The evolution of wind-driven surface waves in partial sea ice cover in the southern Beaufort Sea

by

Yanique Campbell

A Thesis submitted to the Faculty of Graduate Studies of

The University of Manitoba

In partial fulfillment of the requirements of the degree of

MASTER OF SCIENCE

Department of Environment and Geography University of Manitoba Winnipeg

Abstract

Surface waves play an important role in how energy is transported and distributed to both sea ice and atmosphere in Arctic seas. The region of marginal sea ice, termed the Marginal Ice Zone (MIZ), has been increasing alongside temperature, introducing even more open water spaces within the sea ice field. Little research has focused on the development of waves within these open water spaces, and how the wave field evolves under such restricted fetch environments. This study considers a set of observations collected using moorings from ASL Environmental Sciences in the southern Beaufort Sea. These observations suggest local wave development as the dominant source of wave energy tens of kilometers in the MIZ throughout the month of August. The significant wave heights (H_s) and peak periods (T_p) were kept low throughout the month, mainly remaining below a H_s of 0.6 m and a T_p of 6 s in sea ice. At the end of the month, open water waves were able to influence the wave characteristics and there were notable increases in both heights and periods. This study examines how the attenuation of such waves by sea ice differs from the attenuation of open water waves moving into the MIZ. The coherence and positive correlation between H_s and T_p were found to be predominant in the sea ice field. This differs from the classic attenuation of open water waves in sea ice where peak periods increase while wave heights decrease, producing a distinct negative relationship with distance in sea ice. There was no preferential increase or lengthening of the dominant waves under easterly and southerly winds where the wave fetches were long, and the wind speed was found to have limited influence on wave growth after development. Estimations of fetch using empirical relationships, supplemented by satellite imagery, indicate that the short fetches were the dominant factor in terms of wave growth, which indicates an evolution similar to open water waves until they reach an sea ice floe interface and are scattered, a process which depends greatly on the sea ice type, size, rheology and the length of the waves. The interplay among the sea ice (size, structure and concentration) and the wind during a storm event provides an interesting look at the behavior of

locally developed waves and the transition to more open water characteristics and development as the sea ice becomes eroded close to the end of the month. While waves developed locally in sea ice are expected to be fairly low compared to open water waves, they play an important role in the fluxes of energy and momentum in the MIZ and the expansion of this region has implications for the overall energy balance in Arctic marine systems.

Acknowledgements

I would first like to sincerely thank my supervisor Dr. David Barber for granting me this opportunity to study something I am truly passionate about and his positive reinforcement throughout the duration of this project. I would like to thank my co-supervisor Dr. Jens Ehn for his invaluable guidance and support, and for always being the voice of reason. To my other committee members, Tim Papakyriakou and Greg McCullough, thank you for your insight, suggestions and encouragement.

Special thanks to Wayne Chan, who was always willing to help, whether it be with my instruments or my theories. To Sergei Kirillov, who always gave such astute advice and was also always willing to help, thank you very much. I am grateful for Emmelia Wiley, who was so extremely kind and helpful during my preparations for fieldwork as well as all my amazing colleagues at The Centre for Earth Observation Science (CEOS) who helped in any small way or offered encouragement.

I would not be able to complete this project without the financial support of the partnership between the Natural Science and Engineering Research Council (NSERC), Manitoba Hydro, and ArcticNet, nor without the partnership of ArcticNet, Imperial Oil and ASL Environmental Sciences whose Ajurak- Pokak Marine study in the Beaufort Sea 2009 provided me with my main dataset.

Lastly, I would like to say a big thank you to my family and friends for their unwavering support and belief in me throughout this journey.

Dedication

To my absolute biggest fans: mom, dad and Tash. I love you more than words can express.

Table of Contents

List of figures

List of tables

1. Introduction

1.1 Research Motivation & Objectives

Waves in Arctic regions are becoming a key area of interest in the context of climate change. The relationship between waves and sea ice is essentially a feedback mechanism where increased interaction with waves transfers more heat to the sea ice, leading to their decline, and this decline, in turn, supports the development of waves. The large majority of studies that examine the wave-ice relationship focuses on waves of long wavelengths or periods (these terms both refer to the length of the wave spatially and temporally, respectively and are directly correlated in deep water), for example, (Hunkins 1962; Robin 1963; Squire et al. 2009; Prinsenberg et al. 2010; Asplin et al. 2012; Kohout et al. 2014; Collins et al. 2015; Ardhuin et al. 2016). Long ocean waves have been found to be unaffected by sea ice floes, that is, they are able to travel under the sea ice as flexural gravity waves for long distances. The flexure and stress on the floes can result in fractures and breakage which introduces open water, or leads, within the sea ice pack (Collins et al. 2016). The creation of leads in the sea ice pack can also be caused by wind stress on vulnerable sea ice floes.

Long waves measured in these open water segments have been found to decrease in energy (or height) over time as a result of the dampening effect of the sea ice, with the periods of the dominant waves (peak periods) shifting to larger values (Wadhams et al. 1988). This is a result of the sea ice selectively dampening the energy of waves with shorter periods or wavelengths. A dataset of waves in sea ice, therefore, typically consists of wave heights which are lower in comparison to the wave heights in open water. However, it is possible that waves can also be generated within the sea ice cover itself, as concluded by Masson and Leblond (1989). The influence of sea ice, however, changes the physics of wave generation and propagation and as a result, the mechanisms of local wave development in sea ice are more

obscure. Since Masson and Leblond (1989) there have not been any studies focusing on this concept to the author's knowledge. There have been mentions of local wave development in a few studies where unexpected energy increases have been found deep in the sea ice field, which would counteract the idea of long waves decreasing in energy with distance into the sea ice (Wadhams et al. 1988; Doble et al. 2015; Li et al. 2017). Such studies will be considered in the Literature review section.

A focus of this study is such findings of wave energy deep in the sea ice field that go against the typical behavior of long-wave attenuation. Increases of energy in the sea ice field has given rise to a term referred to as the 'rollover effect' which suggests that at a certain point when the waves become short enough, they are dampened less by the sea ice (and hence energy increases). There are varying opinions on this effect which will be discussed further. This study presents a set of observations of wave energy in the sea ice field that are indicative of local wave development and is the first set of wave observations analyzed for local development of waves in sea ice, to the authors' knowledge. The observations were taken during the month of August when sea ice break-up in the study area was in its early stages.

The objectives of this study are as follows:

1. To present evidence for local wave development in the MIZ by examining:
    - The main physical properties of the waves observed by an ice profiling sonar (IPS): the significant wave height (H_s), which is the average of the highest 30% of waves measured, as well as the peak periods.
    - The main influencing factors of waves in ice: the wind forcing and the sea ice field itself.
2. To determine how the sea ice environment, such as the ice concentration, floe size and distribution as well as distance to open water dictated the nature of the waves developed.

3. To explore the ways in which the development of waves in the MIZ could, in turn, affect the actual physics of wave generation and growth in partial sea ice.

1.2 Thesis Outline

This thesis contains 7 main sections. Section 1 describes the rationale for this research as well as an outline of the manuscript. Section 2 gives a description of literature that addresses observations and conclusions made thus far regarding wind waves in the sea ice-covered seas and the implications of persisting climate change in such environments. Section 3 gives the reader the foundational concepts of surface waves, introducing first the properties of waves in the open ocean, then delving into wave evolution in sea ice and the interaction between the two, focusing on short waves. Section 4 describes the study region, how the data were collected as well as an overview of the sea ice and wind conditions during the study period. Section 5 is a presentation and analysis of the results and the discussion in section 6 provides deeper analysis and interpretation of the topic. The conclusions are given in section 7.

2. Literature Review

2.1 The Marginal Ice Zone

The Marginal Ice Zone (MIZ) defines the portion of the sea ice field that is influenced by open ocean processes and acts as a transition region between the open ocean and the continuous sea ice pack. In this region, the influence of the wind, waves and currents allow for the breaking of the solid sea ice pack into arbitrarily shaped floes, ranging from a few meters to hundreds of meters. The MIZ is especially complex; processes resulting from the interplay between sea ice and ocean have important effects on the thermodynamics, chemistry and biology of such an environment. It is also extremely dynamic and is able to move up to 50 km over the course of a day (Perrie and Hu 1996). As such, the delineation of a sea ice edge, or even the distribution of floes within the sea ice field is difficult on short time scales. Even more difficult is developing a feasible model for the MIZ that embodies the diverse mechanisms at play (Zhao et al. 2015; Squire 2018).

Ocean waves are the principal drivers of sea ice deformation and breakup in the MIZ and regulate its extent and characteristics (Dumont et al. 2011). In the context of a changing Arctic, where sea ice extent shows a declining trend and ocean warming an increasing trend, the MIZ is expected to become a more prominent feature. Arctic seas have always been comparably well protected owing to sea ice coverage throughout much of the year, however, an increasing MIZ may significantly modify the fluxes of energy within the system.

Waves are not only able to propagate into the sea ice field from the open ocean, but there is also the potential of waves to evolve locally within the sea ice field (Masson and Leblond 1989).

Because of their vulnerability to wind, waves and current action, MIZs in the Arctic are significantly varied. Consider, for example, strong winds blowing perpendicularly towards the

sea ice pack. The push of the wind and waves create a compact sea ice pack that has a very defined edge (Weeks 2010). The sea ice pack flexes in response to the waves, with the longer waves propagating farther distances, causing stress and eventual breakage in a uniform manner: smaller floes close to the edge and larger floes further in the pack. In the opposite scenario, where the wind is blowing perpendicularly off-sea ice, the stress of the wind creates divergence in the pack and breakage is more haphazard and diffuse, creating various sizes leads and typically bands of sea ice that develop perpendicular to the wind direction (Weeks 2010). A schematic of the MIZ is shown in Figure 2.1.

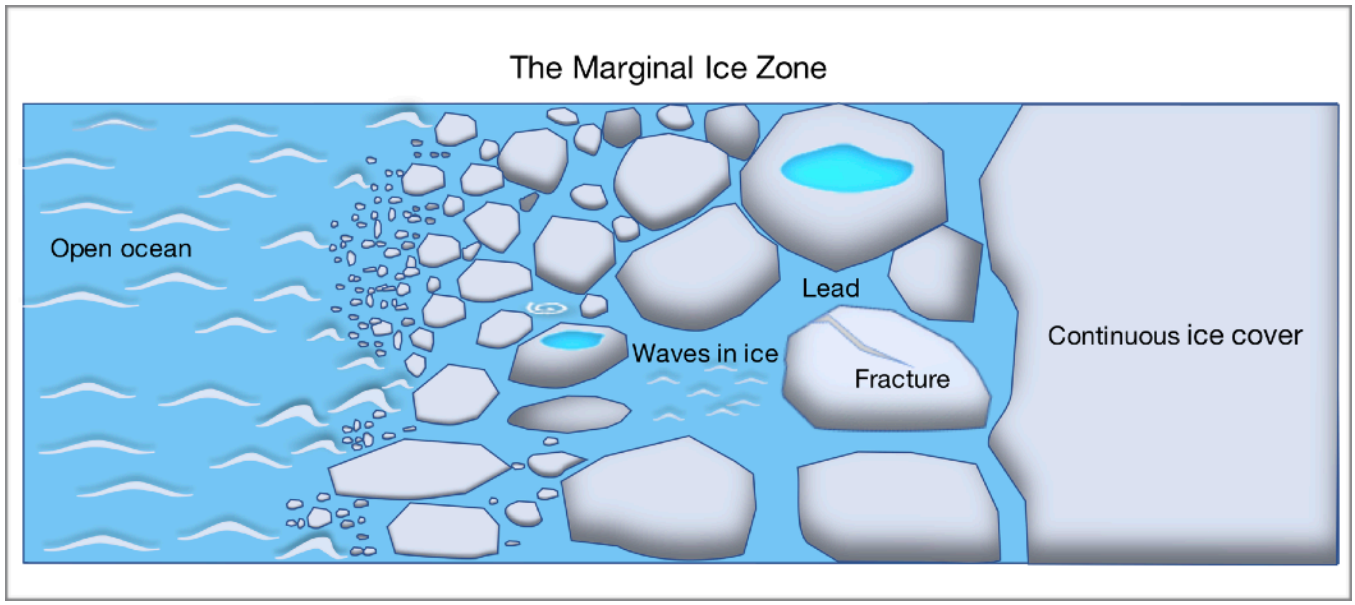

Figure 2.1: The Marginal Ice Zone, an interface between the continuous sea ice cover and the open ocean, where the sea ice is affected by the waves and currents which lead to fractures and breakage.

2.2 Wind-Waves in Changing Arctic Seas

The interaction between waves and sea ice has been studied for quite some time (Robin 1963; Wadhams et al. 1988; Masson and Leblond 1989), but there has been a resurgence in interest owing to the notable decline in sea ice as the climate changes. The effects of decreasing sea ice on the wave environment have already been identified. Asplin et al. (2012) described the decrease in sea ice as a potential positive feedback; as the sea ice decays, a longer fetch is produced which encourages wave growth leading to further erosion of the sea ice by waves. Modelled integrated wave heights over the Beaufort Sea during the years 1979-2009 showed an increase in significant wave heights (H_s) by two and a half fold over the 30 years (Overeem et al. 2011). A 38-year wave reanalysis dataset over the Laptev and Beaufort Seas analyzed by Waseda et al. (2018) revealed that there was an increase in the expected maximum H_s from 2.3 m to 3.1 m during October. The importance of the increasing open water distance (also known as the wave fetch) was highlighted by Thomson and Rogers (2014) who found that waves scaled with fetch over 3 orders of magnitude in the Beaufort Sea. In the Antarctic, Kohout et al. (2014) found that over the period 1997 to 2009, the retreat of the sea ice edge owing to increased melt was correlated with increases in the average H_s.

Open water fetch is therefore instrumental in the development of waves, particularly in an environment where the sea ice limits this fetch. As the open water expands, waves have more space for growth via wind input as well as wave-wave interactions. The influence of fetch, however, has its limitations. As the open water extent becomes much larger than a storm system, for example, and the fetch no longer limits wave development, wave growth becomes more dependent on the nature of the wind (Waseda et al. 2018). Nonetheless, Waseda et al. (2018) also found that winds over open water increased from 1979 to 2016, which had a high correlation with the increasing maximum H_s. The authors noted, however, that there has been no strong evidence, that the intensity and frequency of Arctic storms are actually increasing. In addition,

they found that the correlation between open water distance and the increase in wind speeds was relatively low. Waseda et al. (2018) concluded, then, that the long-term increase in maximum H_s, which is directly dependent on the wind speeds over open water, is a consequence of chance; greater open water fetches increase the probability that high waves will develop as a result of the high winds. Increasing wave heights are therefore not strongly linked to increased storm intensity in the Arctic (at least not thus far), but rather to the reduction in sea ice and consequent increases in fetch, which make wave development and growth possible under strong winds. Even so, the direct correlation between wave growth and wind speed is foundational, as there can be no waves without wind energy input and if given sufficient time and space the wave growth would be almost completely dependent on the wind.

The duration of open water also plays an important role in enhancing the probability of large waves. If open water extends further into fall, for example, when powerful storms are more likely to occur in the Arctic, the probability of strong winds over open water increases, and hence the probability of large waves. Francis et al. (2011) suggested the inhomogeneity in H_s increase throughout the Arctic resulted from the differences in the length of the open water seasons. As an example, the Pacific Arctic showed a greater increase in H_s when compared to the East Chukchi Sea, likely owing to the longer open water season in the Pacific Arctic. Stammerjohn et al. (2012) found that the sea ice edge retreat in springtime Beaufort and Chukchi seas was occurring approximately 1.6 months earlier, and the sea ice edge advance in autumn was taking place approximately 1.4 months later. The result is a notable increase in the open water season duration since 1979.

This increasing trend of a larger open water extent, as well as a longer and earlier open water season, have had significant implications for the position, area, and width of the MIZ (Barber et al. 2015; Strong et al. 2017). While the MIZ has always existed at the sea ice pack periphery to some extent, Lee et al. (2017) found that the width has significantly increased in the western

Arctic Ocean. There is, therefore, a larger area of broken and fractured sea ice with open water segments between floes. These pools of open water increase the absorption of atmospheric heat as well as the transfer of this heat to the sea ice surface, increasing the susceptibility of the sea ice pack to further melt and deformation. Furthermore, the overall sea ice thickness in the Arctic has been decreasing (Stroeve et al. 2012). Multiyear (MY) sea ice extent and area have decreased by -15.1 and -17.2 % per decade respectively, over the period 1979-2011 (Comiso 2012). The thinning and decrease of sea ice caused by warming atmospheric and oceanic conditions, in turn, increases their susceptibility to the atmosphere and ocean, a mechanism termed the ice-albedo feedback. It is plausible, therefore, to expect that increases in the MIZ extent will also increase the total heat transferred to the sea ice from the underlying ocean.

The focus of wave-induced sea ice breakup has largely been on the propagation of long, energetic waves into the sea ice field, which studies have found are highly invulnerable to attenuation by sea ice (Wadhams et al. 1988; Squire 2007). They can, therefore, cause sea ice fracture at incredible distances into the pack. Asplin et al. (2012), for example, observed long swells up to 250 km into a MY sea ice pack, which was almost instantaneously broken up by the waves. As such, the long waves are extremely instrumental in the creation and widening of the MIZ, and essentially pave the way for the development of short waves in partial sea ice cover. This concept was examined in the PhD of Dianne Masson (1987), who developed a theoretical model for wave evolution and growth in partial sea ice. Since then there has been little focus in this area. For waves in general, however, we know that they have a significant impact on energy and momentum fluxes between atmosphere and ocean. Therefore, the development of longer, more energetic waves, enhances the breakup of sea ice in the MIZ, which increases MIZ width, in-ice fetches and in-ice short wave development. These, in turn, modulate the energy balance of the entire sea ice-ocean-atmospheric system.

2.3 Wave-Ice Interactions

The sea ice environment, particularly the MIZ, is both variable and complex, and thus the interactions between waves and sea ice are still not fully understood. This makes the modelling of marginal sea ice environments considerably more difficult than in open water. A wave encountering a sea ice field can be considered in one of the following ways:

1. The sea ice floe is significantly larger than the wavelength.
2. The floe size is significantly smaller than the typical wavelength.
3. The wave and floe or on the same order of magnitude.

In the first case, the large floe, or the continuous sea ice pack is typically modelled as an elastic sheet, with the waves propagating under it as flexural gravity waves (Collins III et al. 2016). In the second case, for very small floes such as pancakes, a mass layer model is the most feasible. The floes are assumed to be mass points with the material properties of floe being unimportant (Zhao et al. 2015). The waves essentially behave as water waves, but with additional mass loading (Collins III et al. 2016). For the even smaller sea ice types such as grease ice, a viscous layer model can be used, due to the dominance of the viscous dampening. The last case describes the most efficient scattering regime, and the ice should also be modelled as infinite, flexible plates (Meylan 2002). However, there is some viscous dampening that takes place alongside scattering and a combination of these modelling techniques might be useful, such as in the model of Bennetts et al. (2012).

The attenuation of wave energy has been the most researched process in wave-sea ice interactions, but it is also inherently complex, comprising of many potential mechanisms for dissipating energy. There are two general categories of attenuation: conservative attenuation and non-conservative attenuation (Collins et al. 2016). Conservative attenuation involves a redirection of wave energy and describes both scattering and reflection mechanisms. The wave gets attenuated in the primary wave direction as the wave gets scattered over other directions.

The overall incident wave energy is thus conserved, just spread out in different directions. Non-conservative attenuation results in the actual loss of energy from the wave spectrum. The wave energy is lost to dissipative processes such as friction, turbulence, wave-induced sea ice breakup and transfer to heat.

The influential field campaign carried out by Wadhams et al. (1988) in the Greenland Bering seas found that wave energy decayed exponentially with distance, with the attenuation coefficient generally increasing with decreasing wave periods:

$$E_x(f) = E_0(f)exp(-\alpha x), \quad (1)$$

where E_x is the wave frequency spectrum at some distance x in the sea ice field, E_0 is the wave frequency spectrum at its initial position x=0, and α is the attenuation coefficient, which, in this case, was based on progressive scattering of the incident waves. While many studies since Wadhams et al. (1988) have also reported this exponential decay, Kohout et al. (2014) found that higher waves, (> 3 m) were attenuated almost linearly rather than exponentially, unlike waves less than 3 m. This allowed the larger waves to propagate further into the sea ice pack. Thus, the largest and longest waves have a significantly greater chance of causing flexural damage to sea ice deep in the pack. Short waves, on the other hand, experience rapid attenuation (Wadhams et al. 1988). The sea ice acts as a low pass filter; as the short waves are attenuated with distance into the sea ice, the longer waves persist, allowing for larger T_p deeper in the sea ice pack. As an example, Smith and Thomson (2016) measured waves in the open water and found T_p ranging from 4 s to 7 s, while the T_p in partial sea ice cover was almost 10 s. According to Stopa et al. (2018), short waves are quickly attenuated over a few kilometers, making them difficult to be imaged by SAR. Zippel and Thomson (2016) compared buoy measurements in open water and in partial sea ice cover and found a significant reduction in the energy of short waves in sea ice, 10-100 times less than the energy of the open water waves under the similar wind conditions. In that study, the maximum distance between the open water buoys and the

buoys in sea ice was 1.5 km, with sea ice concentration extending from zero in open water to 50% in sea ice. The authors observed little wave breaking in the partial sea ice cover, a process associated with short, steep waves, reinforcing the efficiency of the sea ice to dampen short waves. During two separate observations, Asplin et al. (2018) found that the energy of ~ 5 s waves was completely attenuated over a distance of 143 m and 77 m into a sea ice field with 9/10 concentration sea ice.

The only inconsistent result from earlier wave studies was the presence of a so-called 'rollover effect' at short wavelengths (~ 4 - 8 s). At such wavelengths, the exponential increase in attenuation with decreasing peak period that is typically seen slows or even reverses. The result is that these short waves had energy that was higher than expected. Wadhams et al. (1988) first discovered this phenomenon, and suggested two explanations: (1), that the wind could be generating new waves in the short fetches between floes, and (2), there could be a non-linear transfer of energy from long to short waves due to the motion of the sea ice as they interact with the waves. Several studies since then have tested for this rollover effect and its potential causes. Li et al. (2017), for example, created a hindcast of two wave-in-ice events that featured the rollover effect using the Wavewatch III wave model with two different sea ice attenuation parameterizations. The model results showed that the rollover effect was not accounted for when only the attenuation by sea ice was considered. By enabling the other 'source terms' (sources and sinks of wave energy: wind input, nonlinear interactions and dissipation), the attenuation increased with decreasing period over distance, but peaked at some period (around 6 s) after which the attenuation began to decrease. The energy contained in the short waves found deep in the sea ice field (which would not be present if sea ice attenuation was the only factor) was found to be a result of the input of wind energy and the non-linear transfer of energy

from long to short waves. These two effects were found to outweigh the dampening by the sea ice, and hence the attenuation rates were reduced.

Not all studies, however, agree on the presence of the rollover effect. Asplin et al. (2018) specifically examined short wave attenuation in sea ice and found attenuation rates greater than those found in previous studies. The authors found attenuation rates of $\alpha = 2.4 \times 10^{-2}$and $\alpha = 5.4 \times 10^{-2}$ for two different sites in a sea ice field, while previous studies have found attenuation rates on the order of $10^{-5} - 10^{-3}$. They concluded that there is no evidence of this rollover effect. Thomson et al. (2018) addressed this issue by noting that the generation of short waves resulting from local energy input from the wind, at some distance in the sea ice cover, allows for the attenuation to appear that it is less, when in fact, the attenuation still continues to increase monotonically with decreasing period. Distance appears to play a significant role in whether or not the apparent rollover effect is observed. Li et al. (2017) found that the effect increased when the winds were high and the distances between observing buoys were larger. If the distance at the point in sea ice being measured is far enough from the sea ice edge, then it is possible for the energy of the open water to be completely attenuated as suggested by Doble et al. (2015), leaving only that rollover effect from local wave generation.

The concept of wave growth in partial sea ice has not been frequently addressed. Masson and Leblond (1989) first developed an analytical model of wave evolution in partial sea ice and showed that waves can indeed develop in the sea ice field during an off-ice wind, providing that the sea ice concentration is sufficiently low. A more recent study by Smith and Thomson (2016) also identified low amplitude waves in partial sea ice cover, ranging from 0.01 to 0.61 concentration, that were locally generated in off-sea ice conditions. These waves were distance limited, a function of the amount of open water between floes. The authors noted that the waves generated within the sea ice field during on-sea ice wind conditions were likely to consist of

longer waves from the open ocean that were being attenuated, as well as locally generated short waves.

3. Background

3.1 Waves In The Deep Ocean

3.1.1 Description of a simple wave

A wave, in the simplest terms, can be treated mathematically as a linear, sinusoidal wave. Such a wave propagating in the positive x –direction can be expressed as:

$$\eta(x,t) = a\sin(\omega t - k\,x), \tag{3.1}$$

where a is the wave amplitude, $\omega = 2\pi/T$ is the angular frequency, $k = 2\pi/\lambda$ is the wavenumber, T is the wave period and λ is the wavelength. A schematic of such a wave is shown in Figure 3.1. This description of a surface wave is based on linear theory or the Airy wave theory developed by George B. Airy in 1845. Linear theory was built upon idealized assumptions regarding the physical properties of the sea surface, but, nonetheless, has provided the foundational understanding of wave behavior in the deep ocean. It is based on two fundamental equations, the conservation of mass and the conservation of momentum, both expressed in terms of a velocity potential $\boldsymbol{\phi}$. We can show that these equations produce the Laplace and Bernoulli equations, from which we can derive a solution for the linear wave and its properties, when certain boundary conditions are applied. An overview of these fundamental equations is given in the following section.

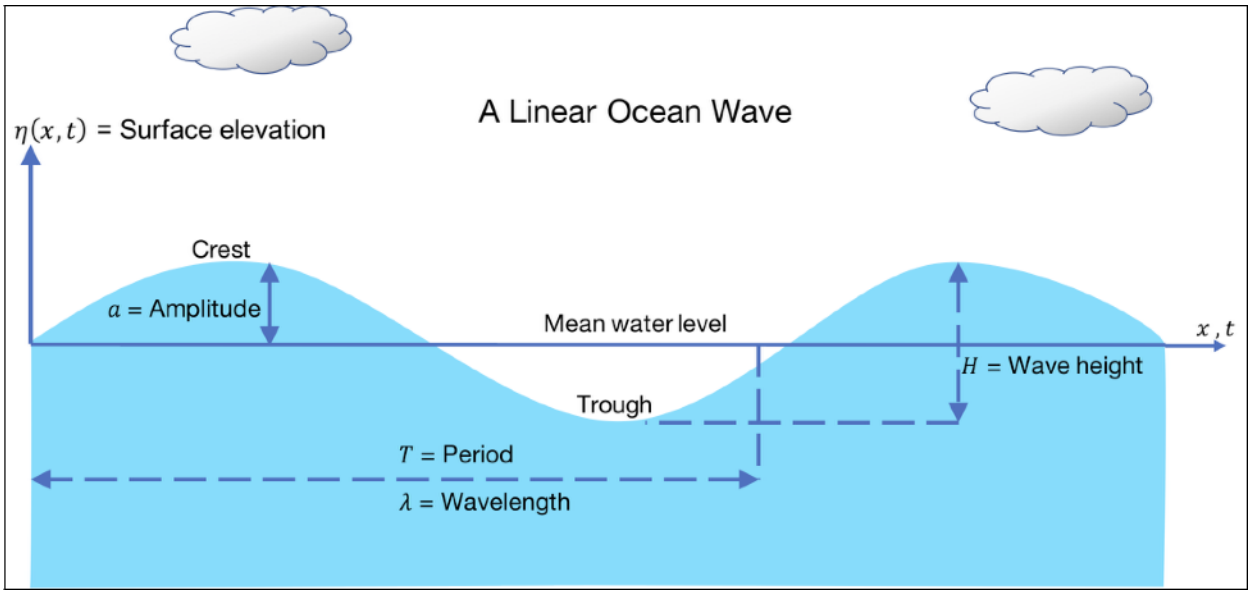

Figure 3.1: Profile of a simple, linear wave. The amplitude is the distance from the mean water level to the crest of the wave, the height is 2 times the amplitude and the wavelength and period represent the distance or time, respectively, between successive crests or troughs.

3.1.1.1 The fundamental equations

Several simplifying assumptions are made in order to satisfy Linear theory:

- The amplitude of the wave is small in comparison to its length and the water depth.
- The water is incompressible. Therefore, for each cell of water (or each water particle), the density is constant, and a continuity equation can be derived within that cell. The changes in ocean density are typically related to temperature and salinity variations, but the spatial scales of these variations are significantly larger than the spatial scale characterizing linear theory.
- Water is considered inviscid. The viscosity is therefore ignored as well as frictional effects.
- The pressure at the surface is considered constant.
- The flow is irrotational, which gives rise to a velocity potential.
- The water particles cannot move through the surface or penetrate through the bottom.

3.1.1.2 Conservation of mass

The mass balance equation for the water surface is given as:

$$\frac{\partial \rho}{\partial t} + \frac{\partial \rho u_x}{\partial x} + \frac{\partial \rho u_y}{\partial y} + \frac{\partial \rho u_z}{\partial z} = S_p, \tag{3.2}$$

where the first term represents the local rate of change of mass density ρ, the following three terms represent the advection or transport of density with water velocities u_x, u_y and u_z in the x, y and z directions, respectively. he right-hand side term, S_p represents the source terms, that is, sources of density. Since density is constant, the derivative of density must be 0 and since there is no generation of water, S_p must also be 0. The result is the continuity equation:

$$\frac{\partial u_x}{\partial x} + \frac{\partial u_y}{\partial y} + \frac{\partial u_z}{\partial z} = 0. \tag{3.3}$$

Because the flow is irrotational, the curl of the flow velocity is 0, that is, $\Delta \times u = 0$. Thus, the velocity potential $\phi(x, y, z, t)$ can be defined such that:

$$u = \nabla \phi \qquad (u_x = \frac{\partial \phi}{\partial x}; \qquad u_y = \frac{\partial \phi}{\partial y}; \qquad u_z = \frac{\partial \phi}{\partial z}) \tag{3.4}$$

The continuity equation for an ideal, incompressible, inviscid and irrotational fluid can thus be written in terms of ϕ, also known as the *Laplace equation*:

$$\frac{\partial \phi^2}{\partial x^2} + \frac{\partial \phi^2}{\partial y^2} + \frac{\partial \phi^2}{\partial z^2} = 0. \tag{3.5}$$

3.1.1.3 Conservation of momentum

The conservation of momentum is similarly solved by taking μ as the momentum density of water. Hence $\mu = \rho u_x$, resulting in the following balance equation in the $x-$ direction:

$$\frac{\partial (\rho u_x)}{\partial t} + \frac{\partial u_x (\rho u_x)}{\partial x} + \frac{\partial u_y (\rho u_x)}{\partial y} + \frac{\partial u_z (\rho u_x)}{\partial z} = S_x, \tag{3.6}$$

where S_x is the production of momentum in the $x-$direction. $S_x$is synonymous with *force* (rate of change of momentum) which is a result of the horizontal pressure gradient in water, $\frac{\partial p}{\partial x}$,

therefore the balance equation in the $x-$direction becomes:

$$\frac{\partial(\rho u_x)}{\partial t} + \frac{\partial u_x(\rho u_x)}{\partial x} + \frac{\partial u_y(\rho u_x)}{\partial y} + \frac{\partial u_z(\rho u_x)}{\partial z} = -\frac{\partial p}{\partial x}. \tag{3.7}$$

The second, third and fourth terms of this equation involves velocities in quadratic terms, thus they are non-linear and can be removed from the equation. The resulting linearized momentum balance equation, is shown below for the $x, y, z-$directions:

$$\frac{\partial u_x}{\partial t} = -\frac{1}{\rho}\frac{\partial p}{\partial x}; \tag{3.8a}$$

$$\frac{\partial u_y}{\partial t} = -\frac{1}{\rho}\frac{\partial p}{\partial y}; \tag{3.8b}$$

$$\frac{\partial u_z}{\partial t} = -\frac{1}{\rho}\frac{\partial p}{\partial z} - g, \tag{3.8c}$$

or in terms of the velocity potential:

$$\frac{\partial}{\partial t}(\frac{\partial \phi}{\partial x}) + \frac{1}{\rho}\frac{\partial p}{\partial x} + gz = 0; \;\Leftrightarrow\; \frac{\partial}{\partial x}(\frac{\partial \phi}{\partial t} + \frac{p}{\rho} + gz) = 0; \tag{3.9a}$$

$$\frac{\partial}{\partial t}(\frac{\partial \phi}{\partial y}) + \frac{1}{\rho}\frac{\partial p}{\partial x} + gz = 0; \;\Leftrightarrow\; \frac{\partial}{\partial y}(\frac{\partial \phi}{\partial t} + \frac{p}{\rho} + gz) = 0; \tag{3.9b}$$

$$\frac{\partial}{\partial t}(\frac{\partial \phi}{\partial z}) + \frac{1}{\rho}\frac{\partial p}{\partial x} + gz = 0; \;\Leftrightarrow\; \frac{\partial}{\partial z}(\frac{\partial \phi}{\partial t} + \frac{p}{\rho} + gz) = 0; \tag{3.9c}$$

where g is weight of the volume due to gravity. The gz term can be added to the linearized equations in the $x-$ and $y-$directions as it would have no effect; the derivative with respect to x would cancel this term out. Hence, a single momentum equation can be derived since $\frac{\partial \phi}{\partial t} + \frac{p}{\rho} + gz = 0,$ is independent of the direction (x, y, z). The resulting equation is the Unsteady Bernoulli Equation:

$$\frac{\partial \phi}{\partial t} + \frac{p}{\rho_w} + gz = 0, \tag{3.10}$$

where ρ_w is the density of water.

3.1.1.4 Boundary conditions

Both the conservation of momentum and the conservation of mass are subjected boundary conditions at the water surface and the seabed.

For the *dynamic boundary condition*, the pressure acting on the free surface is zero ($p = 0$) and thus the Bernoulli Equation becomes:

$$-\frac{\partial \phi}{\partial t} g\eta = 0, \quad at \quad z = 0, \tag{3.11}$$

where $\eta = z$ is the surface elevation from still water level $z = 0$ (the boundary condition is applied at $z = 0$, but the actual surface elevation is considered, which could be positive or negative).

The *kinematic boundary condition* at the free surface restricts the movement of the water particles through the surface, thus the vertical velocity of the water particle must be equal to the velocity of the free surface:

$$w = \frac{\partial \phi}{\partial z} = \frac{\partial \eta}{\partial t}, \quad at \quad z = 0 \tag{3.12}$$

Similarly, at the bed of the wave, the water particles cannot move through the bottom and hence the vertical water velocity is always 0:

$$w = \frac{\partial \phi}{\partial z} = 0, \quad at \quad z = -h, \tag{3.13}$$

where h is the water depth.

The Laplace and kinematic boundary conditions produces all the kinematic aspects of the wave, while the Bernoulli equation and the dynamic boundary conditions provides all the dynamic aspects of the wave. A linear wave profile such as that given by equation 3.1 is a solution of these equations along with their boundary conditions (Figure 3.2).

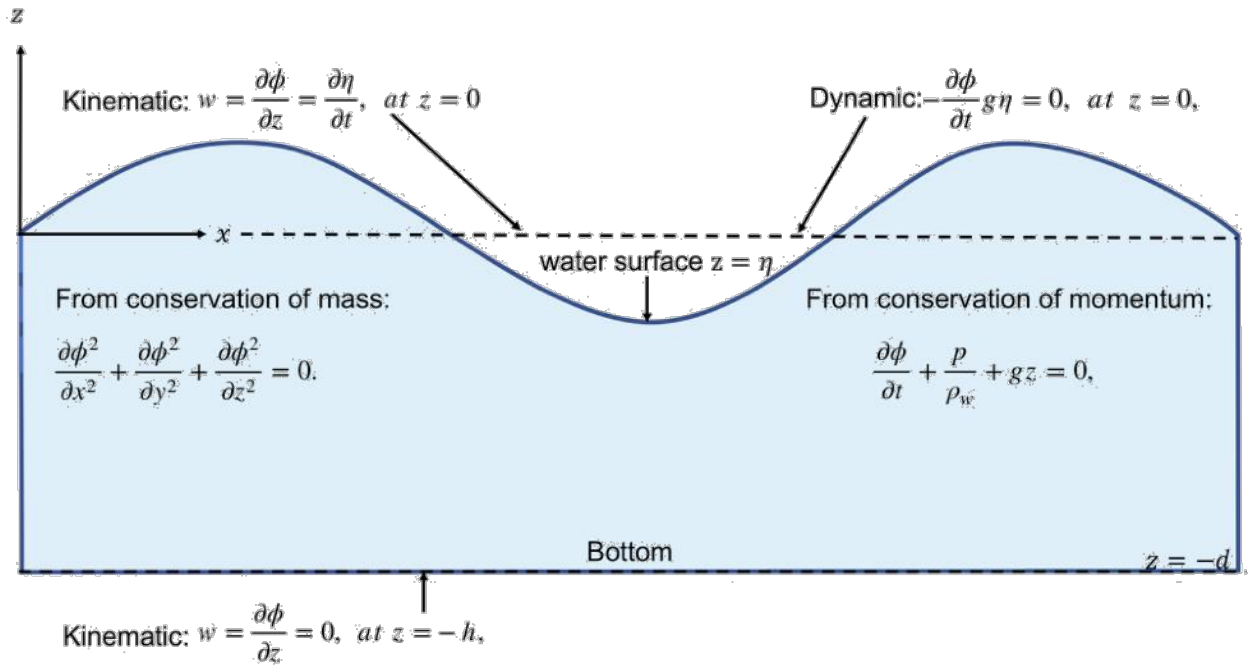

Figure 3.2: The fundamental equations and boundary conditions for linear theory. Adapted from (Holthuijsen 2010).

3.1.2 The wave spectrum

It can be assumed that the sea one typically sees when looking out at the ocean is comprised of many of these simple, linear waves superimposed onto each other to create an irregular, constantly changing sea surface. A combination of frequency (or wavenumber) and direction makes up each wave component and each component is associated with an amplitude and phase. By Fourier analysis, the form of an irregular wave record propagating in space can be obtained as a sum of sinusoidal waves:

$$\eta\left(x, y, t\right) = \sum_{j=1}^{n} a_j \cos(\omega_0 t - \mathrm{k}_j \mathrm{X} + \phi_j), \tag{3.14}$$

where $\eta(t)$ is the recorded elevation of the water surface at time t, a is the amplitude of the wave component and j, $\omega_0, \phi_j, \mathrm{X}$ are the angular frequency, phase angle and horizontal vector of the wave component, respectively. k_j is the wavenumber vector defined as:

$\mathrm{k} = k_x i + k_y j$, where $k_x = k\cos\theta$ and $k_y = k\sin\theta$. Here i and j are the components of the unit vector in the wave propagation direction, θ. In deep water, ($h > \lambda/4$), each wave component will travel at its own phase speed (c) depending on its wavelength or frequency. This relationship describes the dispersion relation, expressed as a function of wavelength and frequency. In deep water the dispersion relation and the corresponding wave speed are expressed as:

$$\omega^2 = \mathrm{gk}\tanh(kh) = \mathrm{gk}; \tag{3.15}$$

$$\mathrm{c} = \frac{\omega}{T} = \sqrt{\frac{g}{k}\tanh kh} = \sqrt{\frac{g}{k}}, \tag{3.16}$$

where g is the acceleration due to gravity and h is the water depth. Each component contains a quantity of energy per surface area, given as:

$$E = \frac{\rho_w g a^2}{2} = \frac{\rho_w g H^2}{8} \quad (H = 2a), \tag{3.17}$$

where ρ_w is the density of water, a is the amplitude and H is the height of the wave. This energy is proportional to the variance of the surface elevation, defined as the mean of the squared deviations of surface elevation, $\overline{\eta^2}$, where η is the surface elevation and the overline means time-averaging. The variance, therefore, is direct measure of the amplitude:

$$\overline{\eta^2} = 1/2\ a^2. \tag{3.18}$$

When all the random wave components are considered, the variance of the random surface elevation (which is the sum of all wave components) is equal to the sum of the variance of each component.

$$\overline{\eta^2} = E\left\{\overline{\eta^2}\right\} = \sum_{j=1}^{n} E\left\{\frac{1}{2}a_j^2\right\} \ for\ E\{\eta\} = 0, \tag{3.19}$$

where $E\{\}$ represents expected value. The distribution of variance across the different frequencies gives rise to the wave-variance spectrum. Since the total energy of all components can be described as:

$$E_{total} = \rho_w g \overline{\eta^2}, \tag{3.20}$$

then by multiplying the variance spectrum by the density of water, ρ_w, and the acceleration due to gravity, g, the *energy spectrum* $E(f,\theta)$ is obtained. The wave spectrum is therefore represented as the variance spectrum, the energy spectrum or just simply a^2 along the y-axis with frequency (or wavenumber) on the x-axis.

The wave energy spectrum, however, is discrete, while in reality the spectrum at sea is continuous with all frequencies represented. An *energy density* spectrum gives a more realistic approach to the distribution of wave energy. The computation of energy for a particular frequency is, in fact, a mean over a small width of frequencies. The energy is divided by this frequency width to produce an energy density at each frequency. Note that the wavenumber can also be used in the place of frequency to produce a wavenumber-direction spectrum, owing to the linear relationship between frequency and wavenumber in deep water: $\omega^2 = gk$, where $\omega = 2\pi f$ is the angular frequency and $k = 2\pi/\lambda$ is the wavenumber. It stands to reason, then, that if the spectrum tends to a very narrow band of frequencies the wave approaches a regular, harmonic wave. If the spectrum is broad, however, the wave profile is irregular as it consists of a large number of wave components of different frequencies.

3.1.3 Statistical Parameters

From the wave spectrum, we can then extract the statistical parameters that are typically used to describe the sea state. The spectrum is characterized by moments, m, where the nth moment is:

$$m_n = \sum_{f_1}^{f_n} E(f) f^n d(f). \tag{3.21}$$

$E(f)$ represents the spectral density integrated over a range of frequencies, f, from the lowest frequencies to the highest. The zeroth order moment, m_0, is of particular importance as it represents the total variance of the of the wave record or the area under the spectral curve which leads to the derivation of the significant wave height (H_s):

$$H_s = 4\sqrt{m_0}\,. \tag{3.22}$$

Since m_0 is a measure of the total variance, $\overline{\eta^2}$, it is also synonymous with the total energy, $E \Leftrightarrow \overline{\eta^2}$, and hence H_s can also be described as $H_s = 4\sqrt{E}$. It must be kept in mind, however, that the total energy is actually $\frac{\rho_w g a^2}{2}$ or $\rho_w g m_o$. The peak frequency, f_p, refers to the frequency associated with the peak energy density in the spectrum, and the peak period describes the inverse of the peak frequency: $T_p = \frac{1}{f_p}$.

Several empirical models of the wave spectrum have been defined over the years, that have set the foundation for our understanding of the evolution of waves in the deep ocean. The most commonly used model spectrum today is from the Joint North Sea Wave Project (JONSWAP) (Hasselmann et al. 1973). This study measured waves along a 160 km transect in the North Sea for four weeks, with respect to frequency, wave direction, space and time. They were able to describe the spectra in fetch limited conditions, where the growth of waves offshore under steady wind conditions was limited by the distance to the shore. An example spectrum from this experiment is shown in Figure 3.3, which shows how energy evolves in the spectra: the wave energy increases as the fetch increases, with the peak shifting from the higher frequencies to the lower frequencies with space and time. Notice the high-frequency tail of the spectrum, where waves are steep and limited in growth by wave breaking as a result.

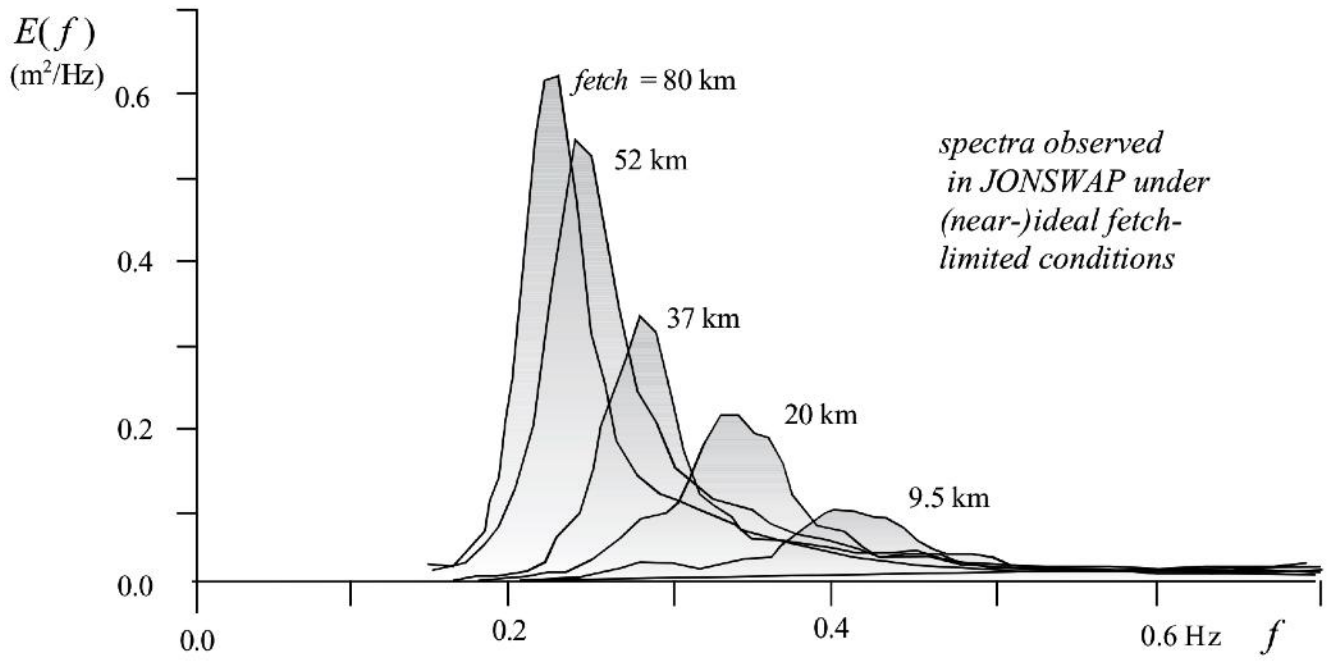

Figure 3.3: Deep water, fetch-limited spectra observed during the JONSWAP experiment, after Hasselman et al. (1973). From (Holthuijsen 2010).

3.2 Wave Evolution In Sea Ice

The governing equation of wave energy propagation in its simplest terms can be described as:

$$\frac{\partial E(f,\theta)}{\partial t} + c_g = S(f,\theta)\,. \tag{3.23}$$

$E(f,\theta)$ is the wave energy density spectrum, which gives the distribution of wave energy across different frequencies, f , and directions θ. Wave propagation occurs as the waves travel in all directions at speeds defined by the group velocity, c_g, which in turn is dependent on the frequency of the wave (in deep water, c_g is half the phase speed, $c_g = g/(4\pi f)$). On the right-hand side of the equation, $S(f,\theta)$ represents the source terms, which accounts for how energy is lost or gained among the different combinations of f and θ. In deep water the source terms that influence wave energy are given as:

$$S(f,\theta) = S_{in} + S_{nl} + S_{dis}, \tag{3.24}$$

where S_{in} represents the input of energy by the wind, S_{nl} describes the non-linear interactions between the waves themselves and S_{dis} account for wave energy dissipation via wave breaking. In partial sea ice conditions, the source terms are altered, and a new source term S_{ice} is introduced, which is typically scaled by the sea ice concentration (Li et al. 2017). The authors found that using only the S_{ice} source term in the WAVEWATCH III wave model allowed for the classic exponential attenuation of energy, without increases of energy within the wave field (typically attributed to the rollover effect where at a certain low periods the attenuation decreases, hence an apparent increase in energy). Since S_{ice} on its own was not useful in producing this effect, they concluded that any increase in wave energy must therefore come about as a result of $S_{in} + S_{nl} - S_{dis}$. They found, however, that S_{dis} was significantly smaller the other two source terms, suggesting that S_{in} and S_{nl} were the main contributors to this energy, which essentially counteracted the attenuation of the waves. Embracing these conclusions, the source terms S_{in} and S_{nl} which contribute to the wave energy in sea ice, and the source term S_{ice} which reduces this energy, are examined in further detail in the following sections.

3.2.1 The governing source terms

3.2.1.1 Wind energy input - S_{in}

The mechanisms of wind-wave generation are still poorly understood today. Two theories, however, were integral in introducing the concept of wave growth based on resonance and are used in wave models today. These ideas of resonance were proposed by Phillips (1957) and Miles (1957) (both scientists were unaware of the other's study at the time). There was a distinct difference between both theories, however. Phillips suggested that turbulent pressure fluctuations at the ocean surface propagate as harmonic pressure waves in the wind direction. These harmonic pressure fluctuations modify the water surface creating freely propagating

water waves. When a pressure wave component happens to move at the same speed, direction and wavelength as a water wave, they are in resonance and energy is transferred from the wind to the water wave. The turbulent pressure fluctuations, in this case, are inherent to the wind, and the airflow is not modified by the wave field.

The modification of a mean shear wind flow by water waves is the foundation of Miles' theory. His idea was that the initial waves on the ocean surface influenced the pressure waves in such a way that the waves themselves became amplified. Miles proposed that the sinusoidal nature of a surface water wave would disrupt the airflow above it, and this disturbance would be greatest at the air-water interface and lessen with increasing elevation. The wind would thus be slower at the surface and faster as elevation increased. At the surface, the weak water wave disturbs the airflow above it and creates a pressure wave in such a way that the pressure is higher over the wave trough and lower over the crest. At some critical level above the surface, the wind speed equals the speed of the water wave, and the interaction of the pressure wave with this critical layer causes the extraction of energy from the wind. This, in turn, allows for a higher pressure to act the windward side of a wave, behind the crest, essentially pushing the water particles down and deepening the wave trough. On the leeward side of the wave, the air pressure slightly decreases pulling the crest upwards. This increase and decrease in pressure at these pivotal points on the wave enhances its growth. As the wave grows in height, its effect on the pressure field above it increases and the resulting transfer of energy from the wind to the wave is amplified. Wave growth in itself is, therefore, a positive feedback mechanism, as the very process of waves increasing in height and energy, produces greater airflow perturbations, which in turn lead to further wave growth. A schematic demonstrating Mile's theory of wave growth is shown in Figure 3.4.

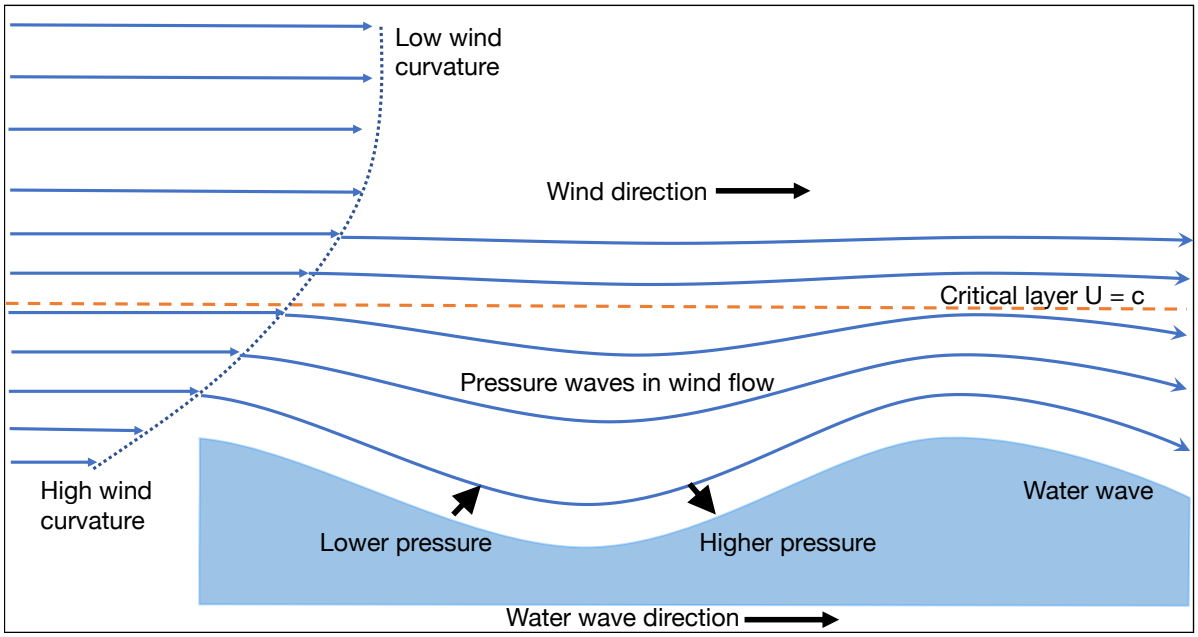

Figure 3.4: Miles theory of wave generation. Close to the surface the water wave disturbs the wind flow creating pressure waves which follow the wave profile. At some critical level above the surface the wind speed equals the wave speed. The interaction of the pressure wave with this critical layer allows for pressure to be higher on the windward side of the wave and lower on the leeward side, amplifying the wave.

The magnitude of the wave energy, however, is not the only consideration in terms of wave growth. There is also a dependence on the ratio of wind speed to wave phase, U_{10}/c_p, termed as the wave age. When the waves are young, their phase speeds are relatively slow (short periods/wavelength waves move slowly) and thus the critical layer where the wind equals the phase speed is close to the surface. At this height, the curvature of the wind profile is very large and more energy is transferred to the waves. For more mature, faster-moving waves, the critical layer is higher, the curvature is very small, and less energy is transferred to the waves. When the wave speed is large enough such that $c_p > U_{10}$, energy transfer from the wind to the wave stops and the waves reach their maximum height for that wind speed. Essentially, the short waves are forced significantly more by the wind than longer waves but their short wavelengths mean that they get steep easily, break and lose their energy. Around the peak frequency, the net influx of wind energy exceeds dissipation by breaking and the waves grow, up to the point where $c_p > U_{10}$ and wave breaking again becomes strong.

Miles described the wind input source term as:

$$S_{in}(f,\theta) = \beta E(f,\theta), \tag{3.25}$$

where $\beta = [Ucos(\theta - \theta_{wind})/c]^2$ is a coefficient depending on the wind speed and direction. U is a reference wind speed and c is the phase speed of the water wave. The spectrum of this source term looks like Figure 3.5 (Holthuijsen 2010). Most of the energy from the wind goes to the peak of the spectrum, however, it also shows that the energy preferentially generates high-frequency waves.

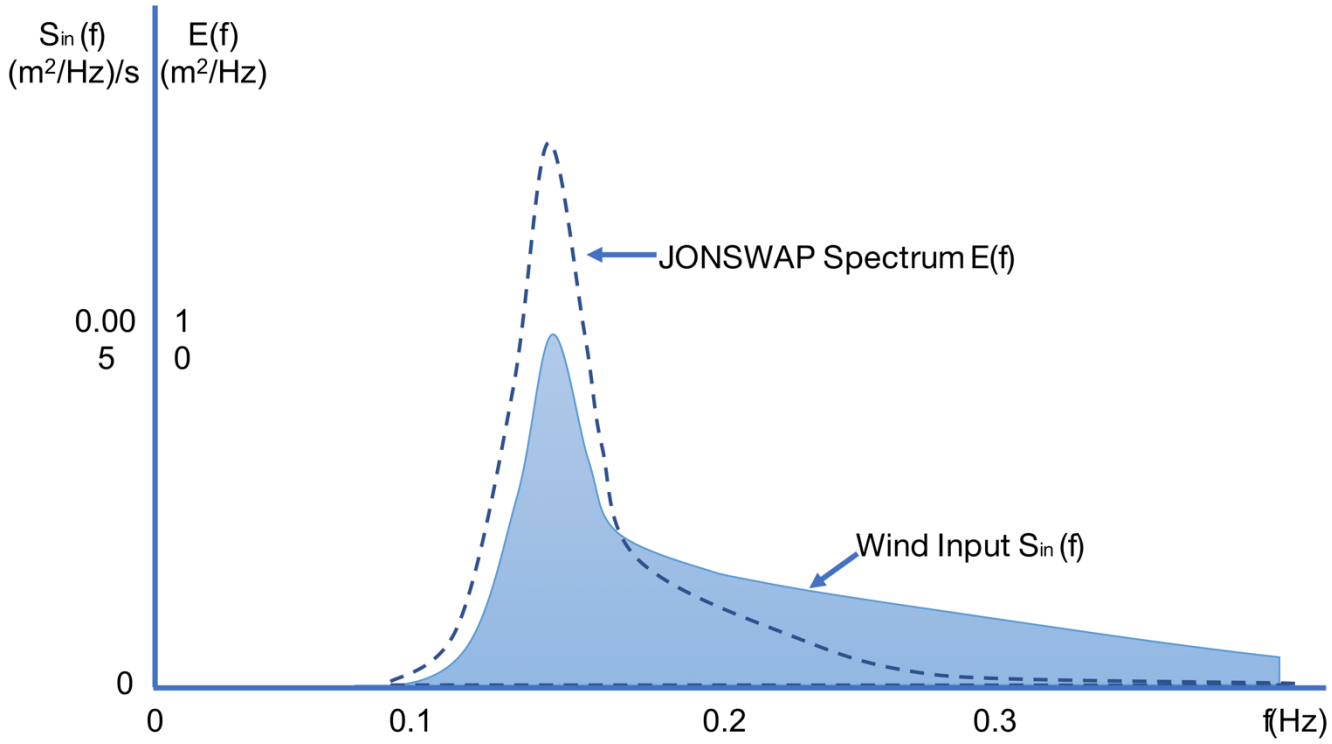

Figure 3.5: Representation of the wind input source term S_{in}, in relation to the total JONSWAP spectrum in deep water.

3.2.1.2 Non-Linear Interactions - S_{nl}

Another important mechanism that enhances wave growth is the resonant, nonlinear interaction that takes place between the waves themselves. These are interactions among the waves themselves that allows energy to be redistributed in the spectrum, keeping the total energy is conserved. At the spectral peak where wind input exceeds dissipation, excess wave energy is transferred to both lower and higher frequencies. At the high-frequency end, the energy is quickly lost through dissipation and there is limited growth. At the low-frequency end, the energy is absorbed with little dissipation and the waves grow. There is, therefore, a characteristic shift of energy to longer waves as the spectrum develops. S_{nl} has a plus-minus signature as shown in Figure 3.6 (Holthuijsen 2010). A narrow positive lobe indicating wave growth sits just below the peak frequency with a broader negative lobe at higher frequencies from which the energy is being redirected. In the early stages of wave development, as the fetch is increasing, the positive lobe is below the spectral peak and energy is efficiently transferred to longer waves. As the spectrum becomes mature, the positive lobe approaches the peak frequency or is just higher than the peak frequency, and the transfer of energy to the longer waves slows. S_{nl} essentially maintains the shape of the energy spectrum, being more active when the sea is young and the spectrum of frequencies is very narrow, then slowing down when the sea is mature and the spectrum of frequencies broadens.

Hasselman (1962, 1963) found that two pairs of wave components can interact and transfer energy if the following resonant conditions were met:

$$f_1 + f_2 = f_3 + f_4; \tag{3.26a}$$

$$k_1 + k_2 = k_3 + k_4, \tag{3.26b}$$

where f is the frequency and k the wavenumber vector. If the frequency, wavenumber and direction of the two pairs match, then the transfer of energy can take place. As this process requires four-wave components it was termed quadruplet wave-wave interactions. It can be expressed in terms of the Boltzmann equation, which shows how energy is transferred to a wave

component with wavenumber k_4, when all four components k_1, k_2 , k_3 and k_4 interact and are in resonance:

$$S_{nl}(k_4) = f \iiint dk_1 dk_2 dk_3 \delta(k_1 + k_2 - k_3 - k_4)\ \delta(f_1 + f_2 - f_3 - f_4) \ldots$$
$$[n_1 n_2 (n_3 + n_4) - n_3 n_4 (n_1 + n_2)]\ K(k_1, k_2, k_3, k_4), \tag{3.27}$$

where n_4 , is the action density which is synonymous with the energy density, that is, $n_4 = \frac{E(f_4, \theta_4)}{f_4}$). The frequencies f_1, f_2, f_3 and f_4 correspond to the wave component with wavenumbers k_1, k_2 , k_3 and k_4. The delta functions δ, ensure that the resonance conditions are met and the kernel function, K, describes the amount of energy being transferred to the wave component associated with k_4, f_4, θ_4.

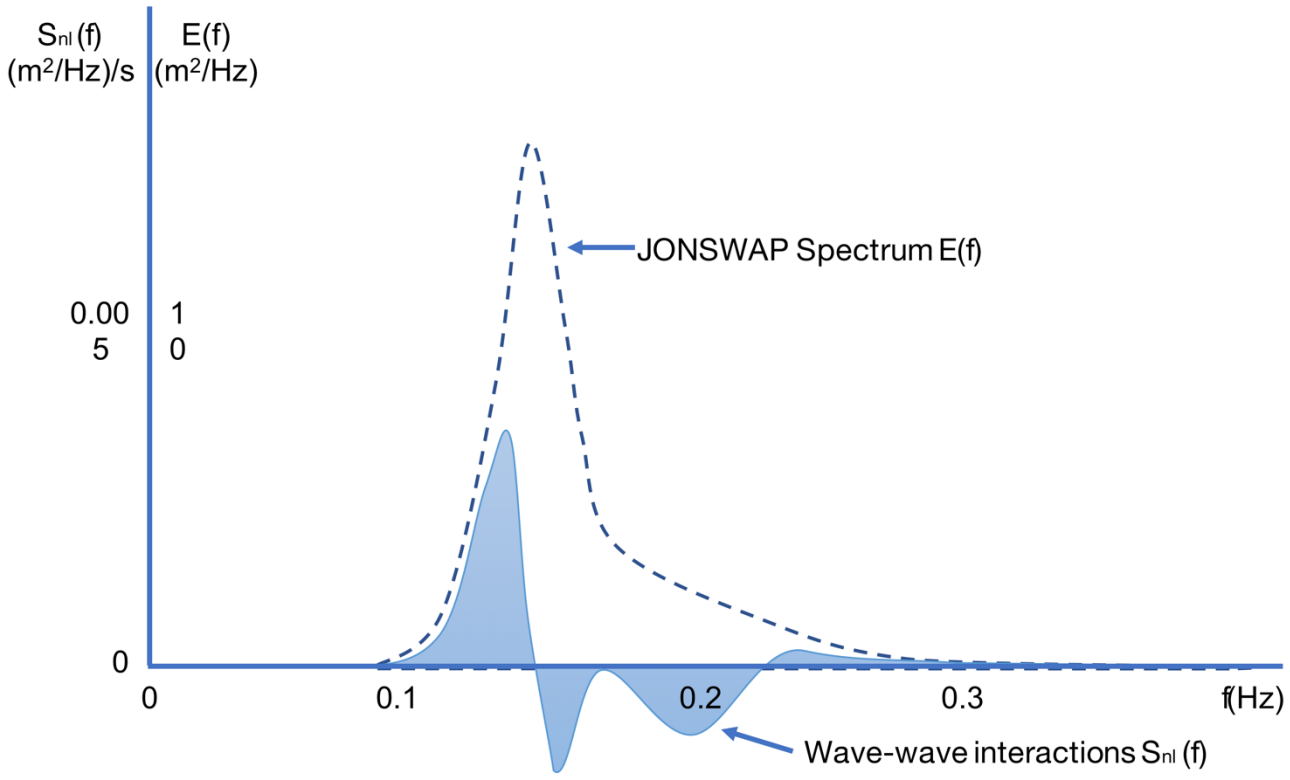

Figure 3.6: Representation of the wind input source term S_{nl} , in relation to the total JONSWAP spectrum in deep water.

3.2.1.3 Ice-wave interactions - S_{ice}

The two main contributing source terms to wave growth in partial sea ice are described above. The introduction of the S_{ice} represents the effect of sea ice on the wave evolution. The PhD work of Masson (1987) was the first to assess the three-dimensional evolution of the wave spectrum in partial sea ice cover. Masson and Leblond (1989) and Perrie and Hu (1996) produced publications drawing on the work of Masson, where the concept of wave growth in partial sea ice was considered. Masson and Leblond (1989) discussed this idea theoretically, (Perrie and Hu 1996) incorporated the idea in their numerical model. The models of both pairs of authors, however, considered floes as rigid, cylindrical bodies and thus was not suited for large floes which experience flexure during wave advance. Their model was based on multiple scattering theory which assumed that the geometry of the floes was fixed. An alternative to the multiple scattering theory is the linear Boltzmann equation for wave propagation, which was first used by Meylan et al. (1997). In this case, the floes were modelled as flexible plates. Meylan and Masson (2006) proved that the scattering equation of Masson and Leblond (1989) was equivalent to the Boltzmann equation of Meylan et al. (1997) and thus it is useful to examine both methods together. The full evolution of waves propagating in partial sea ice as described by Masson and Leblond (1989) was:

$$\frac{\partial E}{\partial t} + c_g \,.\, \nabla E = (S_{in} + S_{ds})(1 - fi) + S_{nl} + S_{ice} \,. \tag{3.29}$$

In this case the wind energy and the dissipation source terms are scaled by the sea ice concentration, fi. The linear Boltzman equation used by Meylan et al. (1997) which describes the energy spectrum resulting from the influence of S_{ice} can be given as:

$$S_{ice} = -\alpha(x,t,k,\theta)E(x,t,k,\theta) + \int_0^{2\pi} S_k(x,t,k,\theta-\theta')E(x,t,k,\theta')(f,\theta)d\theta' \,. \tag{3.30}$$

The absorption coefficient α represents the fraction of the wave energy lost via scattering and dissipation, while the scattering function S_k represents the redistribution of the incident wave

energy in different directions. Since scattering conserves the total energy, then it would be equivalent to the energy loss in a given direction.

3.2.2 Wave scattering by ice

The scattering in the MIZ is a combination of scattering from multiple, individual floes. As a wave encounters a floe, its energy is reflected and scattered at the floe edge (Figure 3.7). A portion of the energy also gets transmitted under the floe and if it is not fully dampened before it reaches the other end of the flow, is scattered again on exit. This attenuated energy will go on to interact with another floe as well as other scattered waves. Eventually, the incident energy spectrum becomes isotropically spread out. Short waves have been found to be preferentially scattered by sea ice compared to longer wavelengths, which essentially pass through floes largely unperturbed. As the focus of this study are waves of shorter wavelengths, we will consider two cases: the first, when the waves are significantly short relative to the size of the floes (waves just being formed, for example) and the second, when the waves are longer or more mature, but still considered short waves, i.e < 10 s. In the case of the former, the waves are mainly backscattered so that wave energy is unable to penetrate under the floe. In the latter case, some of the energy is transmitted under the floe while a large amount is scattered in different directions. One can consider this problem, then, a balance between the transmission and the reflection of the incident wave energy, i.e.: $|R^2| + |T^2| = 1$.

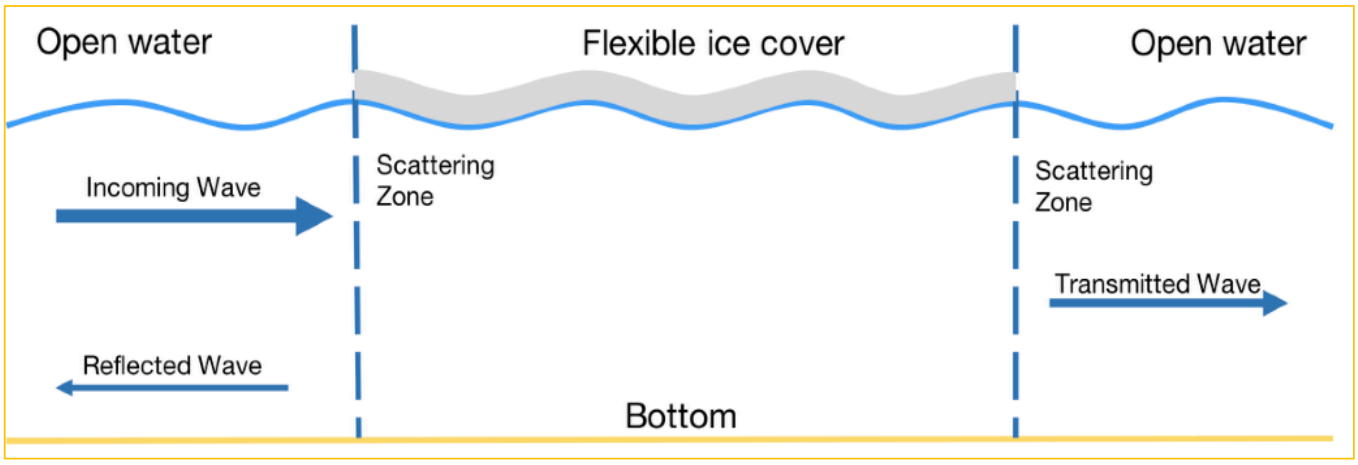

Figure 3.7: Schematic showing the physical interaction between an incoming wave and an sea ice floe. Adapted from (Broström and Christensen 2008).

Regulators of wave scattering and transmission

The ratio of floe size to wavelength, $k\,a$, has significant control over the scattering of an incident wave, where $k = 2\pi/\lambda$ is the wavenumber and a is the size of the floe. When the wavelength is comparable to the floe length, maximum scattering takes place at its edges. When the floe is large, it is able to flex in response to the waves, causing scattering at the edges, but also the transmission of unattenuated energy beneath it (Kohout and Meylan 2008). As the floe becomes less than two or three times the size of the length of the wave, the scattering at its edges significantly lessens and the floe essentially moves along the contour of the wave. Thus, for very small floes wave energy attenuation is mainly a result of viscous dissipation as opposed to scattering. A field of pancake sea ice, for example, would not scatter waves of moderate length to any extent because of the short diameters of the pancakes (Squire 2018). Similarly, swells greater than 19 s were found to be slowly dissipated rather than uniformly scattered (Ardhuin et al. 2016), although the dissipative mechanisms are still unclear.

An example of the S_{ice} spectrum is shown in Figure 3.8, adapted from Masson and Leblond (1989). The floes in this work were modelled as small and cylindrical, and in this example, the floe size was set to 10 m and the peak frequency was 0.3 Hz, equivalent to a peak wavelength of

17 m. The most efficient scattering regime according to the authors is between a ka value of 1 and 4. Table 3.1 shows the ka values for varying frequencies and a floe size, a, of 10 m. From the table, the efficient scattering regime would fall roughly between frequencies 0.15 and 0.33 Hz. Therefore, most of the scattering would be taking place at the peak and at the forward face of the spectrum (just below the peak). At the high-frequency end, isotropic scattering lessens and backscattering increases, leading to less energy being extracted from the incident direction.

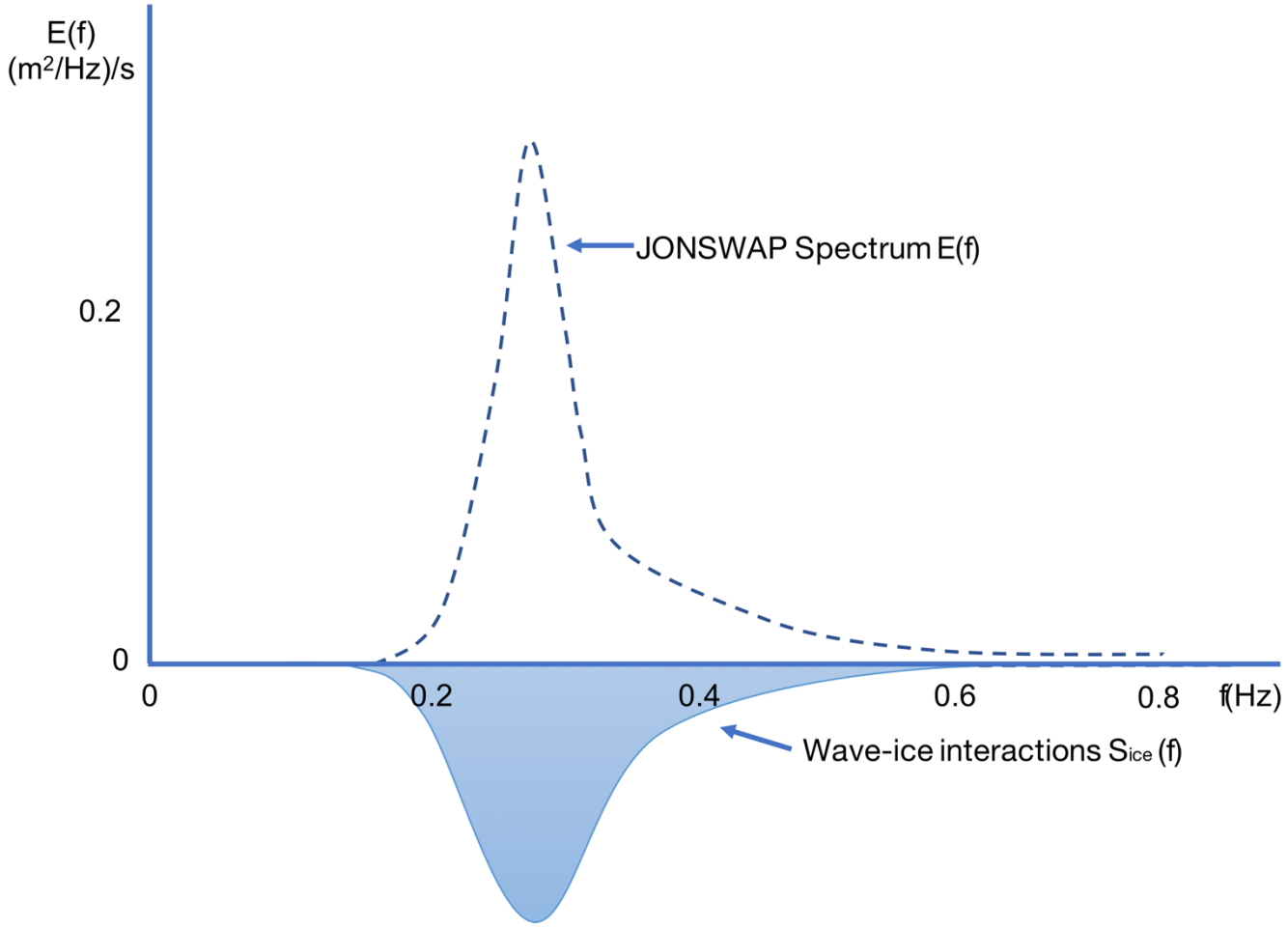

Figure 3.8: Schematic showing the sea ice field source term, S_{ice}, in relation to the total JONSWAP spectrum in deep water.

Frequency (f)	**Peak period (T_p)**	**Wavelength (λ)**	***ka***
0.10	10.00	156.00	0.4
0.15	6.67	69.33	0.9
0.16	6.25	60.94	1.0
0.20	5.00	39.00	1.6
0.25	4.00	24.96	2.5
0.30	3.33	17.33	3.6
0.31	3.23	16.23	3.9
0.32	3.13	15.23	4.1
0.33	3.03	14.33	4.4
0.35	2.86	12.73	4.9

Table 3.1: ka values for different peak frequencies, f, where ka is the ratio of floe size to wavelength.

Floe size is not only a key parameter when considered relative to wavelength, but it is also crucial in determining the density of the sea ice field. Perrie and Hu (1996) found that a reduction in floe size from 20 m to 15 m produced significantly higher attenuation rates, which suggests that more energy is lost when the floes are smaller and more compact. The authors also found that larger floe sizes were associated with wave growth at a significant distance in the sea ice field. While attenuation increased from the sea ice edge towards the sea ice pack, at some point, the increasing floe sizes also allowed the generation of wave energy. When the authors reversed the orientation of the sea ice field, with larger floes at the edge and increasing smaller floes towards the sea ice pack, they found that the total energy decreased with distance into the

sea ice field and, hence, with the decreasing floe diameters. The authors concluded that the floe diameters were more influential than the thickness of the sea ice floes.

Nonetheless, sea ice thickness has been identified by many studies as being a notable component in the wave attenuation process (Fox and Squire 1990), (Meylan and Squire 1994), (Kohout and Meylan 2008). Thinner floes have a lesser effect on wave scattering and allow for a larger transmission of the incident energy, while a thicker wave essentially blocks more transmission and increases scattering at the sea ice edge, leading to choppy seas at the front of the floe (Fox and Squire 1990). According to Boutin et al. (2018), thicker floes increases the wave energy and hence heights at the sea ice edge as well as increasing the directional spread of the spectrum that is transmitted to the sea ice. Since more wave energy is dampened and less transmitted by the thicker sea ice, there is less sea ice breakup by flexural motion, which in turn leads to greater attenuation, a feedback effect pointed out by Boutin et al. (2018). Meylan and Bennetts (2018) found, however, that the effect of thickness on scattering is only significant at low thicknesses, and becomes insignificant once a critical thickness was reached, a parameter dependent on the wave period.

Wave attenuation also increases with sea ice concentration as one would expect. In the numerical model of Perrie and Hu (1996), a steady increase in sea ice concentration from the edge to the continuous sea ice pack produced increasing wave attenuation with distance into the sea ice. It is important to note that there can be interdependence between the sea ice concentration and the sizes of the floes. Kohout and Meylan (2008) found that the attenuation coefficients produced by their scattering model (not considering dissipation) in a small-floe sea ice field were particularly sensitive to the concentration of the floes. Their model underestimated the attenuation of waves when the floes were small and the concentration was high. They concluded that scattering was not the dominant attenuation mechanism in these environments, but rather viscous losses from the bottom of the sea ice. Owing to the small size of the floes the

sea ice field could become more compact, resulting in less surging of the floes and hence less scattering. Kohout, Meylan, and Plew (2011) went on to improve upon the model by Kohout and Meylan (2008), including the viscous effects of sea ice bottom roughness, which improved the attenuation results in more compact sea ice fields. The PhD results of Masson (1987) also provided valuable insight into the modification of the energy balance as a result of scattering. When the waves are young, (consider the possible generation of new waves in an open water segment in the sea ice field), the spectrum is initially allowed to grow but is limited by the short fetch between floes. The interaction of these very short waves with the sea ice floes produces significant backscatter, keeping a large amount of energy the concentrated along the incident direction. Because of their inability to lengthen significantly, however, they quickly become steep and dissipation can occur. If they are given more fetch to develop and lengthen, the peak frequency lowers and the scattering takes on a larger directional spread. With time, isotropic scattering increases, causing a reduction of energy in the incident propagation direction (recall that the most efficient scattering takes place when the floe length and wavelength are of similar sizes, at which point the scattering becomes rapidly isotropic for short waves). The dissipation of energy as a result of the sea ice, S_{ice} , at this point, is a significant contributor to the overall energy balance and is roughly twice as much as S_{dis}. In addition, the input of wind energy, S_{in} , is a function of the amount of energy that the wave already possesses. Thus, when scattering is efficient, the energy in the main propagation direction is reduced, resulting in diminished energy transfer from the wind. The energy of the wave, therefore, decays even further.
The effect of wave-wave nonlinear interactions, S_{nl}, are also diminished as a result of scattering. Since the redistribution of energy in the spectrum by S_{nl} is dominant close to the peak (the region where the energy influx is the largest), the spread of energy as a result of scattering diminishes the peak energy and thus the strength of $S_{nl.}$ The overall effect of the partial sea ice, then, is to inhibit the shift of energy to longer waves (waves do not grow efficiently in length),

increase attenuation and reduce the input from the wind, leading to an overall inhibition of significant wave growth.

4. Study Region, Data & Methods

4.1 The Study Region

Twelve sub-surface moorings were deployed in the southern Beaufort Sea as a part of the ArcticNet Industry Partnership Program, which collected data over the course of a year, from summer 2009 to summer 2010. The data used in this study cover the months August to October 2009 for nine of the moorings mentioned. Seven moorings (A1, C, F, G, H, I and J), were located offshore and in the sea ice field during August, while two moorings (D and E) were further inshore at a depth of ~15 m and were in open water for the entirety of the month (Figure 4.1). The in-ice moorings were located in a cluster that extended 80 km, west to east, from the innermost mooring, F, to the outermost mooring, J. There was a distance of ~60 km from the southernmost sea ice mooring, C, to the northernmost moorings, G and H. C was located 110 km north of Inuvik. As a general location, the cluster of in-ice moorings was located between 70 and 71 °N and to the north of the Mackenzie River delta as shown in Figure 4.1 and will be the focus of this study. These moorings remained in the sea ice field for the entire month, with the two outermost moorings I and J just at the edge of the marginal sea ice by August 28. Measurements taken up to the August 27 will be therefore be referred to as 'in-ice' values.

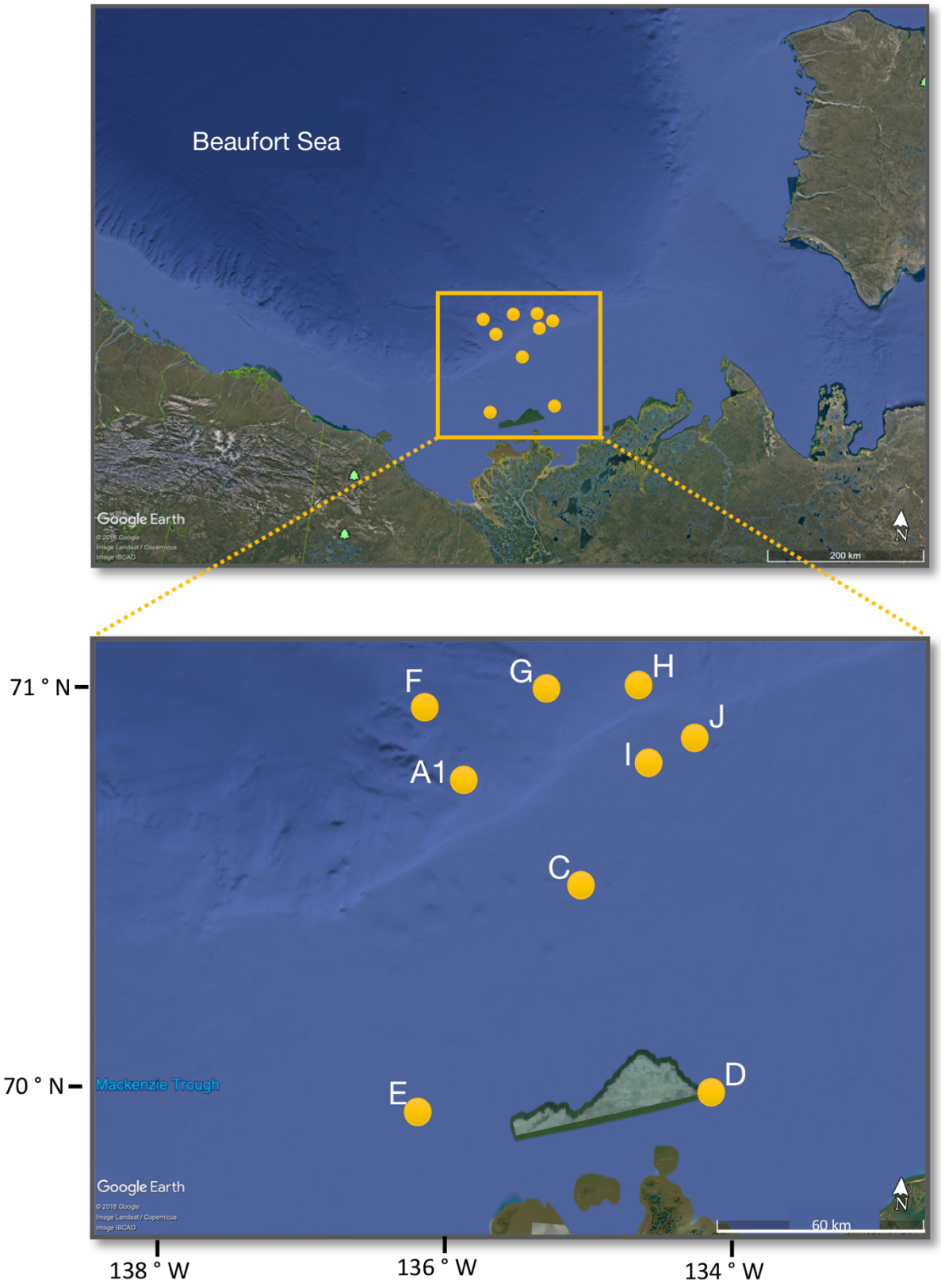

Figure 4.1: Study site in the Beaufort Sea. Yellow circles represent the 9 moorings deployed with sea ice profiling sonars.

4.1.1 August 2009 sea ice conditions

The sea ice pack in the southern Beaufort Sea in August 2009 was a combination of thick, first-year sea ice as well as old sea ice. The MIZ experienced consistent sea ice breakup and melt throughout the month, unlike the successive months where sea ice growth occurred. There were no especially powerful swells during the month and so the breakup was gradual but nonetheless very pronounced. This resulted in a progressively more dynamic sea ice environment throughout the month, as both floe sizes and overall concentration decreased. The MIZ region, with the in-ice mooring locations indicated by yellow circles, is shown in Figure 4.2. At the beginning of the month, the sea ice field consisted of large, arbitrarily shaped, old-sea ice floes reaching up to 25 km in size, clearly identifiable from visible satellite imagery. Figure 4.2a shows such conditions on August 4. In the second half of the month, the floes decreased noticeably in size and the sea ice field became a mixture of larger floes between 5 and 10 km and smaller floes that were tens to hundreds of meters (Figure 4.2b). By the end of the month and early September, most of the larger floes had melted and the MIZ consisted mainly of smaller floes, ~ 1km or less, organized into band-like features and individual floes unidentifiable from visible imagery (Figure 4.2c). For this study, the fact that the majority of floes were large, old sea ice floes is an important distinction to make, as opposed to the floes being predominantly new grease-sea ice or pancakes, for example. These sea ice types, which tend to be much smaller, dissipate waves in a different way, in that not much of the wave energy is actually scattered, but the energy is actually lost to other forms and so completely dissipated.

A.

B.

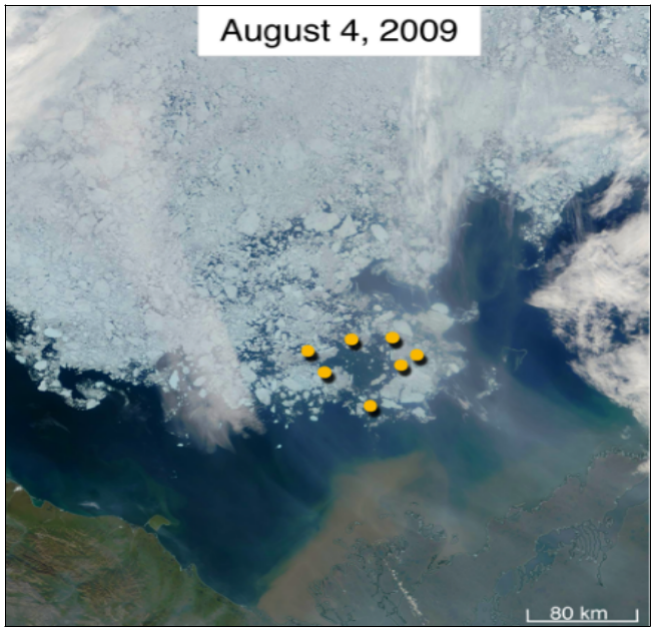

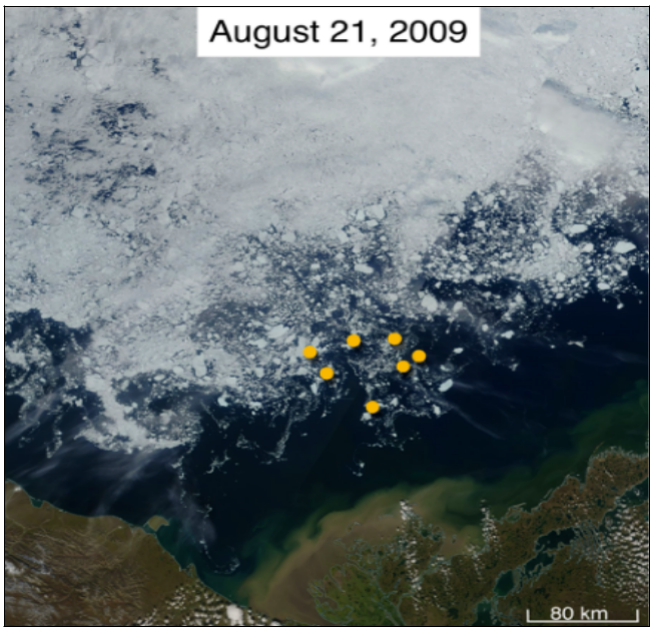

C.

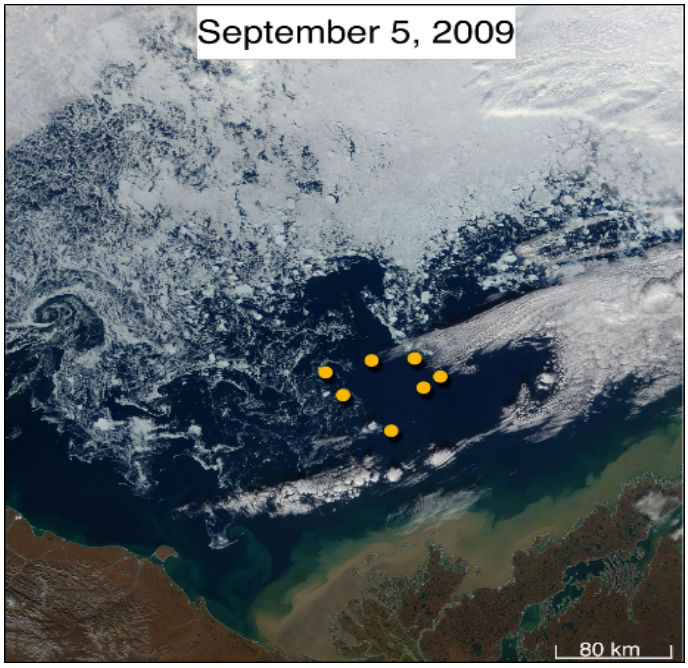

Figure 4.2: The MIZ on a) August 4, b) August 21 and c) September 5. Yellow circles indicate the position of the in-ice mooring locations.

Despite a relatively calm month, the MIZ was very dynamic throughout August. The sea ice concentrations from the CIS charts showed considerable changes in the daily sea ice conditions in response to wind and wave forcing. North of the Mackenzie Delta, the main sea ice pack of 90-100% concentration sea ice had retreated ~160 km to the north by the end of the month and was replaced by concentrations of 60% or less. The sea ice was eroded mainly from the eastern side of the pack, where the open water fetch was the longest. Because of the large scale of the domain as well as the dynamic environment, it is not always an easy task to define an 'sea ice edge'. A more fitting term in this context would be the marginal-sea ice boundary (MIB), which will be taken as the general line where there is a transition from sea ice floes to open water as inferred from optical imagery.

It is evident that sea ice degradation in August 2009 did not occur strictly at the sea ice edge in response to ocean waves at the MIZ. Leads also formed within the MIZ itself due to the dynamics of the sea ice under divergent wind stress or the upwelling of warm water in specific locations (Zhang et al. 2018). However, they tended to be predominant in areas of thinner sea ice (relative to the continuous sea ice pack) which typically is the case in the MIZ. Leads can be up to tens of kilometers long and kilometers wide (Wadhams 2014).

4.1.2 August wind conditions

The Beaufort Sea typically experiences monthly average wind speeds of 5-6 m/s in August (Stegall and Zhang 2012). Small, Atallah, and Gyakum (2011) studying the wind regimes over Tuktoyaktuk from 1971 to 2006, found that the median wind speeds were higher in the warmer months but the tendency towards higher wind speeds increased in the colder months. The months of August and September tended to be skewed towards higher wind speeds than in July but were less skewed towards these higher winds than October and November. The Beaufort

high which is present almost year-round over the Beaufort Sea is typically responsible for prevailing northeast winds, however, the high is usually at its weakest in August. As a result, north-easterly winds were also found to be at their minimum in August (Stegall and Zhang 2012). In fact, Small et al (2011) found that the frequency of northwesterly winds measured at Tuktoyaktuk in August was greater than north-easterly winds, and nearly all the winds that exceeded 10 m/s were also from the northwest. They suggested the strong northwesterly winds were associated with a region of anomalous low pressure to the northeast of Tuktoyaktuk and a high-pressure ridge over the Bering Sea and eastern Siberia. In this study, the wind speeds and directions were examined at 2 moorings: the northernmost mooring E, with position 69.85 °N, 136.17 °W and 72 km north from the coast of Ellice Island, as well as the southernmost mooring H, located at 71 °N, 134.7 °W and roughly 164 km north of the mainland. Mooring H had an average wind speed of 5.4 m/s in the month of August. The north-easterly winds were slightly more frequent than northwesterly winds (151 and 171 counts, respectively), however, both were significantly less than the frequency of southeasterly winds which had 264 counts (Figure 4.3). Unlike H, mooring E which was much closer to the coastline had a strong predominance of northwesterly winds compared to north-easterly winds, 290 and 124, respectively (Figure 4.3). This agrees with the results of Small et al who noted this dominance of northwesterly winds at the Beaufort coast. The frequency of southeasterly winds was also high for mooring E, with 237 counts. The average wind speed of 5.7 m/s was only slightly higher than at H.

A. B.

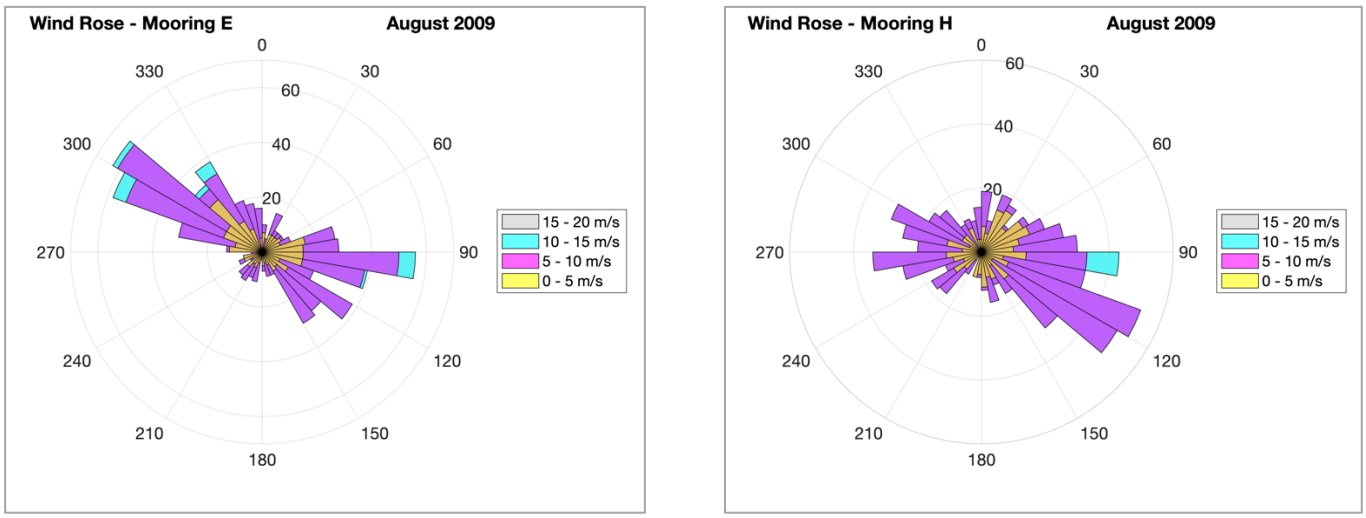

Figure 4.3: Wind rose for: (A) the southernmost mooring E and (B) the northernmost mooring H during August 2009. Wind data was obtained from the ERA5 reanalysis.

4.2 Data Collection

4.2.1 Wave data collection

In the absence of sea ice above the moorings, waves were measured using an Ice Profiling Sonar-5 (IPS-5). When used in wave-mode, the IPS was able to collect bursts of data at up to 2 Hz. The instrument sends out an acoustic pulse and measures the return travel time from the ocean surface. It then converts the time-of-travel measurements to a time series of acoustic ranges (the distance from the IPS to the interface between air and water). The significant wave heights (H_s) and the peak periods (T_p) were then computed from autospectra obtained using the Fast Fourier Transform (FFT) method. H_s was calculated as four times the square root of the area under the autospectral curve, which is the zeroth-moment of the wave spectra: $H_s = 4 \times \sqrt{m_0}$. T_p was calculated as the corresponding period where the autospectra was at its maximum.

At the inner shelf locations, sites E and D, wave measurements were taken using an Acoustic Doppler Range Profiler (ADCP). The ADCP was developed for measuring current velocities by

calculating the Doppler shift of acoustic echoes from water particles. Much like the IPS, however, it has provided a new way of measuring ocean waves. The ADCP sends out acoustic pulses at constant frequencies and the reflection of these altered frequency pulses from the water (or sea ice) particles back to the sensor enables the instrument to determine particle velocities as well as the return time series. In this way, it can measure the movement of the currents or sea ice as well as the distance to the ocean surface. Moorings E and D were equipped with a 150 kHz Workhorse QuarterMaster (WH QM) ADCP, which was mounted near the ocean floor and sent out pulses upward at a 20° angle (from vertical).

4.2.2 Reanalysis wind and wave data

To complement the data collected in field, wind and wave data from the latest product of the European Centre for Medium-Range Weather Forecasts' (ECMWF's) global reanalysis, ERA5, was used. ERA5 assimilates previous forecasts from the ECMWF's wave and atmospheric model and combines that information with observations at specific intervals, in such a way as to provide the best estimate of the atmosphere and ocean surface. The wave model computes the two-dimensional energy spectrum at each grid point, discretized into 24 directions and 30 frequencies. This gives a complete description of the wavefield at any point. The statistical parameters from the reanalysis used in this study are computed as follows:

- The significant wave height (H_s) - As described above this is computed as: $H_s = 4\sqrt{m_0}$
- The peak period (T_p)- This is the reciprocal of the peak frequency. It is obtained from a parabolic fit around the discretized maximum of two-dimensional wave spectrum.
- The mean wave direction (θ)- This is computed as $\theta = atan(SF/CF)$, where SF is the integral of $sin\theta\ E(f,\theta)$ and CF is the integral of $cos\theta\ E(f,\theta)$, over f and θ.

The wind data is given as the horizontal, u, and vertical, v, wind components at 10 m above sea level. The spatial resolution for the wind data is 0.25°, while all ocean parameters have a 0.5° resolution. The temporal resolutions for both wind and wave data are hourly.

4.2.3 Ice data

Information regarding the sea ice concentration was obtained primarily from the Canadian Service Ice (CIS) charts. These are daily, operational sea ice charts created by means of the manual analysis of in situ, satellite, and aerial reconnaissance data over the Canadian Arctic. The concentrations are given in intervals ranging from 10-30% sea ice concentration to 90-100% sea ice concentration. The concentration charts are also supplemented by sea ice-type charts which describe the maturity of the sea ice, for example, old sea ice, multiyear sea ice, new sea ice. For a better picture of the sea ice conditions, the MODIS true color corrected reflectance images visualized in NASA Worldview was used when feasible.

5. Results & Analysis

The graph in Figure 5.1 shows the significant wave height (H_s) recorded throughout August 2009 for all mooring locations in the MIZ. It is evident that the majority of waves do not exceed 0.5 m throughout the month. Towards the end of the month, there is a marked increase in wave heights, particularly at locations close to the MIB. The cumulative distribution function (CDF) in Figure 5.2 shows that ~90% of waves measured were less than 1 m, and ~80% were less than 0.5 m. After August 27, the wave heights showed similarities to open ocean wave heights at the outermost moorings, as the ice floes at those locations were largely eroded by the end of the next day. Low wave heights are expected in sea ice cover, but the underlying cause of low waves is usually attributed to attenuation of longer waves propagating into the MIZ. In this study, there is an argument for local wave growth in the sea ice as the primary source of the energy observed in this dataset. This is not to say, however, that the selective attenuation of shorter wavelength waves relative to longer wavelength did not occur. It is hypothesized that attenuation was dominated by two processes:

1. The scattering of locally generated waves by sea ice similar in size to the waves. In this case, the very short waves were preferentially scattered and their energy reduced, resulting in a decrease in H_s and an increase in T_p. Since this type of attenuation has been well mentioned in literature, it will be referred to hereafter as the classic attenuation mechanism.
2. The scattering of locally generated waves by large floes, significantly larger than the wavelengths. In this case, the 'longer' of these short waves were scattered more efficiently, leading to a decline in both T_p and H_s.

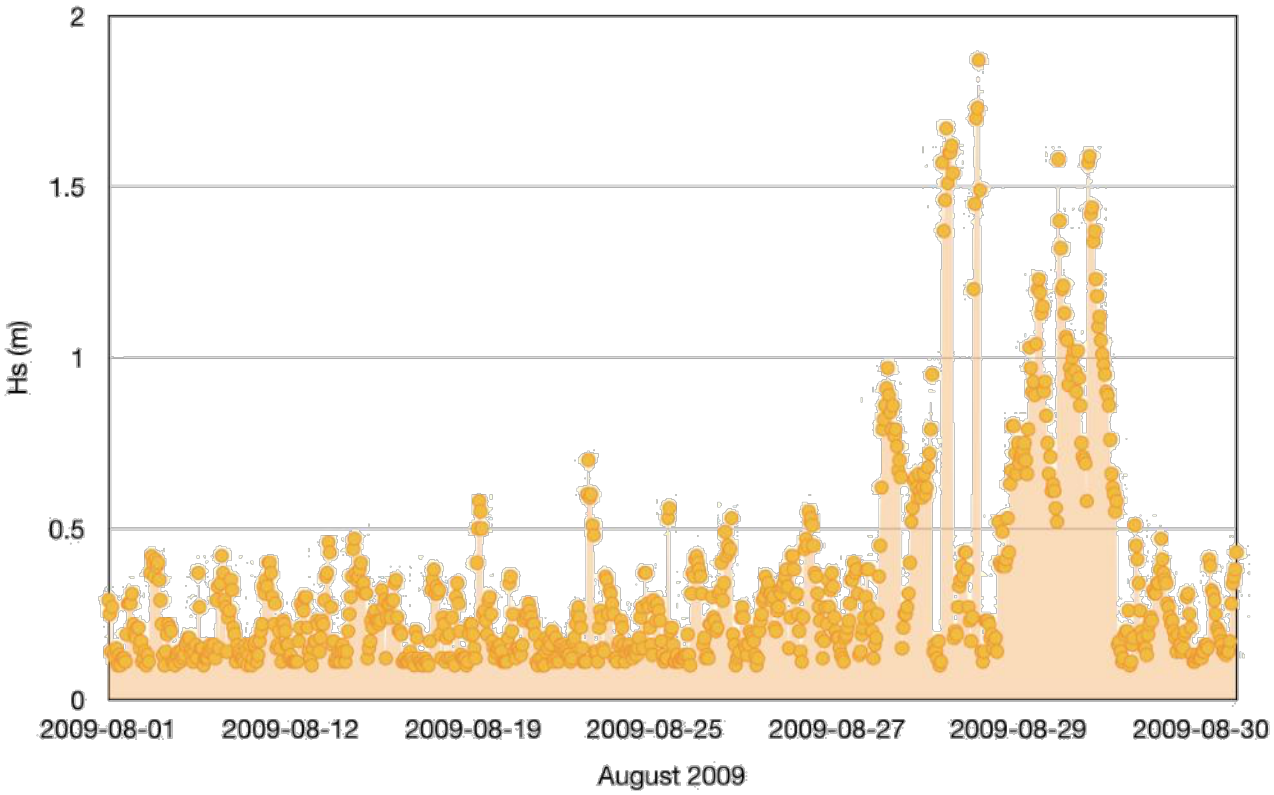

Figure 5.1: Significant wave heights (H_s) throughout August 2009.

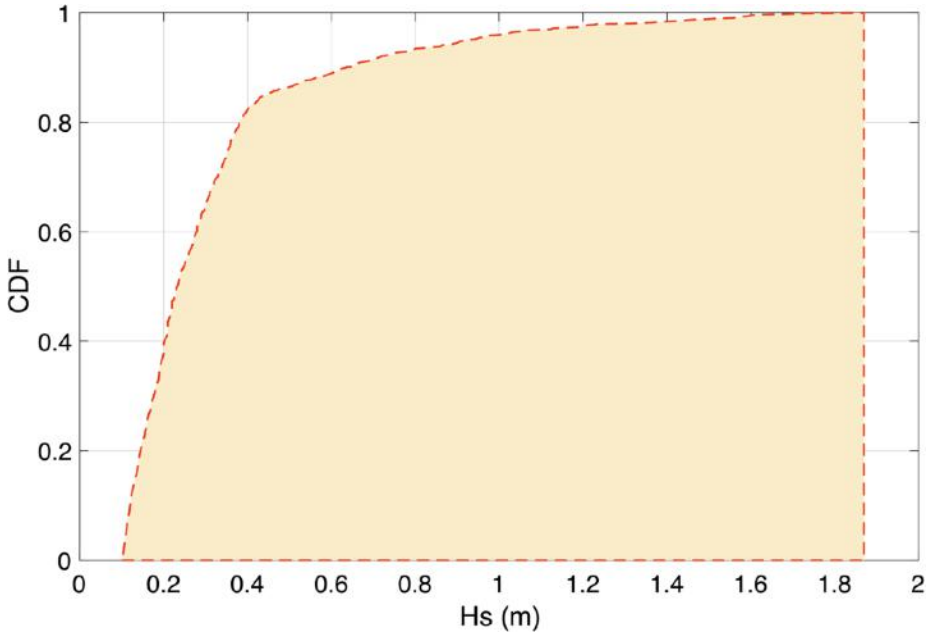

Figure 5.2: Cumulative distributive function of H_s throughout August 2009. 80% of the waves measured were under 0.5 m.

The H_s measurements, on their own, did not provide a conclusive picture of waves developing locally. This is as a result of the structure and dynamics of the sea ice field at the point of measurement; the sea ice field at any point is constantly changing and even when the sea ice is fairly immobile, the fetch is so small that wave growth occurs only over a short period of time. These short-wave growth periods can be identified throughout the month, occurring typically over 2-4 hours. As such, there is rarely evidence of steady growth from calm conditions in the H_s data alone, with increases often appearing as 'jumps' in heights due to the presence, or the lack thereof, of sea ice over a mooring. As a result, it is necessary to examine the wave field as a composite of factors in addition to wave heights: the wind and the sea ice which are the chief regulators of the wave development, and the peak periods which can give us further information on the wave field, as described in the next section.

5.1 Peak Periods

Because the process of growth or attenuation in sea ice is so dependent on the wave height (H_s)-peak period (T_p) relationship, we begin by examining the T_p records. Overall, the in-ice T_p values were relatively low, with the majority remaining under 4 seconds as shown by the density distribution graph in Figure 5.3a. This distribution of very short waves does not give the impression that peak periods were increasing due to attenuation by ice. For comparison, T_p recorded at the open water moorings to the south of the in-ice moorings, D and E, were also quite low but the frequency of T_p exceeding 4 s was significantly higher. Note, however, that these two moorings were much closer to land, hence, southerly and easterly fetches would also be much shorter, resulting in lower T_p values (land is 72 km south and 163 km east of E; 38 km south and 100 km east of D). The effect of non-linear interactions in open water is to transfer energy from shorter to longer waves as the sea develops. This would have happened to the waves at D and E. Essentially, a similar behaviour is expected for wave attenuation in ice, that is, the

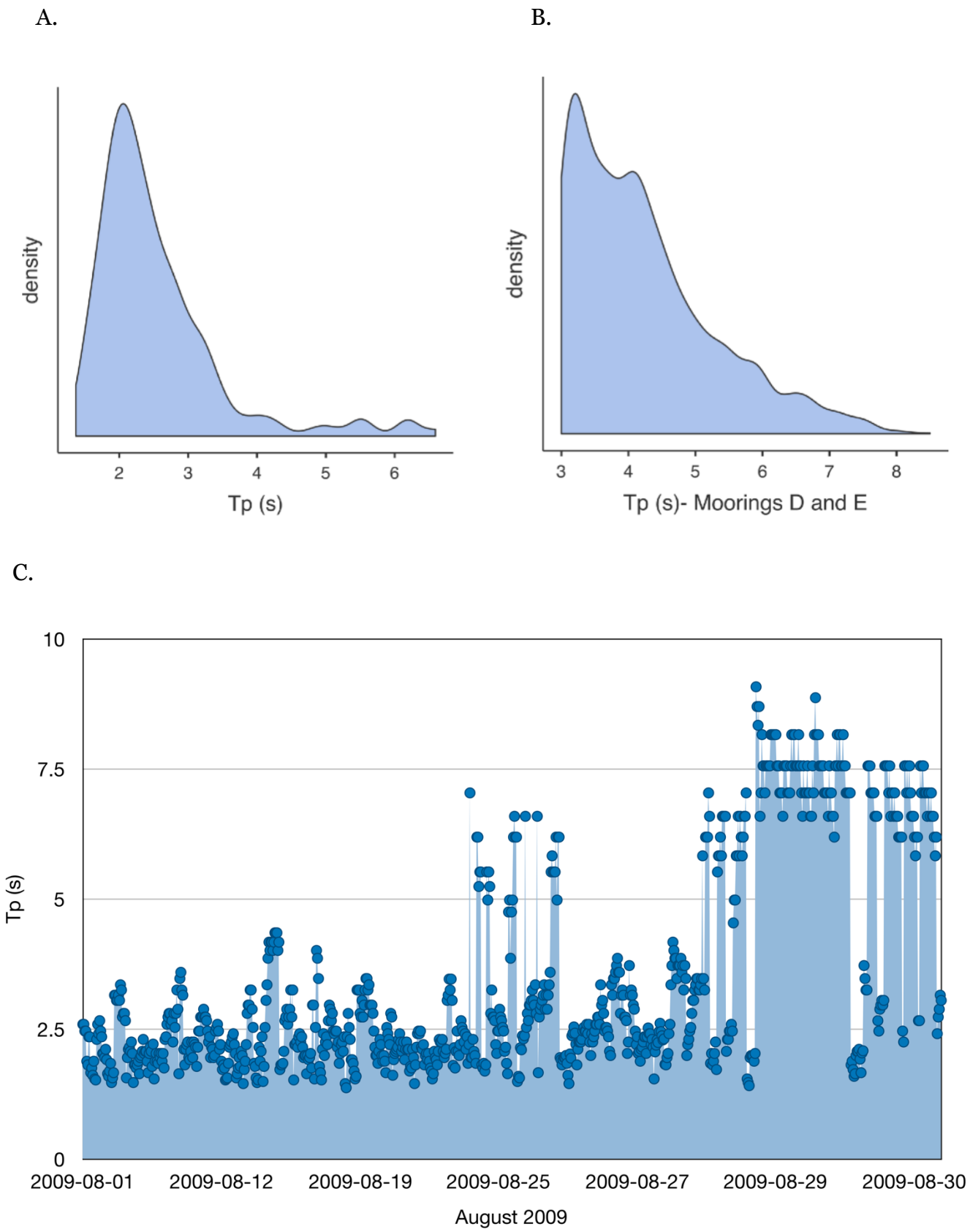

Figure 5.3: A) shows the density distribution of the in-ice peak period (T_p) values during August 2009. B) shows the density distribution of T_p values from moorings E and D located in open water to the south. C) shows all T_p values throughout August 2009.

energy being shifted to longer wavelengths, albeit the mechanisms behind the shift in each case is different. Thus, if this behaviour was dominant in the MIZ, there would at least have been a higher frequency of values exceeding 4s. After August 27 the influence of open water waves is evident as the T_p values show a marked increase (Figure 5.3c).

A closer look at the relationship between H_s (white line graph) and T_p (dark blue area graph) for the different in-ice moorings throughout August is shown in Figure 5.4a-f. The H_s measurements were filtered in order to remove any potential noise, so that the lowest value was 0.1 m. Spikes in T_p occurring only for a single measurement were also removed to eliminate any potential instrument errors. Owing to the varying ice conditions at a specific mooring point, the hourly wave data is not continuous; some days will have very few wave measurements at a specific mooring location, or none at all, and hence the inconsistency of the dates on the x-axis. The solid, black vertical lines in the graphs represent the beginning of the wave record for key days: August 24 and August 27-30. The black dashed boxes with numbers represent specific wave events referred to. It is easy to see, in all the graphs, the sparseness of wave events occurring before August 24, relative to the last seven days of the month. Nonetheless, two types of T_p behaviour is evident:

1. T_p is low and *generally* coherent with H_s, that is, they have a similar pattern of increase or decrease. Note that a change in one variable will not always correspond with a change in the other at exactly the same time. Also, there can be cases of the classic attenuation effect, but on such a short scale (spatially and temporally) that there is no distinct increase in T_p. T_p therefore, remains low and are likely to be associated with locally developed waves. This coherent behaviour is depicted by the blue shading in Figure 5.4a-f.
2. T_p is notably higher with variable H_s responses. This behaviour is depicted by the green shading in Figure 5.4a-f. The increase in T_p suggests the influence of open water waves, either being attenuated by the ice (classic attenuation) or uninhibited by ice.

This section will look at examples of coherent behaviour, as well as examples where T_p shows a distinct increase. The moorings can be grouped into three categories: moorings J, I and H being the outer moorings, mooring G the intermediary mooring, and moorings A1 and F the inner moorings.

Coherency

The blue shading in Figure 5.4a-f represents a general coherency between T_p and H_s. This was the dominant behavior at all mooring locations throughout the month. This indicates that throughout much of the month, short fetches between large floes regulated the growth of local waves. It is clear that the positions (not necessarily the distance) of the different moorings in the sea ice field affected the length of this coherent pattern before marked increases in T_p were able to occur. For example mooring A1 (Figure 5.4e), which was quite far in the ice cover (~66 km west of J), but closer to the MIB than F (Figure 5.4f), had no higher than average T_p events throughout the entire month. Mooring F, on the other hand, experienced some of the highest in-ice T_p values of all the moorings once the ice field had eroded significantly on August 28-29. The difference was simply that the ice field throughout the month was arranged in such a way that non-local waves could not reach mooring A1, while being able to reach mooring F. For the remaining moorings, however (Figure 5.4a-d), the ice configuration corresponded with distance in the sea ice field, such that the moorings further in the partial sea ice, such as moorings H and G, had a longer period of undisturbed coherency, while moorings closer to the MIB such as moorings J and I, had a shorter period of undisturbed coherency (or greater occurrences of marked T_p increases).

A longer coherent pattern indicates that there was a longer period where sufficiently large, high concentration floes were dominant, allowing this location to be more resistant to open water waves. Earlier duration high T_p events indicate that the ice field was becoming less

concentrated and floes were becoming smaller, at an earlier date. The duration of these high T_p events also indicate the extent to which the ice field was becoming more open.

The classic attenuation mechanism

A large number of the wave events in the green shaded region at mooring J (Figure 5.4a) experienced the classic attenuation of open water waves propagating into the sea ice field. For example, at the start of August 24, mooring J was only around 4 km to the west of the low concentration ice field. Moderate easterly winds of around 8-8.5 m/s gradually pushed ice to the west, allowing the mooring location to become closer to the open water boundary. Local waves were recorded up until 20:00 UTC where T_p jumped notably (Figure 5.4a, at the start of wave event 1), indicating that the sea ice to the east of the mooring was eroded enough to allow open water waves to move into the area. Even so, there was enough sufficiently small sea ice to attenuate the open water waves, causing an increase in T_p while significantly lowering their H_s. Waves with T_p values of around 5-5.5 seconds and H_s values of around 0.15 to 0.3 meters were recorded at mooring J (Figure 5.5a, wave event 1). The data for the same hours at mooring I (Figure 5.4b, wave event 1), to the west of J, shows further decreases in H_s (0.14-0.16 meters) and increases in T_p (5.2-6.2 seconds). Reanalysis T_p data shows open water T_p values to the east of the moorings being around 4.3-4.5, while open water H_s values being around 0.8-0.9 meters. Although the change in T_p from open water to partial ice cover was not especially drastic, the T_p values stand out in the in-ice data as being notably higher than typical in-ice values, making it easy to pinpoint possible instances of the classic attenuation effect. In-ice H_s values, on the other hand, are likely to already be low, and thus identifying decreases caused by the classic attenuation effect presents a greater challenge. Another example of the classic attenuation effect

can be seen during August 29-30, particularly at moorings J and I (Figure 5.4a-b, wave event 2). The storm on August 28 had caused the ice field to the east of the moorings to erode significantly, and open water waves were reaching moorings J and I with T_p of around 6-7 seconds by the end of August 28. During the early hours of August 29, the winds steadily decreased as the storm subsided, prompting the waves to decrease gradually in height and length as well. The wind direction then began to shift from easterly to north-westerly, but measurements at moorings J and I still reflected the open water waves, indicating that the storm generated waves had become swell and were still propagating westward despite the changing wind direction. The north-westerly wind gradually began to increase and is likely to have pushed small ice floes back to the east, past moorings I and J, allowing for greater attenuation of the incoming swell waves. Thus, H_s continued to decrease, while T_p maintained slightly higher values than the open water values of 6-7 seconds obtained from Reanalysis data (Figure 5.4a-b, wave event 2). As the wind had died down in the direction of swell propagation, the increase in T_p was limited and also, the moorings were quite close to the open water boundary, limiting the energy transfer process to longer waves (peak periods increase with distance in sea ice field). The sharp drop in T_p at the end of August 30 (Figure 5.4a-b, purple arrow) indicates the dying out of the swell for the August 28 storm, which was validated by reanalysis data.

Even mooring F, tucked away deep in the ice field, seemed to experience the influence of the open water swells from the August 28 storm, unlike mooring A1 (Figure 5.4f). Owing to the position of the ice field under wind forcing, the mooring location actually had less concentrated ice to the east than at mooring A1 on August 29. As a result, for a few hours on August 29, waves with the highest T_p values of the dataset were recorded along with very low H_s (Figure 5.4f, green shaded region). At this time the wind direction was north-westerly and low, and therefore was unlikely to produce such long period waves, eliminating the possibility of locally grown

waves. Thus, it is possible that the swells from the August 28 storm, had propagated through the low concentration ice field to arrive at F, ~ 80 km east of J (which was practically at the MIB). With such a long distance, the waves were almost completely attenuated with T_p values reaching 9 seconds.

A.

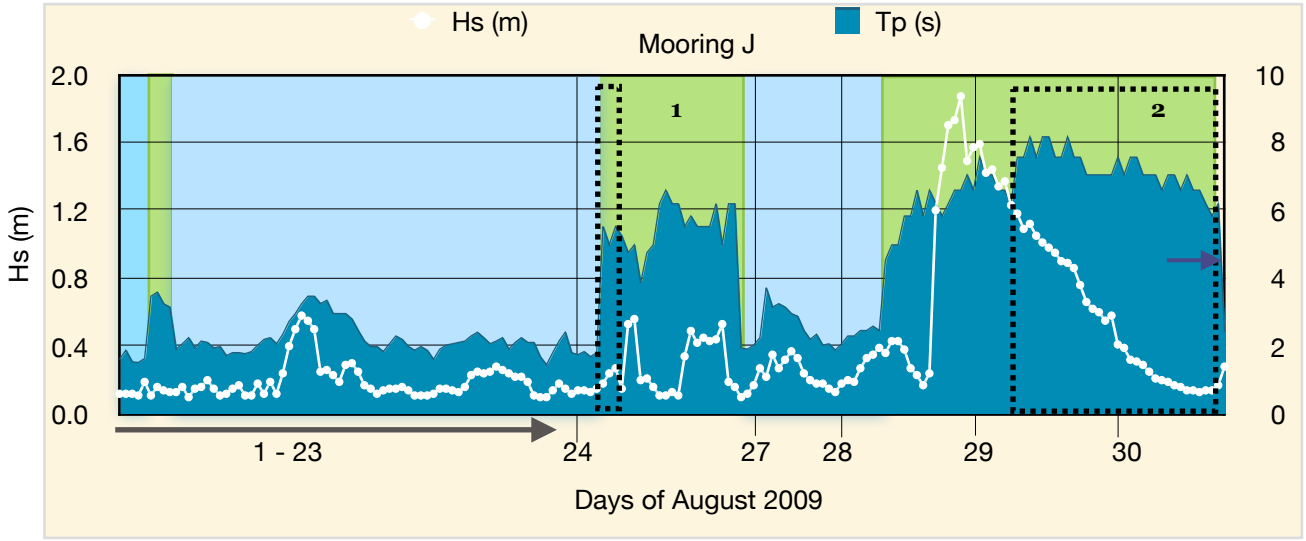

B.

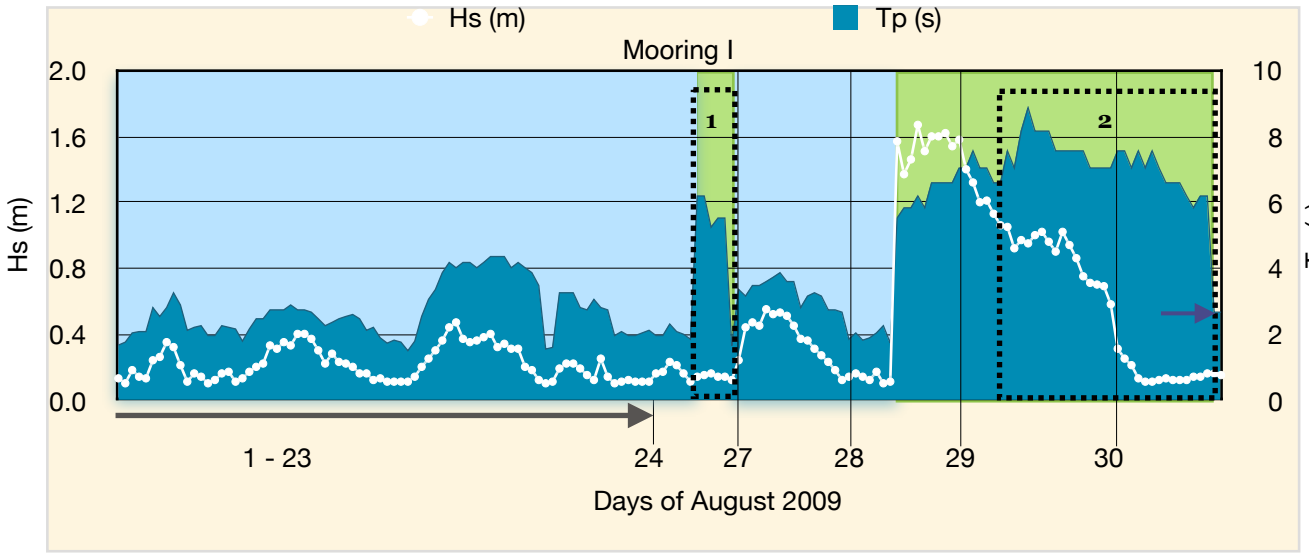

C.

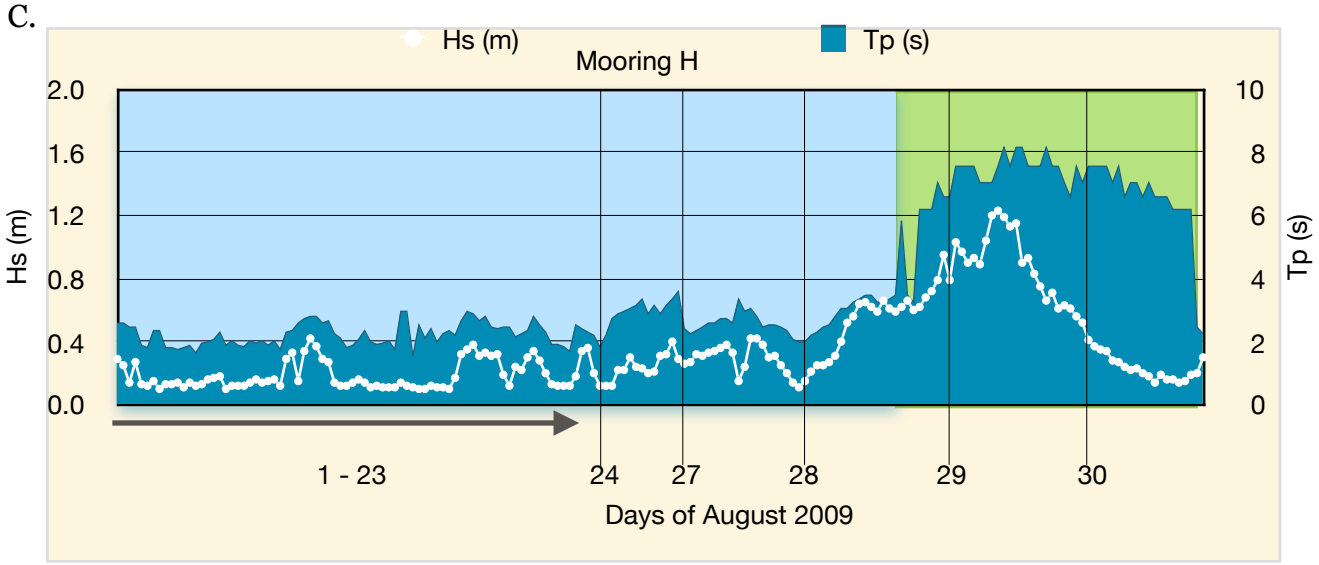
Hs (m)
Tp (s)
Mooring H
2.0
1.6
1.2
0.8
0.4
0.0
10
8
6
4
2
0
Hs (m)
Tp (s)
1 - 23
24
27
28
29
30
Days of August 2009

D.

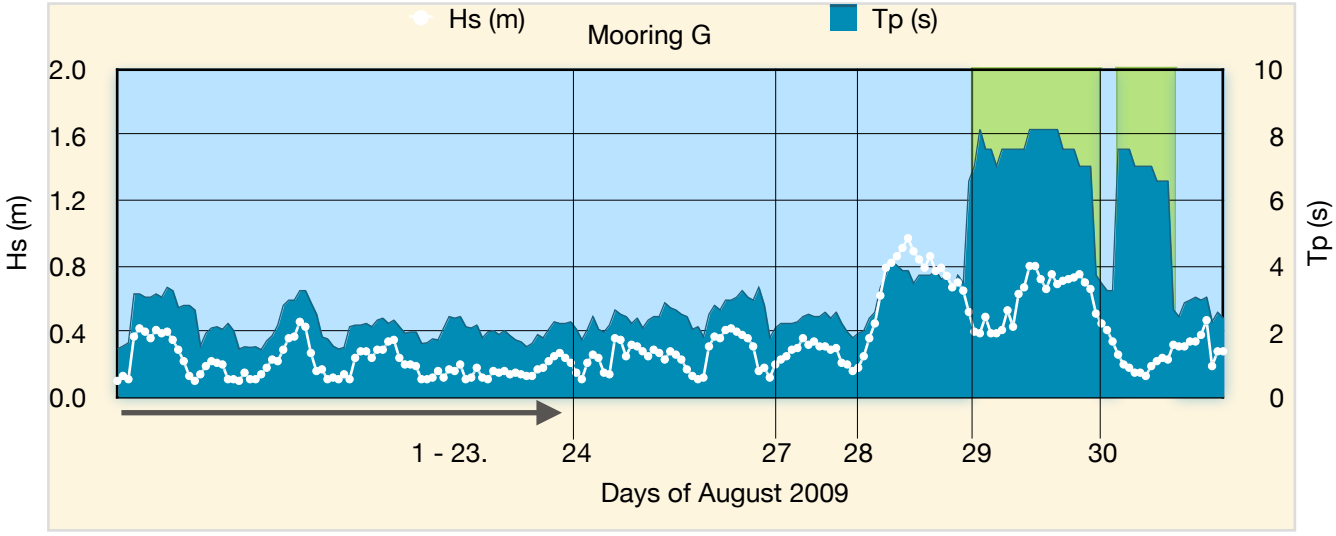
Hs (m)
Tp (s)
Mooring G
2.0
1.6
1.2
0.8
0.4
0.0
10
8
6
4
2
0
Hs (m)
Tp (s)
1 - 23.
24
27
28
29
30
Days of August 2009

E.

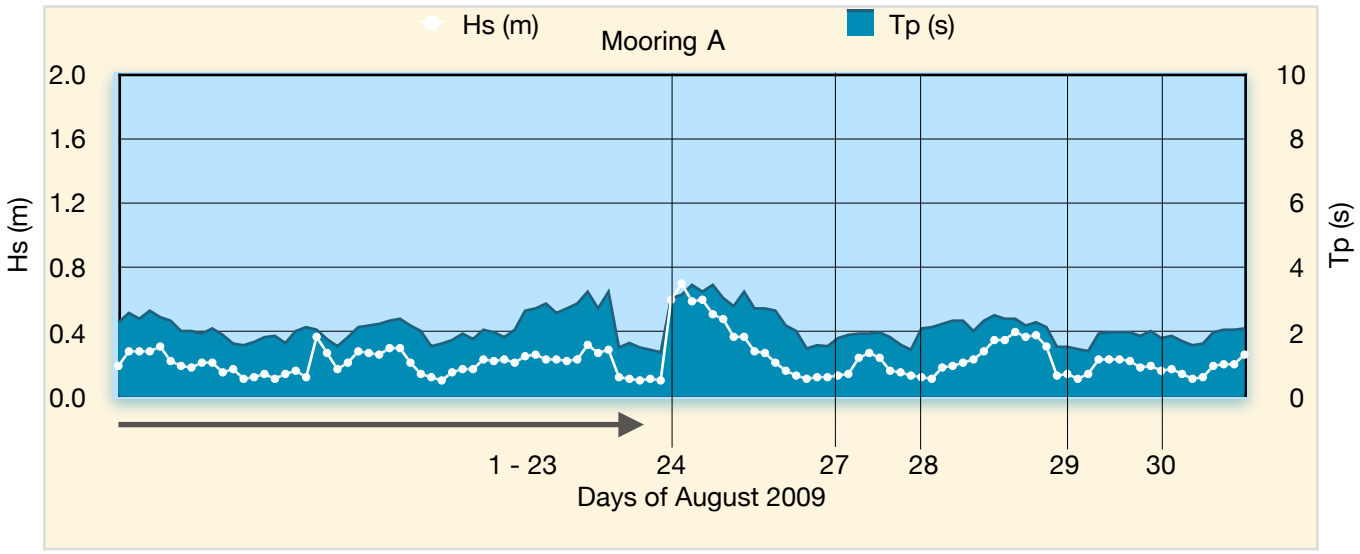

F.

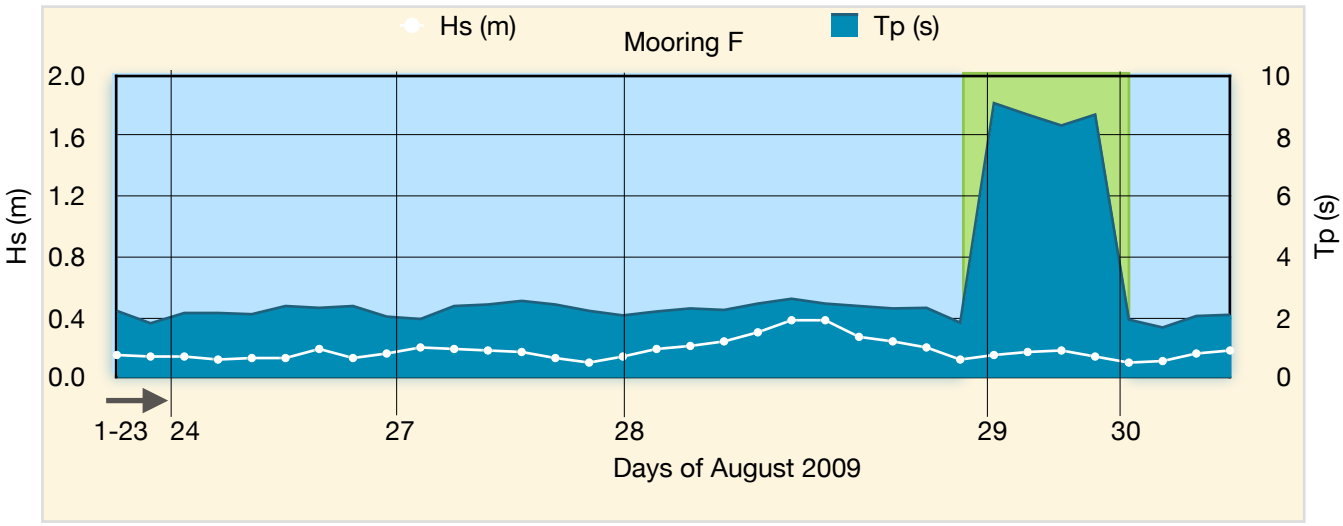

Figure 5.4: A-F) shows the relationship between H_s and T_p for the different moorings J, I, H, G, A1 and F, respectively during August 2009 (from outer to inner moorings). H_s is represented by the dark blue area plot, while the white line plot represents H_s. The blue shading shows the period of time when T_p was low and generally coherent with H_s, indicating that these waves were locally developed waves. The green shading shows notable increases in T_p as a result of the classic attenuation effect, which tended to start occurring earlier at the outer moorings and later at moorings further in the ice. Distance is not necessarily the controlling factor, however, and more so the structure of the ice field as melting occurs, as seen at mooring F, the furthest in the sea ice field, where the classic attenuation effect occurred while not occurring at all at mooring A.

For most of the month of August, then, local wave generation dominated, with coherent growth/decay patterns also dominating. Figure 5.5 shows a non-parametric regression of H_s and T_p. The regression is smoothed using the LOWESS method to obtain a more visible functional relationship between the two variables. There is a strong positive relationship between the majority of H_s and T_p in-ice records, and this positive relationship is associated with lower values of both variables (H_s less than 0.5 meters and T_p values less than 5 seconds). This corresponds with local growth and decay between large floes, where fetch limited conditions hinder significant growth. Thus, a decrease (increase) in one variable, tended to be associated with a decrease (increase) in the other more often than not. As T_p gets larger, however, the relationship becomes more spread out and there is less correlation (or coherency) between the two variables, which is associated with the classic attenuation effect.

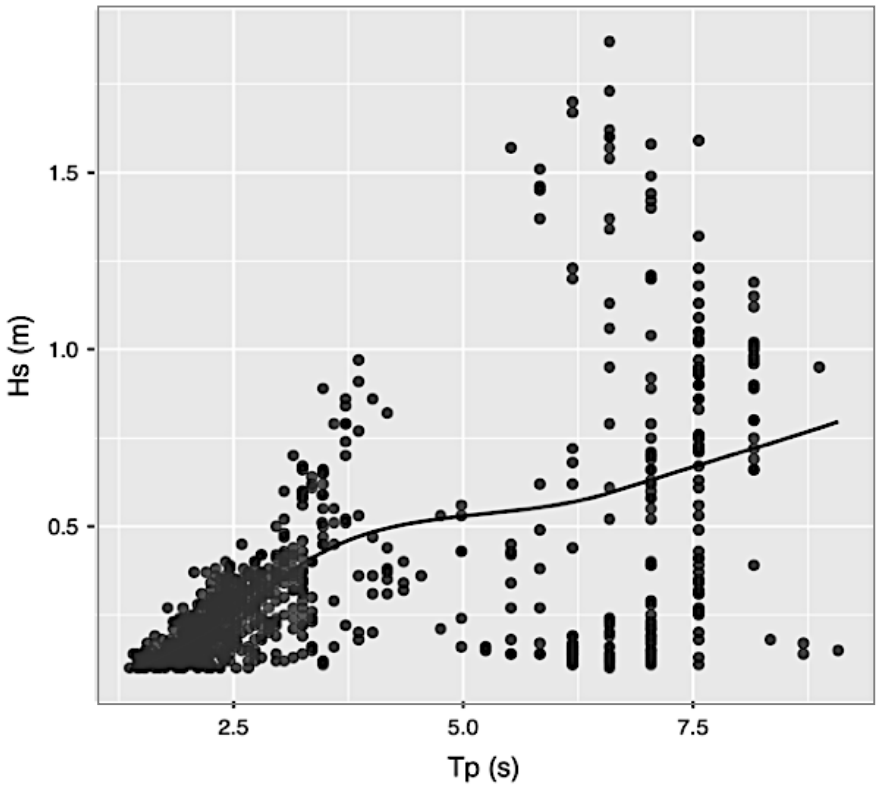

Figure 5.5: Scatterplot showing the overall positive correlation between H_s and T_p for August 2009. A stronger correlation is associated with lower values of H_s and T_p and local wave evolution. A weaker correlation exists as T_p values get larger indicating the classic attenuation mechanism.

5.2 Wind Speed and Direction

It has been well established that the frequency and intensity of storms in the Beaufort Sea in August tend to be lower in comparison to September and October. The average wind speed for the month from ERA5 reanalysis data at mooring A1 was 5.4 m/s. To what extent, however, does the strength of the wind affect the wave energy observed in areas with partial sea ice coverage? In Figure 5.6, H_s against wind speed over the in-ice IPS locations are shown. The graph shows that wind speeds (light orange) exceeded 6 m/s throughout a significant portion of the month. Wave response (bright orange) to moderate or strong winds, however, is seen only towards the end of the month. Furthermore, the response to high winds was only seen at the outermost moorings where the floes had become smaller and less concentrated.

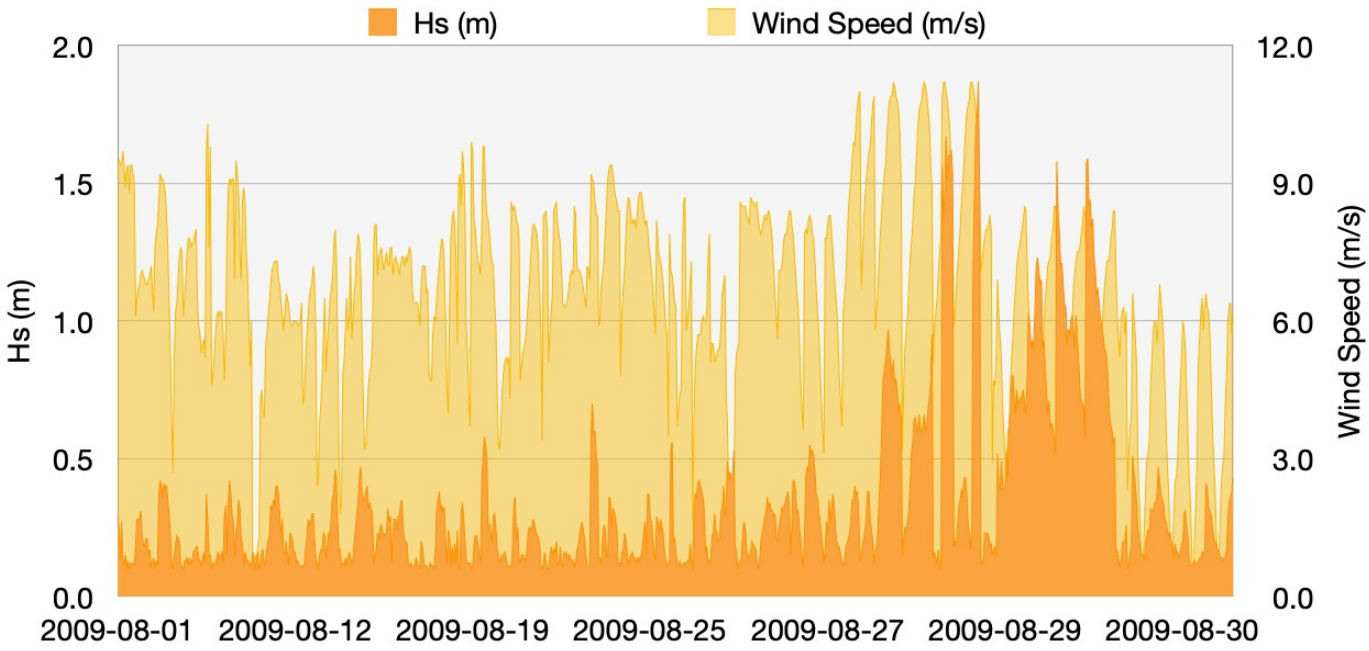

Figure 5.6: Significant wave heights (H_s) from all in-ice moorings represented by the area plot in bright orange overlaid on an area plot of wind speed (light orange) during August 2009.

The maximum H_s achieved at F, the innermost mooring, was ~0.4 m under 10 m/s winds, while this same H_s was reached under winds of 5 m/s at mooring G, where the ice concentration was lower. This indicates that at a fixed point, the wind speed on its own cannot directly suggest the wave height in the sea ice field. In Figure 5.7, all in-ice H_s values (orange diamonds) are plotted against increasing wind speeds. The figure shows that there is very little relationship between wind speed and the in-ice H_s, if the dataset is considered in its entirety. That is, a 9 m/s wind event was associated with waves that were as low as those recorded during a 2 m/s wind event. It is clear to see, however, that the highest H_s occurrences tended to be more towards the higher winds (although many low waves *also* occurred at high winds). The average and maximum H_s values (blue circles and red diamonds, respectively) calculated for each 1 m/s wind speed interval, indicate that there is some positive correlation between wind speed and potential wave growth when wind speeds exceeded 6 m/s. Thus, it is feasible to say that moderate to strong winds will likely (though not necessarily) produce higher maximum and average waves throughout the month than lower wind speeds.

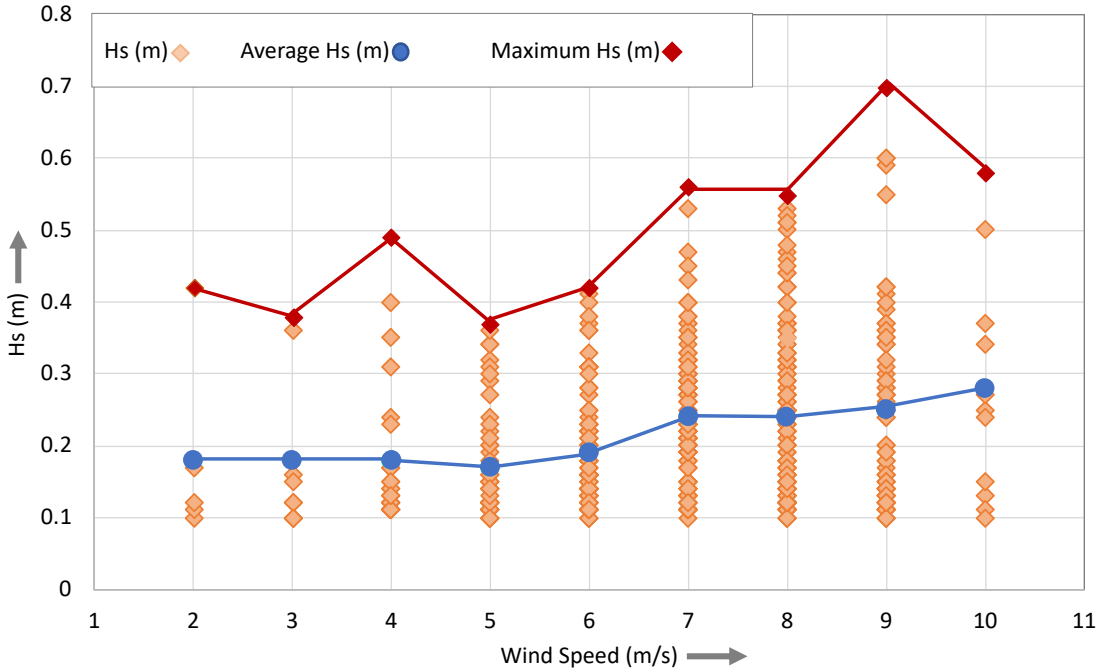

Figure 5.7: Average H_s (blue circles), maximum H_s (red diamonds) and all H_s (orange diamonds) for all mooring locations against increasing wind speeds. For wind speeds > 6 m/s average and max H_s values are likely to increase with wind speeds.

Prior to August 27, H_s values were all under 0.6 m. The dynamic sea ice field made measurements of steady increases in H_s for a useful amount of time essentially impossible. Figure 5.8 illustrates an example from August 26th, where H_s (blue line) increased over three hours, 12:00 - 14:00 UTC. It then began to decline despite the steady and then increasing wind speeds, depicted by the yellow line. A similar duration of growth was found in all the cases where the waves were at least 0.3 m, either as a result of the dissipation by sea ice (short fetch) or by decreasing wind speeds before encountering sea ice. Estimates of open water fetch from satellite data for these cases (for those with minimal cloudiness) were ~ 5- 20 km. For this fetch range and wind speeds 6-9 m/s, empirical wave equations produced comparable wave height estimates (0.3-0.6 m). An example of the fetch estimation from satellite imagery is shown in Figure 5.9.

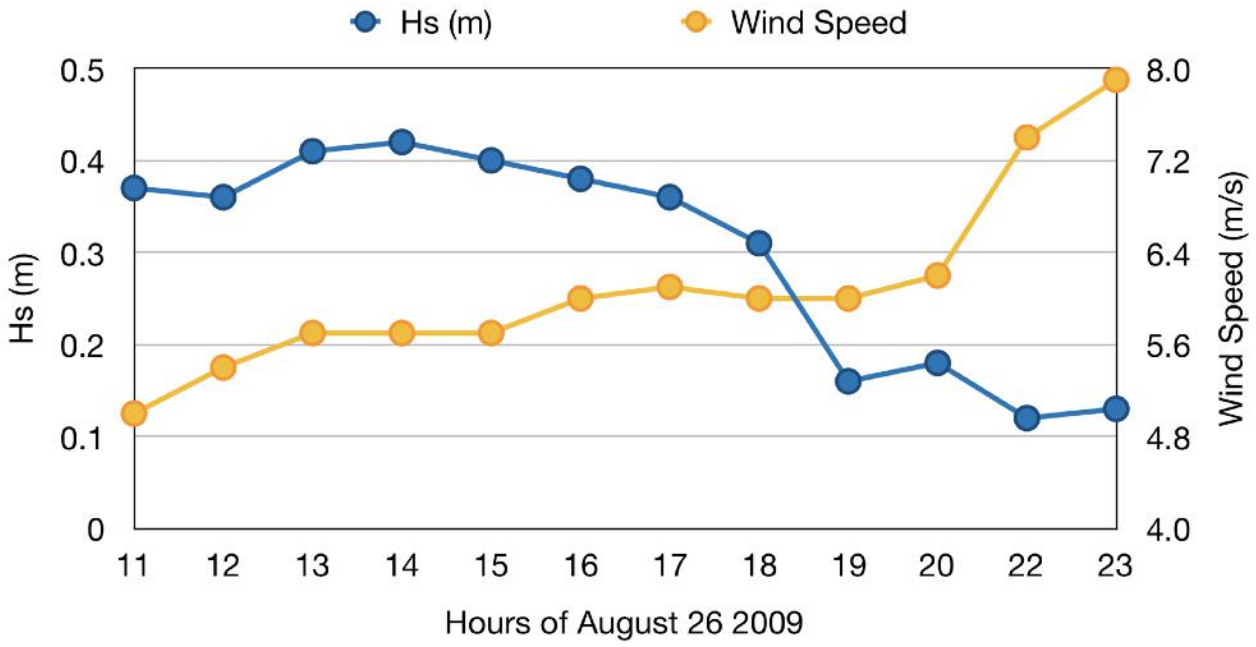

Figure 5.8: Evolution of a wave event under increasing wind conditions. H_s (blue line) shows a short increase over three hours (12-14), after which it begins to decrease despite increasing wind speeds (yellow line).

A. B.

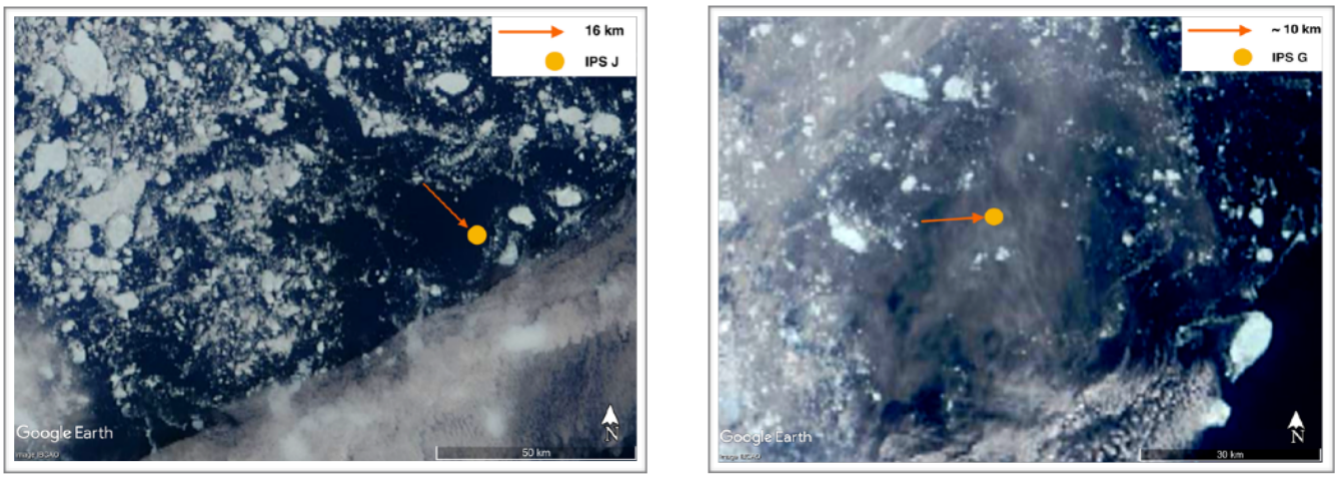

Figure 5.9: Example of fetch estimation form satellite imagery on two separate days, A) August 19 and B) August 24. The yellow circle represents the mooring position and the orange arrow represents the distance and direction of wave propagation towards the mooring.

While the wind speed on its own does not directly suggest wave growth in the sea ice field, the wind direction can reveal key differences in waves formed under on-sea ice (blowing towards the sea ice field) or off-ice winds. Since the large open water fetches are located to the east and south of the MIZ, there is the potential for more energetic waves to penetrate the sea ice field from these directions, as well as more energetic locally generated short waves. In Figure 5.10 and 5.11, the graphs illustrate the density of varying H_s and T_p in sea ice (up to the 27th), respectively, for each of the main wind directions. For all wind directions, H_s measurements were in a similar range of values and H_s in easterly and southerly wind conditions were not preferentially higher. In fact, there were fewer waves exceeding 0.2 m during easterly winds than westerly winds. Similarly, the differences in T_p between northerly and southerly winds were very small, and the same for easterly and westerly winds, indicating no preferential influx of longer waves from the east and south. Overall, there were no particularly long waves measured in the MIZ, which points to local wave growth being the main source of energy in the sea ice.

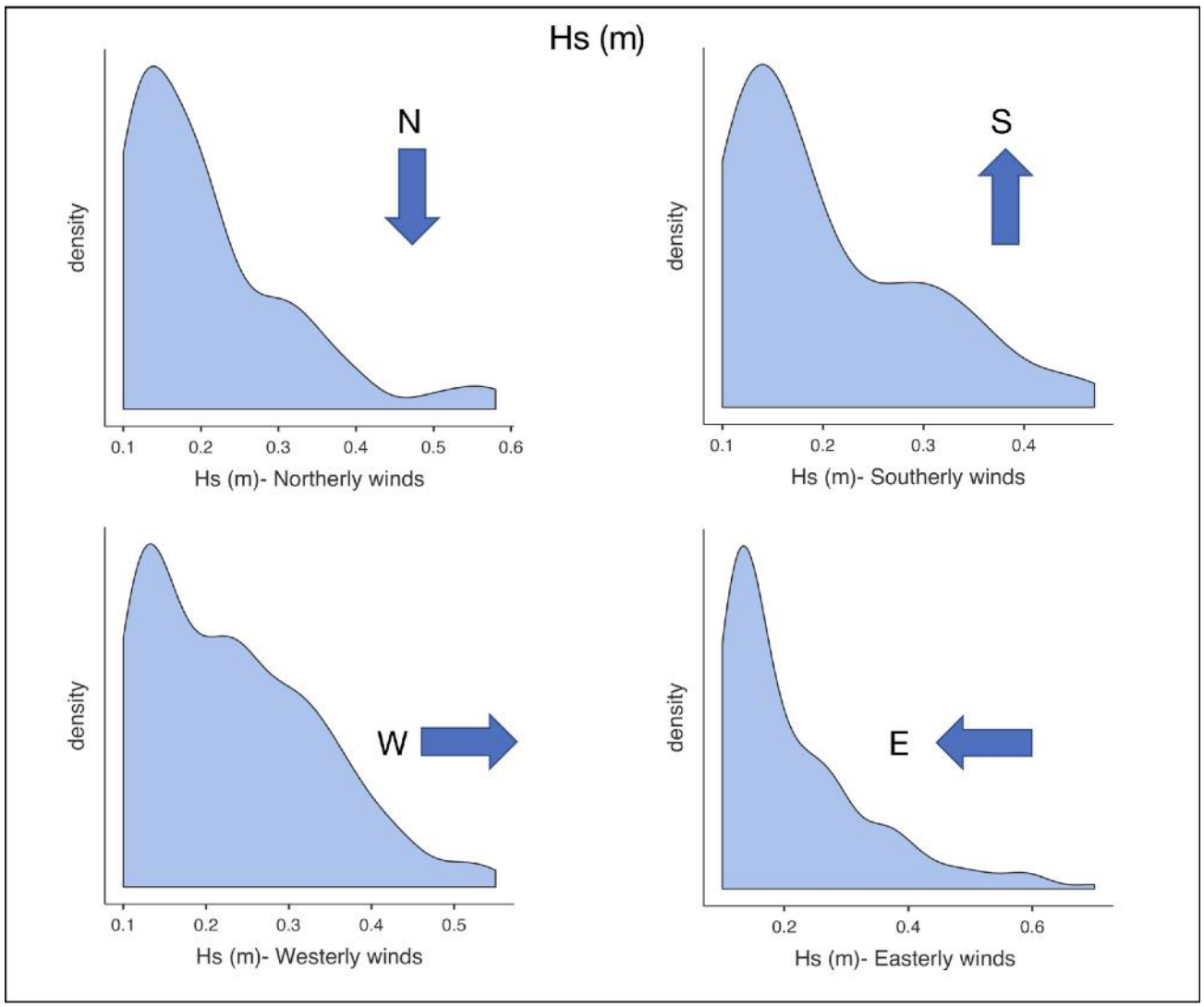

Figure 5.10: Density distributions of H_s values recorded under different wind directions, northerly, southerly, easterly and westerly winds, where a northerly wind is wind coming *from* the north. Open water fetch is located to the east and south of the MIZ, however, there are no significant differences between the height and length of waves generated under winds from the different directions.

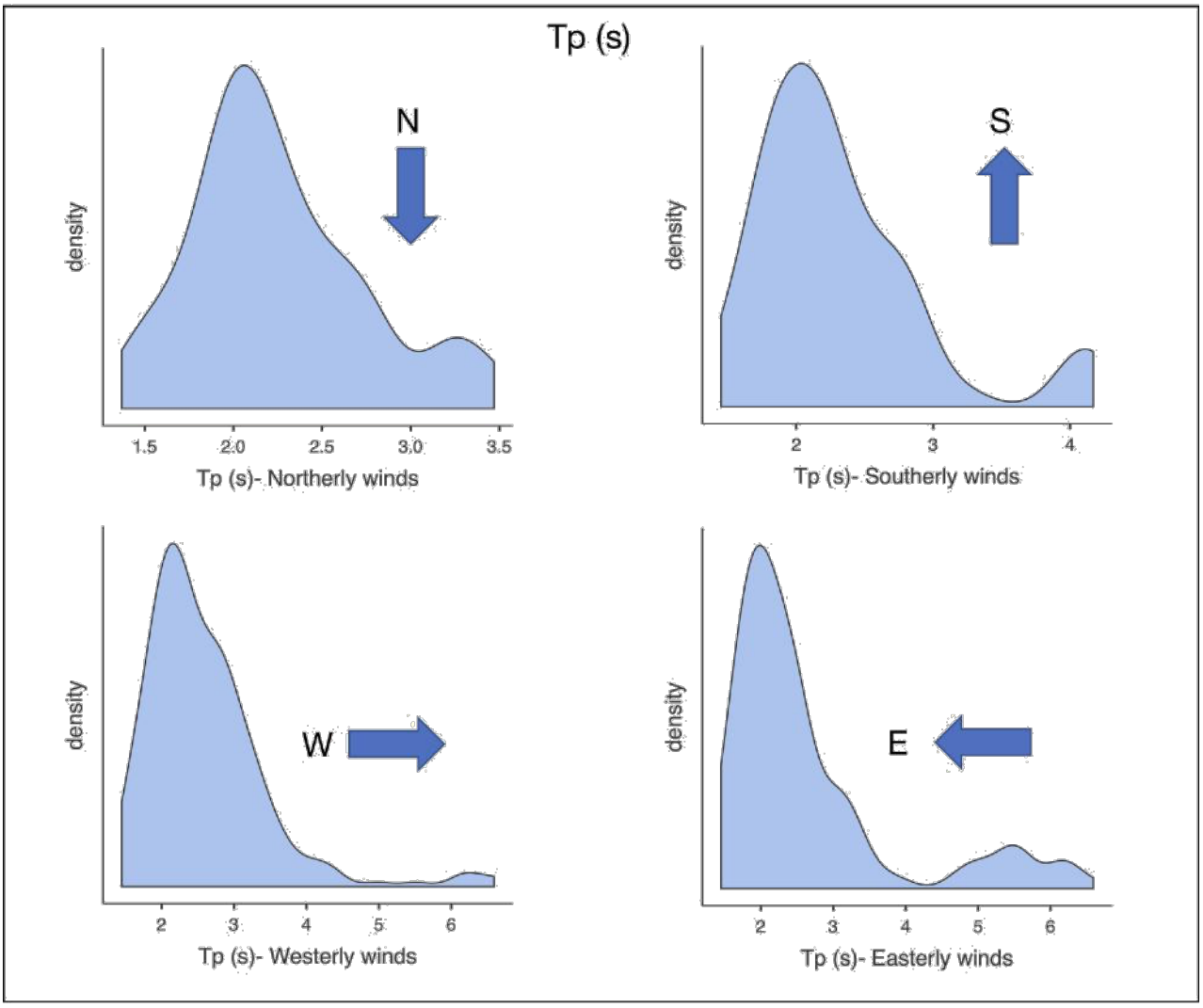

Figure 5.11: Density distributions of T_p values recorded under different wind directions, northerly, southerly, easterly and westerly winds, where a northerly wind is wind coming *from* the north. Open water fetch is located to the east and south of the MIZ, however, there are no significant differences between the height and length of waves generated under winds from the different directions.

5.3 Sea Ice

The average sea ice concentration over all mooring locations showed a decreasing trend throughout the month, an expected observation as the sea ice field decays. The importance of sea ice concentration (SIC) is seen during the August 28 storm event, where the SIC increased from mooring J at the MIB, to the innermost mooring, F. Figure 5.12 shows the effect of this type of structure, as it relates to concentration, on the development of waves. The moorings are ordered from the innermost mooring F to the outermost mooring J. The open red circles and open blue diamonds represent the maximum H_s and T_p, respectively, while the closed red circles and closed blue diamonds represent the average H_s and T_p. Mooring J was essentially in open water at the end of this storm, and hence the maximum values recorded were synonymous with the open water conditions. We will, therefore, consider the position of mooring J the MIB. It is evident that with increasing distance into the sea ice field, there is an overall decrease in the maximum and average values of both H_s and T_p. This situation is likely towards the end of the month when the sea ice field has opened up considerably closer to the MIZ compared to the regions closer to the continuous sea ice cover, and there is an overt transition from low to high concentration. In essence, the sea ice field is not always structured in an ideal way where sea ice concentration seamlessly increases with distance in the sea ice field. For example, when considering all in-ice values up to August 27 against distance in sea ice as shown in Figure 5.13 (here moorings are ordered from the innermost, F, to the outermost, J), one can observe that the highest waves do not always occur closer to the MIB. Mooring A, for example, had some of the highest waves and was located significantly further in the sea ice than mooring J. Nonetheless, in cases where the ideal situation manifests (or almost ideal for the August 28 case), typically towards the end of the month, then there is a clear trend in the average and maximum values of H_s.

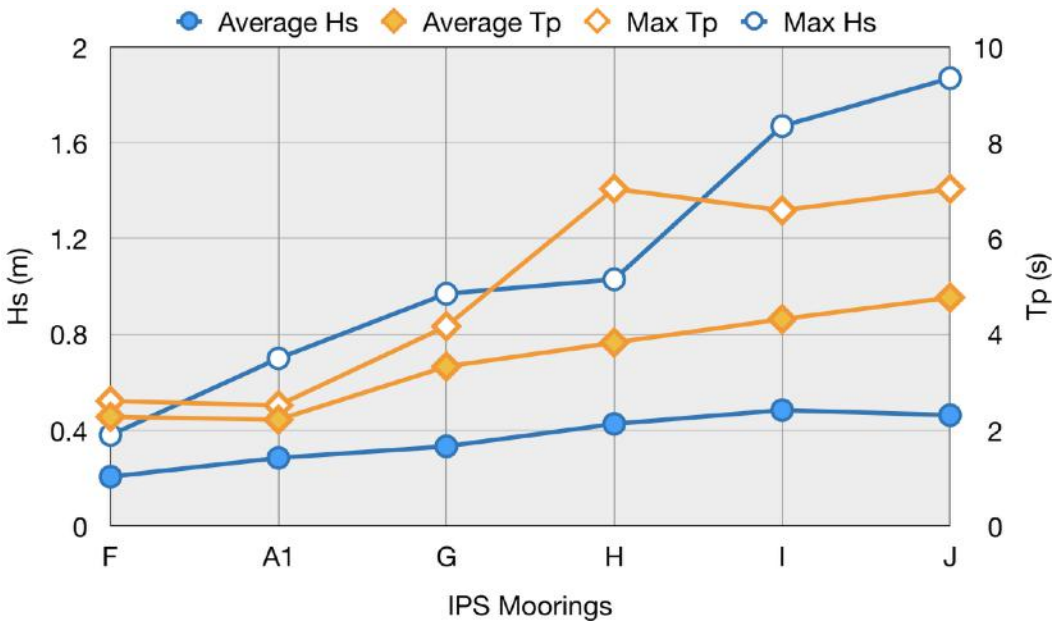

Figure 5.12: Average H_s (blue closed circles), average T_p (yellow closed circles), max H_s (blue open circles and max T_p (blue open circles) for a storm event on August 28 2009. The moorings are arranged form the innermost mooring, F, to the outermost mooring, J. In this case the sea ice concentration in general was lowest at I and J and increased with distance in the sea ice so that F had the highest sea ice concentration.

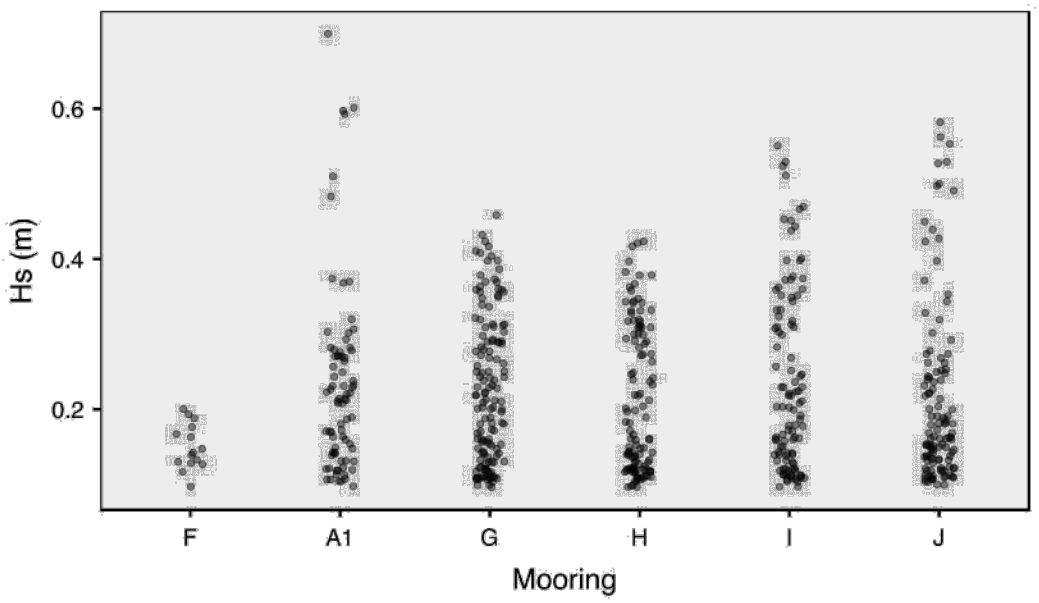

Figure 5.13: H_s distributions at the different mooring locations during August 2009, with the moorings arranged from the innermost F, to the outermost, J. J and I had the highest number of H_s > 0.4 m, however, the highest H_s was measured at A.

An estimate of in-ice fetches can be made by using the JONSWAP empirical relationships (Hasselman 1973). While this model was not developed for use in a sea ice field, because of the short wavelength of locally developed waves compared to the size of the majority of the floes during August, any transmission of wave energy to the other side of a floe is not expected to be significant. Therefore, if the point of interest is not directly at a sea ice edge (in which case the reflections may influence the wave heights) then the problem can be reduced to an (extremely) fetch limited wave spectrum starting from initial conditions (at some floe edge) to the point of interest. Therefore, it stands to reason that these empirical estimations would be useful in estimating fetch distances for the recorded H_s values.

The method by Carter (1982) is a further analysis of the initial JONSWAP data, which was based on fetch limited observations in the North Sea, west of Denmark in 1969. Hasselman developed a spectrum for a sea that was still growing under offshore winds, limited by the presence of the shoreline. The foundation of this spectrum was the Pierson-Moskowitz (PM) spectrum (Pierson and Moskowitz, 1964) which was intended to characterize fully developed seas. Carter developed a relationship between the wind duration, speed and the fetch for local wind conditions. A critical duration (CD) is defined, which discriminates between fetch limited and duration limited seas. For $D > CD$, where D represents the duration of the steady wind, the sea is considered fetch limited. Where $D < CD$, the growth is limited by the wind duration. A minimum fetch and duration are then computed by assuming that the fetch and duration limits for both the JONSWAP and PM spectrum are the same. Beyond this minimum value the sea is considered fully developed. For seas still growing under fetch limited conditions, H_s and T_p can be calculated as:

$$H_s = 0.0163 \times U \times F^{1/2} \tag{5.1}$$

$$T_p = 0.566 \times U^{0.4} \times F^{0.3} \tag{5.2}$$

In the case of partial sea ice, it can be assumed that the waves are fetch limited owing to the presence of the sea ice. We can, therefore, estimate fetches based on measured H_s and wind speed values.

It was extremely difficult, however, to validate these empirical relations from optical satellite imagery due to cloud conditions (which make ice difficult to distinguish) as well as the fact that the images are daily and as such will fail to capture any ice drift on a smaller time scale (such as hourly). We did find very few examples where the ice position in the wind direction did not vary significantly over two days: the day under consideration as well as the previous day. This allowed for a more concrete estimation of the 'ice edge' or the start of the fetch. An example from August 24 at mooring I is shown in Figure 5.14. The wind direction is between 100° and 104°. The red line indicates the length of the fetch from the mooring location to the visible ice edge on August 23, while the yellow line represents the fetch on August 24. The measured fetch length is 4-5 km. Table 5.1 shows a subset of hours from August 24. Growth under a steadily increasing wind occurred over 11:00 to 13:00 UTC, after which H_s began to decrease despite the wind continuing to increase. This suggests that the fetch ended at this point.

The available parameters for the fetch limited empirical relation is thus:

F=5 km;

U=7 m/s (taking the highest wind speed)

From equation 5.1, H_s= 0.25 m, which is similar to the maximum height 0.23 m recorded 13:00 UTC. From equation 5.2, T_p =2 s, which is also similar to the maximum T_p, 2.3 s, during that interval at 13:00. To determine the wind duration that is associated with this wave height, we can again use Carter's relations where:

$$Duration = \left(\frac{H_s}{0.0146 \times U^{9/7}}\right)^{7/5} \quad (5.1)$$

This gives a duration of 1.4 hours, that is, it only took 1.4 hours to create the maximum H_s within that fetch (even though the actual steady wind duration was much longer). It makes sense then, that the maximum H_s was recorded by the IPS after a two-hour period: 11:00 to 12:00 and 12:00 to 13:00.

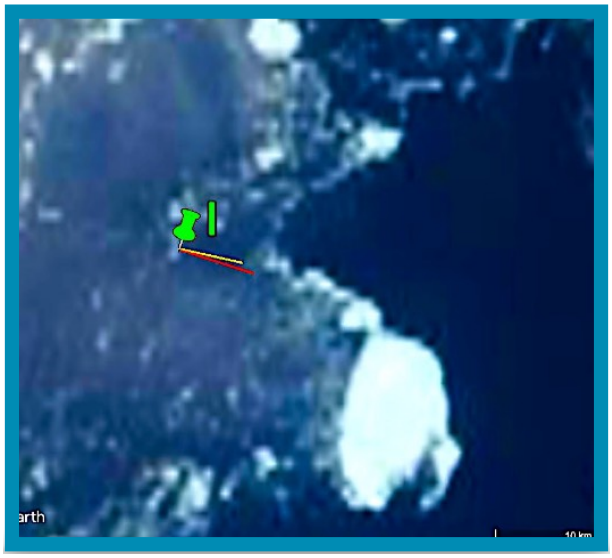

Figure 5.14: Fetch estimation from optical imagery. Yellow line represents the fetch on August 24, and red line is the fetch on August 23. Two days were used so as to get the best estimate of the start of the open water fetch.

Hour of Aug 24	Hs (m)	Tp (s)	Wind Dir °	Wind Speed m/s
9	0.11	7.04	104.3	4.8
11	**0.16**	**1.95**	**104.9**	**6.2**
12	**0.17**	**1.95**	**102.8**	**6.7**
13	**0.23**	**2.3**	**100.2**	**7.1**
14	0.21	2.07	98.4	7.8
15	0.16	1.99	99	8.4
16	0.11	1.84	99.4	8.7

Table 5.1: Data subset for a period of wave growth (bold) from 11 to 13:00 and then a decline in H_s and T_p despite increasing winds.

Figure 5.15 highlights the distribution of H_s (> 0.3 m) with fetch, calculated using these empirical relationships. The majority of these fetches that produced waves > 0.3 m were between 5 and 10 km (shown by the density distribution at the top of the graph), with the frequency of fetches exceeding 15 km increasing towards the end of the month (Figure 5.16).

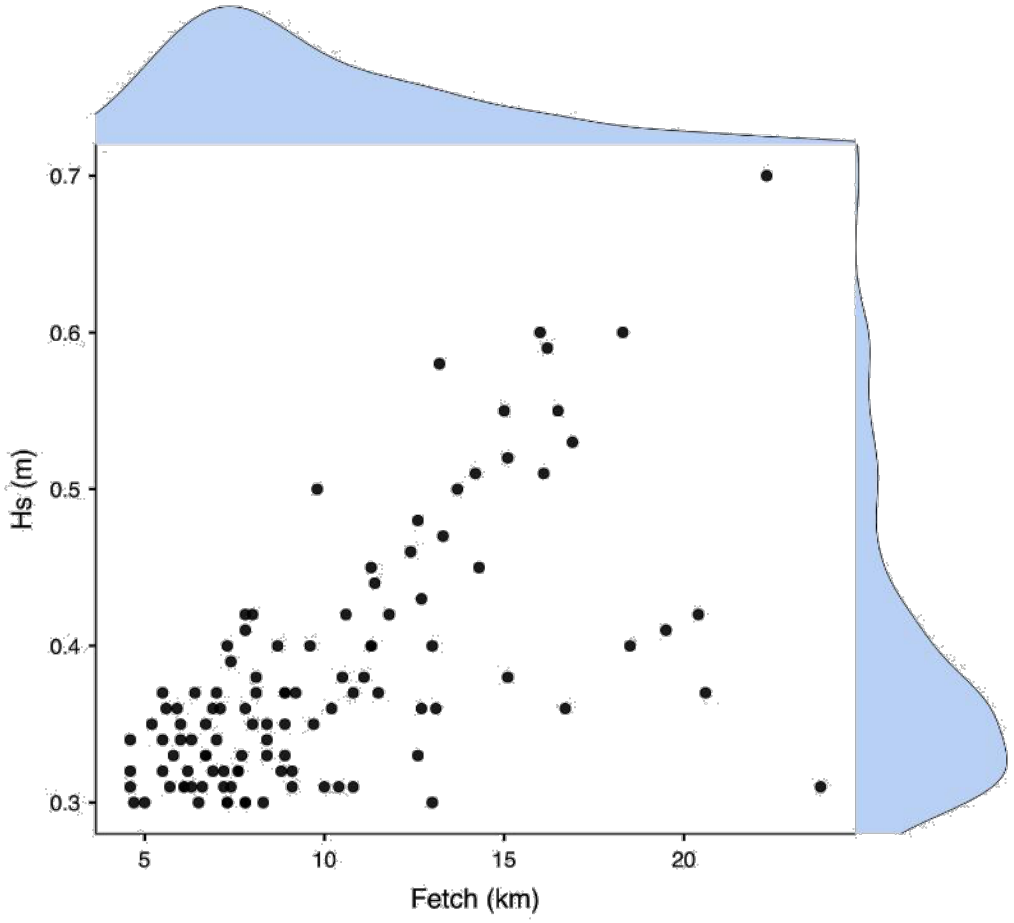

Figure 5.15: Scatterplot of H_s > 0.3 m with Fetch. Blue density marginals show the density distribution of H_s to the right and Fetch to the left. Fetch was calculated using modified JONSWAP equations (Carter 1989) using observed H_s and ERA5 reanalysis wind speed data.

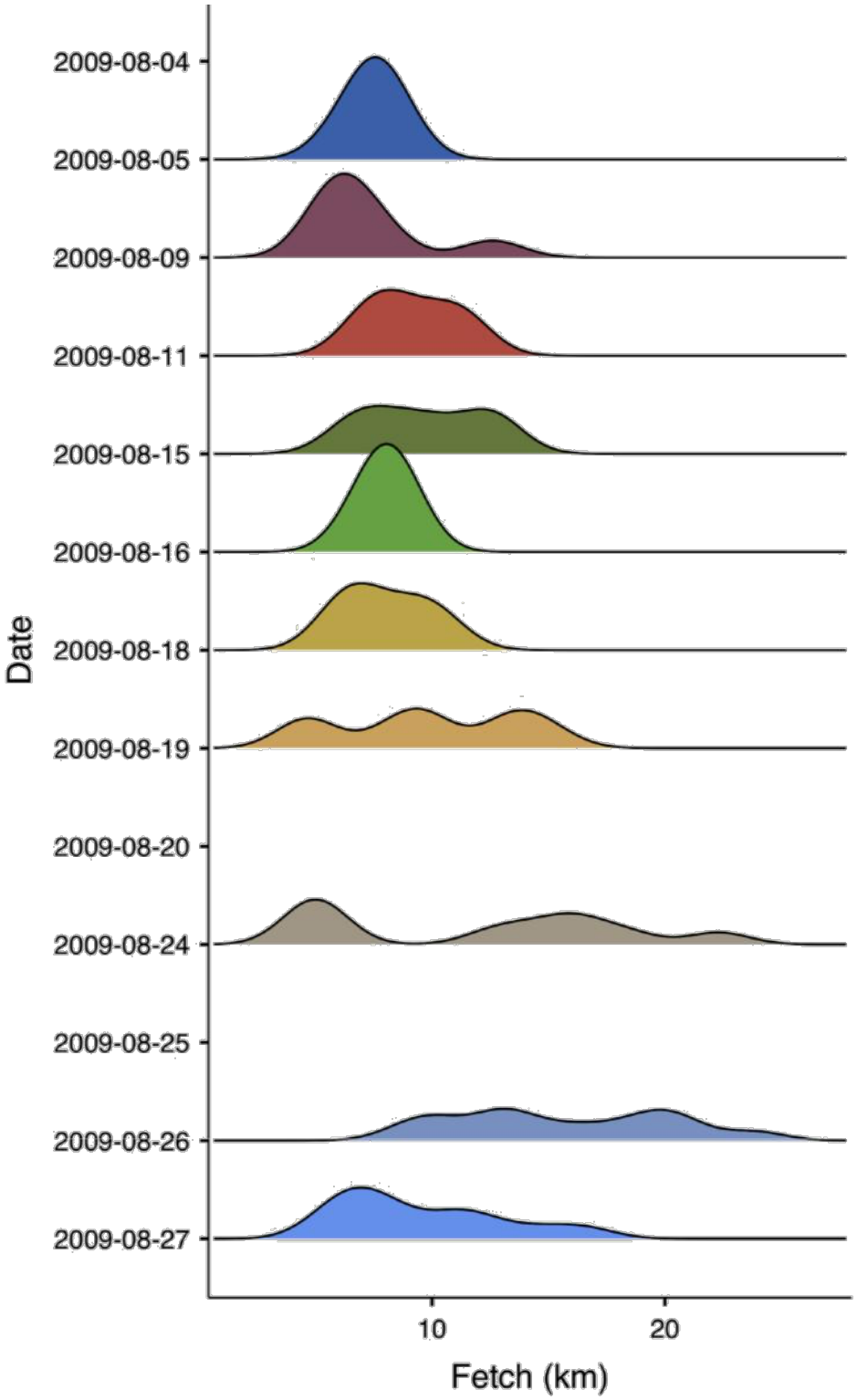

Figure 5.16: Density distributions of H_s > 0.3 m with Fetch for different days of the month. Fetches exceeding 15 km increased towards the end of the month

5.4 The Interplay of Winds, H_s, T_p and Sea Ice

The high wind event that took place on August 28th presents an interesting view of how both the wind and the sea ice influence H_s and T_p uniquely, and how the interactions differ depending on the position in the sea ice field. In the first example, Figure 5.17 shows the relationship between wind speed, H_s and T_p at mooring G during this high wind event. Mooring G is the intermediary mooring, not as close to the MIZ as moorings H, I, J and not as far in the sea ice field as moorings A1 and F (see Figure 4.2 and Figure 5.19). For this storm, the wind was blowing from the east, pushing waves into the MIZ as shown in Figure 5.19. The wind speed increased gradually from 6 to 11 m/s during 3:00 to 18:00 UTC. At the same time, both H_s and T_p increased steadily from 3:00 to 10:00 UTC, after which H_s increased at a slower rate up to 13:00, while T_p began to fall. The decrease in T_p after 9:00-10:00 UTC is a likely indicator of the effect of the sea ice field. The wind was still increasing, and hence not the cause for the decrease. At this point, it is likely that the waves attained their longest periods based the available fetch, as the non-linear transfer of energy to longer periods becomes more efficient with adequate space (Lin et al. 2010). H_s, on the other hand, still continued a slow increase, and this is unsurprising due to the strong winds. Limited fetch combined with strong winds is likely to produce short, steep (choppy) waves (high heights relative to length/period). For example, Healy (2005) explains how fetch limited winds can produce choppy waves in semi-enclosed seas or estuaries. Essentially, the wind energy input outweighs the ability of non-linear wave-wave interactions to take place as a result of the limited space. A similar concept can be applied here and would explain the decrease in T_p with time while H_s still increased slowly under increasing winds. While the growth in height seems to have had a delayed response to the ice field, it eventually reaches its limit for the given fetch, ~ 1 m, at 13:00. The values of H_s then began to decrease, and eventually both H_s and T_p attained a fairly steady signature contingent on the wind and ice

conditions. The maximum H_s at 13:00 (Figure 5.17b), was in fact similar to open water values around the same time. However, the periods in sea ice (~4 s), were lower than those in open water (~4.5-5 s) and, more importantly, were also decreasing under increasing winds, which suggests that these waves were not open water waves.

A.

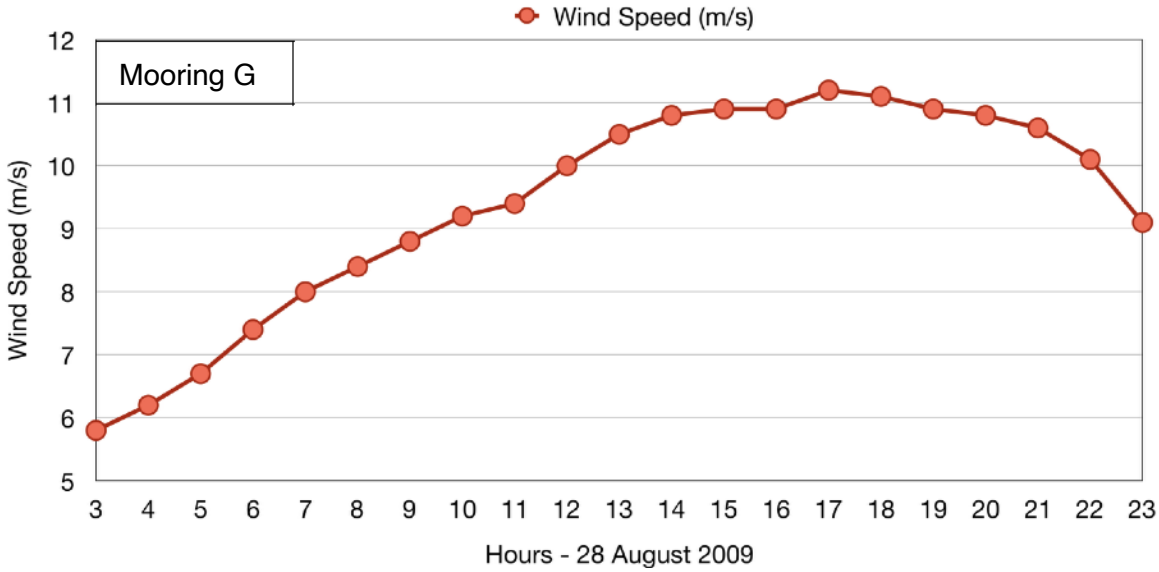

B.

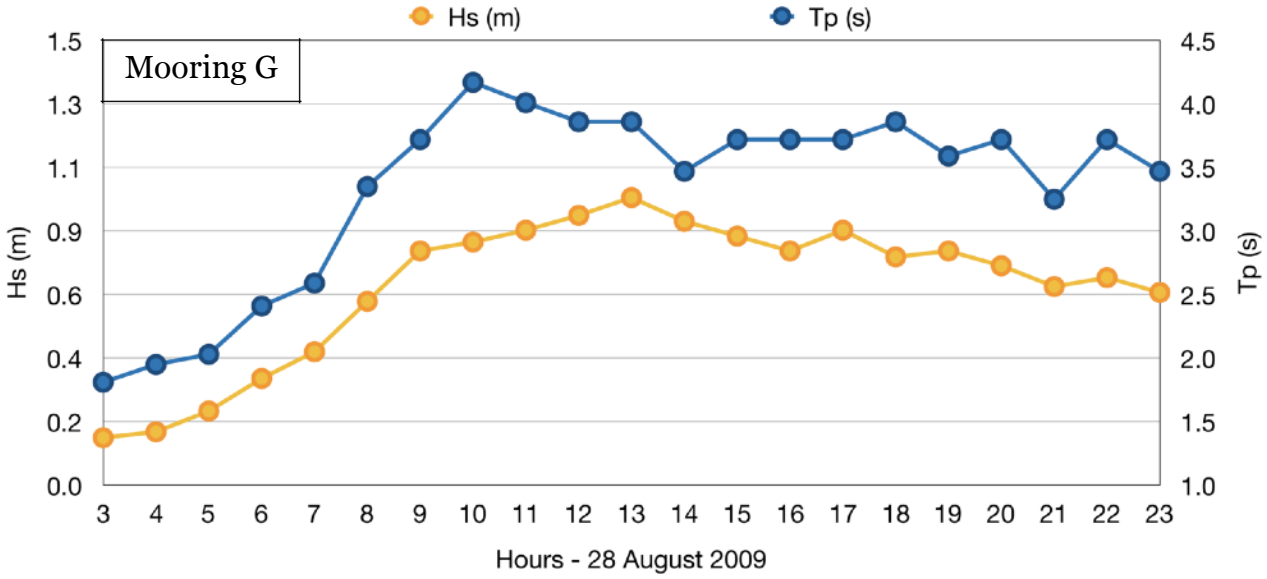

Figure 5.17: Evolution of A) wind speed, B) H_s and T_p at mooring G, over the course of 3:00 to 23:00 UTC during the storm event on August 28. Local wave growth is seen from hours 3 to 9, after which the influence of sea ice affects wave development causing a decrease in T_p despite the increasing wind speeds.

In the second case, the outermost mooring, J (Figure 5.18), is examined during the storm on August 28. By the end of the day, mooring J was essentially in open water. In Figure 5.18a-b, three types of interactions can be observed in this case:

1. Wave growth in partial sea ice- As the wind picked up, increasing from 6 to 9 m/s, during 4:00 to 10:00 UTC, there was also an increase in H_s as well as T_p, indicating wave growth in sea ice (The wind continues to increase after 10:00, however, wave growth ceases around that time).
2. Ice acting as a low pass filter- By around hour 11- 12, T_p increased notably, and without a clear increase in H_s, suggested that the classic attenuation mechanism was occurring. The sea ice floes close to the MIB were relatively smaller and more mobile at this time, allowing the wind to push them westward, including floes that were to the east of mooring J. As such, it is likely that the ice concentration increased for a while at mooring J, allowing for the classic attenuation of the open water waves moving into its location. This is supported by the fact that H_s began to decrease in time at around hour 13, despite increasing winds. Therefore, although waves were being attenuated at mooring J, the ice field must have been increasing in concentration in order to induce more attenuation with time.
3. Open water growth and decay- The final stage represents the transition to open water conditions around hour 18 to 20. The gradual increase in H_s is evident. The fact that T_p does not increase after this point (it actually decreases during hours 18-20) suggests that T_p in-ice values had likely exceeded open water values during the attenuation stage. As the wind speed begins to slow down, H_s drops at the end of the day (hour 23), while T_p shows a slight increase suggesting the transition to swell conditions.

A.

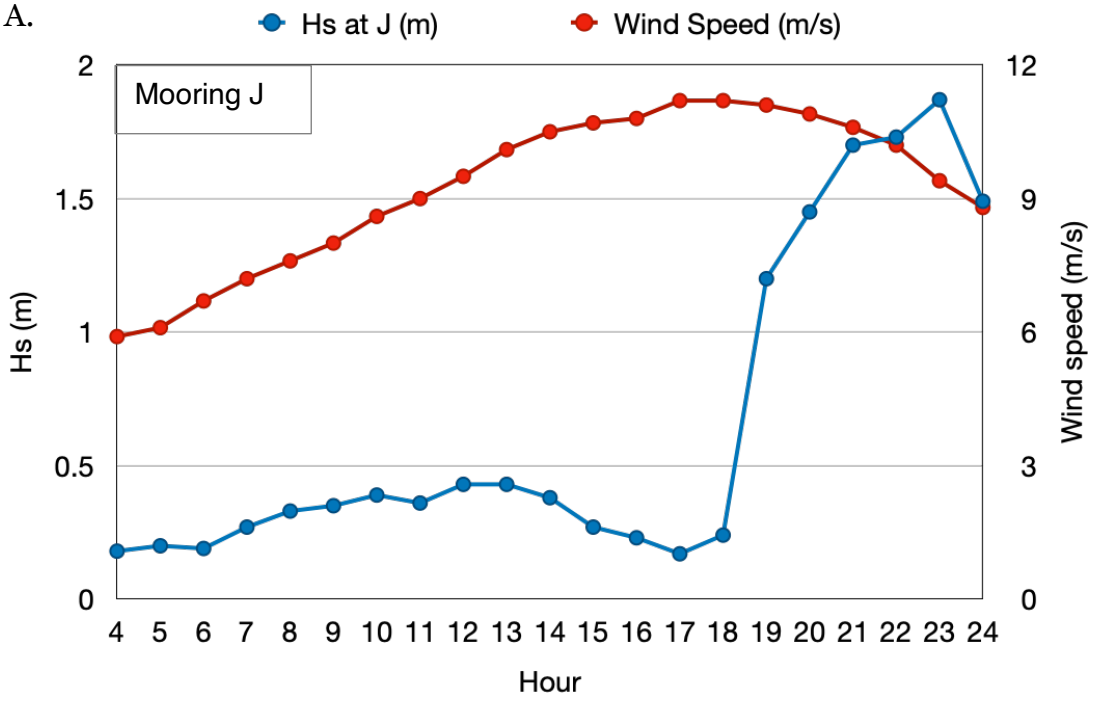

B.

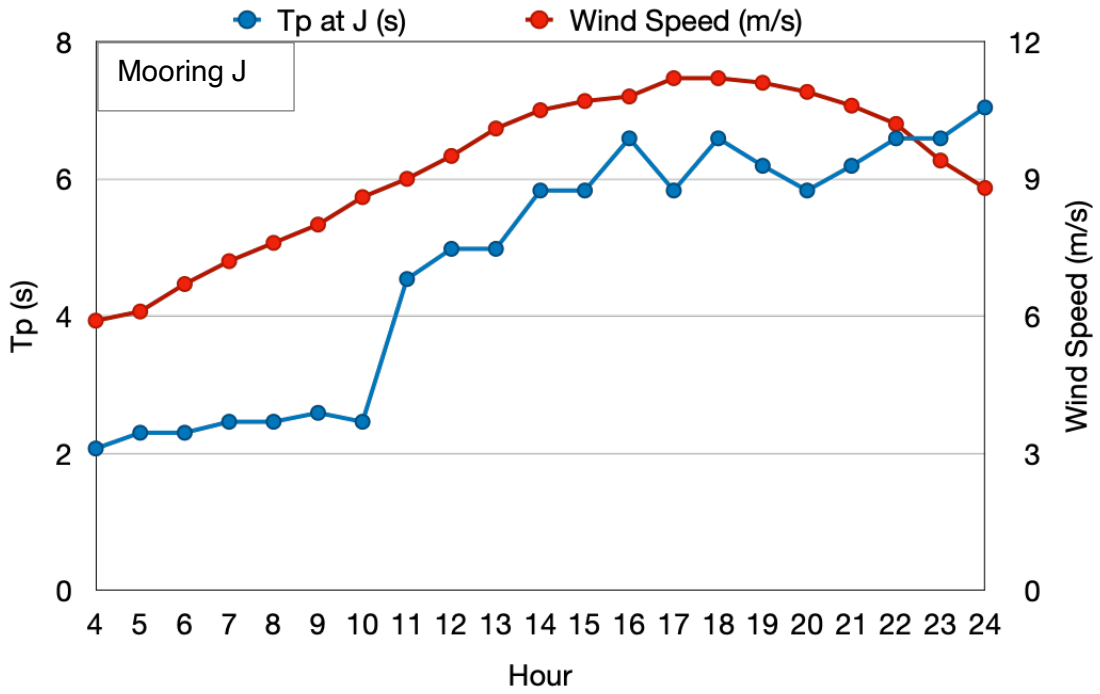

Figure 5.18: Evolution of A) observed H_s and B) observed T_p at mooring J (blue line) over hours 4 to 24 on August 28-29. Wind speed is represented by the red line in both. Three separate events can be identified: local wave growth under increasing winds, wave attenuation of open water waves by sea ice and open water wave growth and decay.

It is interesting to note that after the growth of H_s and T_p at both moorings G and J, the T_p began to decrease at mooring G where the floes were larger, while it began to increase at mooring J where the floes became much smaller, indicating the preferential attenuation of the longer waves at mooring G and the shorter waves at mooring J.

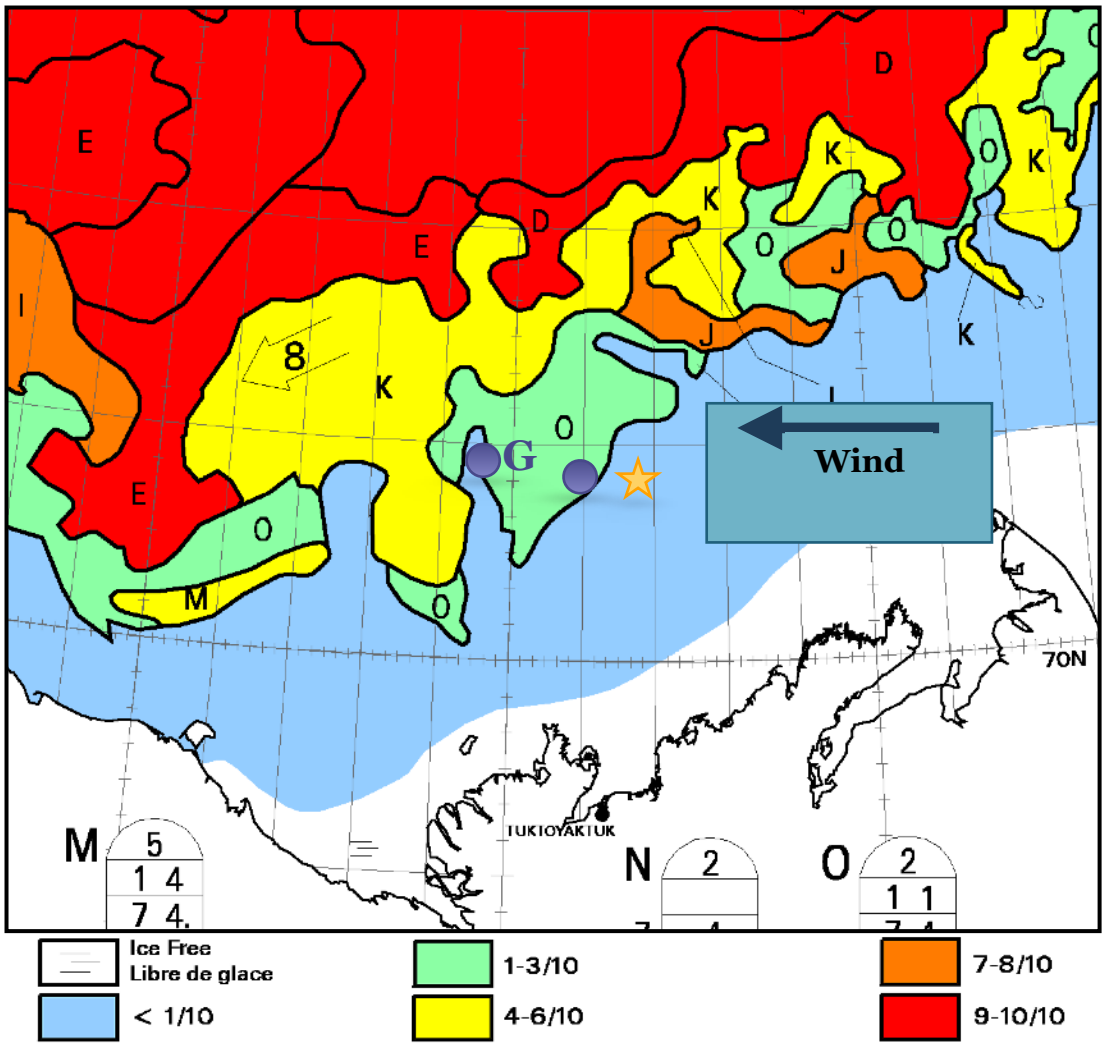

Figure 5.19: Canadian Ice Service chart showing ice concentration on August 28 2009. Purple circles indicate positions of moorings G and J. Mooring G was surrounded by larger floes and more distance within the ice field while mooring J was just at the edge and was in open water by the end of August 28. The yellow star indicates the open water observation point to the east of J. Waves were travelling from east to west.

So far, we have identified the main relationships that regulate wave growth in partial sea ice cover. Using the empirical formulations for the fetch estimation, model ERA5 wind speed data and observed T_p data, the correlation matrix in Table 5.2 shows the factors that co-vary the strongest with wave heights in partial sea ice. The different factors are shown within the red box, and as expected, the fetch and T_p correlate the strongest with H_s (0.65 and 0.64, respectively) with the wind speed having a lower correlation of 0.4. This is a rational outcome as fetch limited conditions would carry the greatest weight for wave growth and as a result of the local wave evolution dominating, wave periods would be largely concurrent with the wave heights (positively correlated).

Correlation Matrix

		Hs	Tp	Wind Speed	Fetch
Hs	Pearson's r p-value	—— ——			
Tp	Pearson's r p-value	0.645 <.001	—— ——		
Wind Speed	Pearson's r p-value	0.4 <.001	0.081 0.4	—— ——	
Fetch	Pearson's r p-value	0.64 <.001	0.514 <.001	-0.405 <.001	—— ——

Table 5.2: Correlation matrix showing the contributions of the different factors to the determination of Significant wave height (H_s). Fetch (determined by the open water distance between sea ice floes) carries a greater weight than wind speed- 0.64 and 0.4, respectively. The peak period (T_p) is also highly positively correlated, indicating the dominance of local wave development.

6. Discussion

6.1 The Physical Characteristics of Waves in Partial Sea Ice Cove

Short waves

The limited fetch that waves in partial sea ice cover have for their development means that there is less space for them lengthen significantly and so they remain short. In the early stages of wave generation, however, the wave will grow and lengthen for a short period of time given that there is sufficient open water (Masson and Leblond 1989). Nonlinear wave-wave interactions are more dominant in young seas (newly formed waves) when the wind forcing is strong and will tend to shift excess energy away from the peak to opposite ends of the spectrum. The waves at the very high frequencies (short waves) will very easily become steep and break. At the peak, for H_s greater than 0.3 m, calculated values of steepness ranged between 0.02 to 0.06, and were smaller than the approximate threshold for wave breaking: $\frac{H}{\lambda} = 0.14$. Thus, our dataset shows that wave breaking was not occurring at the peak. The dissipation at the very short wavelengths and the shift of energy to longer waves by S_{nl} means that the waves in the early stages were allowed to grow and lengthen, similar to open water conditions. Of course, in this scenario, they have not encountered a large sea ice floe, but waves can also encounter small floes along their path, which do not completely stop their propagation but create reflection and refraction patterns. If the floe is smaller broken piece of a large, solid floe, then it will scatter some of the wave energy but also allow for the transmission of the remainder (Kohout et al. (2011), Bennetts et al. (2015)). If the floe is similar in size to the wave, then the shorter wavelengths are preferentially scattered. The wave, then, that is transmitted has a longer period but decreased energy. This in turn affects the energy balance of the spectrum, reducing both S_{in} and S_{nl} . This lengthening of the peak period (in this particular study) does not last very long. As the wave encounters large floes the lengthening of the wave stops. As suggested by Masson (1989), the

wave field could begin to filter the relatively 'longer' (or less short) waves with respect to the very short waves, reducing the overall T_p of the wavefield with time. The longer waves of this short-wave spectrum approach isotropic scattering to a greater extent than the shorter waves (where backscattering dominates the reflections). Thus, the energy is more spread out at longer periods, leading to greater attenuation, and the peak shifts to shorter waves with less energy. Thus, in the early stages, of wave evolution, the peak waves are allowed to lengthen, the effectiveness of which depends on the frequency of small floe collisions, and the distance to collision with a large floe, after which the longer waves become more efficiently scattered and the peak again shifts to the shorter waves.

Low, but possibly choppy waves

As mentioned above, collisions with small floes will tend to reduce the energy of incident waves, so that the transmitted wave is a lower height. This allows for the actual process of wave generation to become less efficient. Since the waves are kept short, as well as low, the feedback mechanism proposed by Miles' theory is weakened. Recall that the feedback relied on the idea that as the waves grow, they modify the airflow in such a way that increases the growth. If the waves remain low, this process is severely limited. Therefore, the transfer process is dependent on the amount of energy the waves already have. Having more energy increases the amount the waves are able to receive. Collisions with large floes, essentially stop transmission and finalize the extent to which waves can grow via wind forcing. Thus, even in the presence of increasing wind speeds, wave growth was maintained for only a short time. However, the interaction with the floe can bring about changes in the height of the waves on the incident side of the floe due to the reflections of the waves. In a similar way to waves impugning on a barrier in the ocean (a scenario that is well studied in marine technology/engineering), a wave that is reflected in such

a way that it superimposes with the incident wave arriving head-on at a floe edge, can cause an increase in wave height, up to two times the height of the incident wave. This is referred to as a standing wave, as the phase velocities of each wave, incident and reflected, cancel each other out and the wave is essentially no longer propagating (similar to waves sloshing about in a bathtub). In reality, reflections might not be perfect at the sea ice edge, they may only be partial in which case the resulting wave heights will be less than $2H_i$, where H_i is the height of the incident wave.

Partial reflections can be represented as follows:

Consider an incident wave of

$$\eta_i = \frac{H_i}{2} cos(k x - \omega t), \tag{6.1}$$

and a partially reflected wave of

$$\eta_r = \frac{H_r}{2} cos(k x - \omega t), \tag{6.2}$$

where η is the surface elevation and H are the heights of the incident, i, and reflected, r, waves. The wavenumber and frequency in space (x) and time (t) are given by k and ω respectively. The water surface after the partial reflection is then a combination of both waves:

$$\eta_{ir} = \frac{1}{2}(H_i + H_r)\, cos(k x)\, cos(\omega t) + \frac{1}{2}(H_i - H_r)\, sin(k x)\, sin(\omega t), \tag{6.3}$$

with a reflection coefficient of

$$\frac{H_r}{H_i} = \frac{H_{max} - H_{min}}{H_{max} + H_{min}}. \tag{6.2}$$

In the simple case of waves arriving obliquely at a barrier (in this case a straight floe edge as shown in Figure 6.1), the superposition of incident and reflected waves occurs in such a way that a pattern of superimposed crests (yellow circles) and troughs (blue circles) is formed which propagates sideways along the floe edge (Lynn 2013). It is easy, then, to see how the water

surface on the incident side of a floe of arbitrary geometry can become choppy, with varying increases in wave heights.

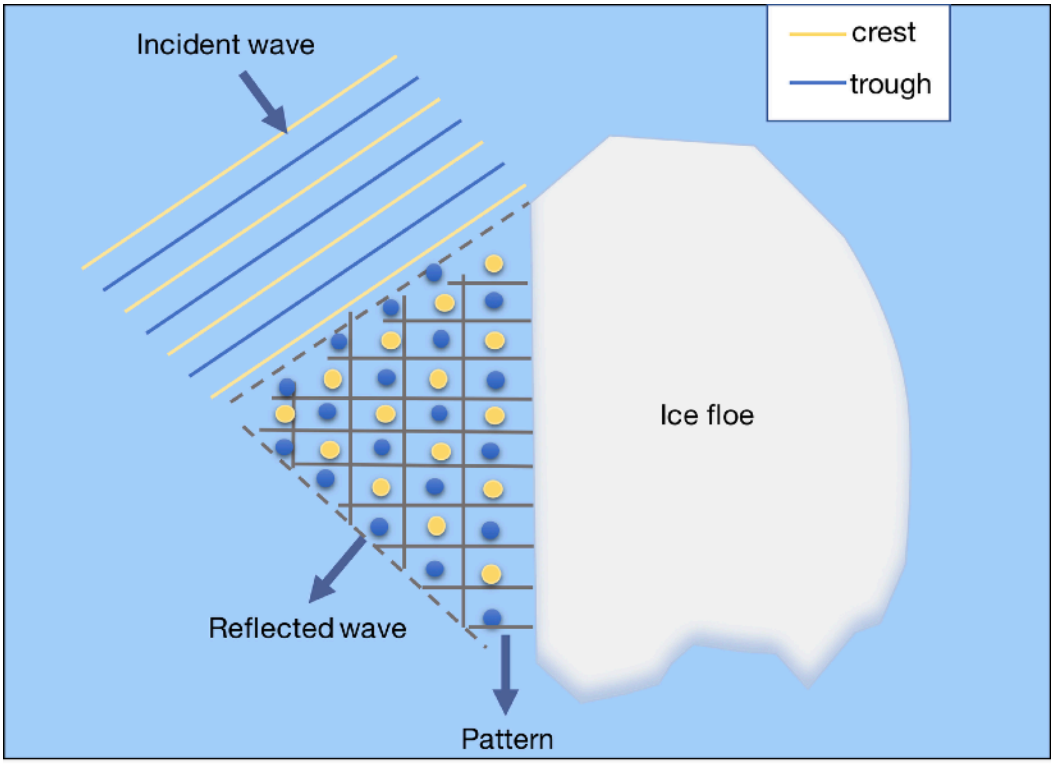

Figure 6.1: Schematic showing a simple case of oblique reflection from a straight sea ice floe edge. The yellow circles represent the superposition of the crests of the incident and reflected waves, and the blue circles for the superimposed troughs. The pattern itself moves sideways along the edge of the floe. Adapted from Lynn (2013).

6.2 The Role Of Wind Forcing On Wave Development

While the wind is the main driver of wave evolution in open water, this relationship becomes significantly more complex within the sea ice field. The amount of energy that can be transferred to the ocean surface is limited by the availability of actual open water surface. The severely fetch limited conditions in a sea ice field means that the sea ice cover will have more weight in terms of the extent to which the waves can grow, as opposed to wind speed or duration. The confirmatory factor analysis of this idea indeed confirms that the sea ice limitation, and hence the available fetch, have greater weight (Figure 5.18). The table shows a factor of 0.64 for the

relationship between H_s and fetch (regulated by the sea ice) and a lower factor of ~0.4 between H_s and wind speed.

On-ice winds are typically associated with long waves propagating not the MIZ. This is not always the case, however, particularly when considering distances that exceed a few kilometers. The similarity of H_s and T_p in all directions suggest that on-sea ice winds are not always associated with larger waves than off-sea ice winds on these scales. It must therefore not be assumed that long waves are being attenuated with distance in sea ice, as the opposite could be happening- the growth of short waves in sea ice (even though if the concentration increases with distance in the sea ice, the former could seem like the case, if only H_s is observed). Overall, the wind is the controlling factor within the limits of the fetch it is given. If the fetch limit is not reached, then any decrease in wind speeds will cause the wave to correspondingly decrease. Higher winds increase the chances of higher waves developing; the average and maximum waves over time will tend to be higher during periods of high winds (> 6 m/s). However, the wind speed, direction or duration is not enough to estimate wave growth in sea ice as the waves will almost always be fetch limited, and hence their growth-dependent primarily on the fetch.

6.3 The Role of Ice Floes on Wave Development

While it may be easier to conceptualize that large floes would have the effect of diminishing wave growth in comparison to small floes in the MIZ, this is not always the case. In fact, the maximum H_s was recorded at an inner mooring location, where the floes were larger than those closer to the edge (Figure 5.14). Smaller floes have the potential to become compact if the wind direction causes convergence of the floes, significantly reducing any open water spaces. Larger floes are,

for one, less susceptible to the push of the wind, and two, less likely to fit neatly with other large floes, allowing for leads to persist between them even under converging winds. For the very large floes close to the continuous cover, fracture and breaking may occur in such a way that the floes are more uniform, preventing any significant fetch. This is evident early in August, where waves were measured in leads between large floes, but severe fetch limitation kept them below 0.3 m. Furthermore, wave growth in the vicinity of small floes close to the MIZ, where the diameters are similar to the wavelengths of the waves (which, in this study was an average of 13 m for H_s > 0.3 m), could enhance the scattering of the waves Several studies have noted that scattering occurs most efficiently in such a case where both wave and floe are of similar length ((Masson and Leblond 1989, Meylan et al. (1997), Meylan (2002)). Masson (1989) had concluded that in off- ice winds, the waves would become more efficiently scattered with distance from the interior ice pack towards the MIB, as the floes would be expected to get smaller and become similar in size to the short waves. In the current study, the majority of floes around the moorings for much of the month were significantly larger, and so the scattering regime was likely not the most efficient for the most part. As a result, the majority of the scattering would take place at the longer periods since the periods overall were very short in comparison to the floes. Thus, the growth in the vicinity of the larger floes may, in fact, be more efficient owing to the scattering being less efficient. However, the increase in scattering and subsequent decrease in wave growth that would happen close to a MIZ containing small floes as suggested by Masson (1989) would be pronounced only if the floes were relatively close together so that the waves travel only a short distance before impinging on the floes in order to get scattered. In this study, the region of the smallest floes also became much less concentrated towards the end of the month and so it was possible for the highest (1.9 m) and longest waves (7.6 s) on average to occur in that region (see Figure 5.1 and Figure 5.4c). Another possibility for increasing growth in sea ice is the scattering of waves from the floe edge which has been found to increase the heights close to the

sea ice edge up to twice the original height leading to choppy (short, steep waves) at the sea ice edge (Boutin et al. 2018). It can be assumed, owing to the short wavelengths (average of 13 m) compared to the much larger floe sizes (mainly >500 m), that backscattering was a dominant process in the study area and therefore it is likely that choppy seas and increases in incident H_s were common occurrences.

6.4 Estimating Waves in Partial Ice Cover - Considerations and Future Work

As mentioned in section 5.4, the fetch is the most important factor regulating wave development in partial ice. This poses a significant challenge for modelling waves in the MIZ as the MIZ itself is poorly resolved in most publicly accessible wave models. This results in two situations: the waves developed in the partial ice cover are simply absent in such models, or the open water waves propagating into the ice are grossly overestimated as the unresolved MIZ is taken as open water. As an example, Figure 6.2a and 6.2b shows H_s interpolated from two reanalysis datasets, ERA5 and Wavewatch III, on August 28 2009, with the position of mooring F indicated by the green circle. With a spatial resolution of 0.5° for both wave products, a significant portion of the MIZ is unresolved, thus completely eliminating the short fetches present between scattered floes within that region. The interpolated H_s at the location of mooring I from both reanalyses is ~ 2m, while the actual observation at the same hour was only 0.2 m, with the wave growth being local (in-ice) as opposed to waves generated in open water.

A.

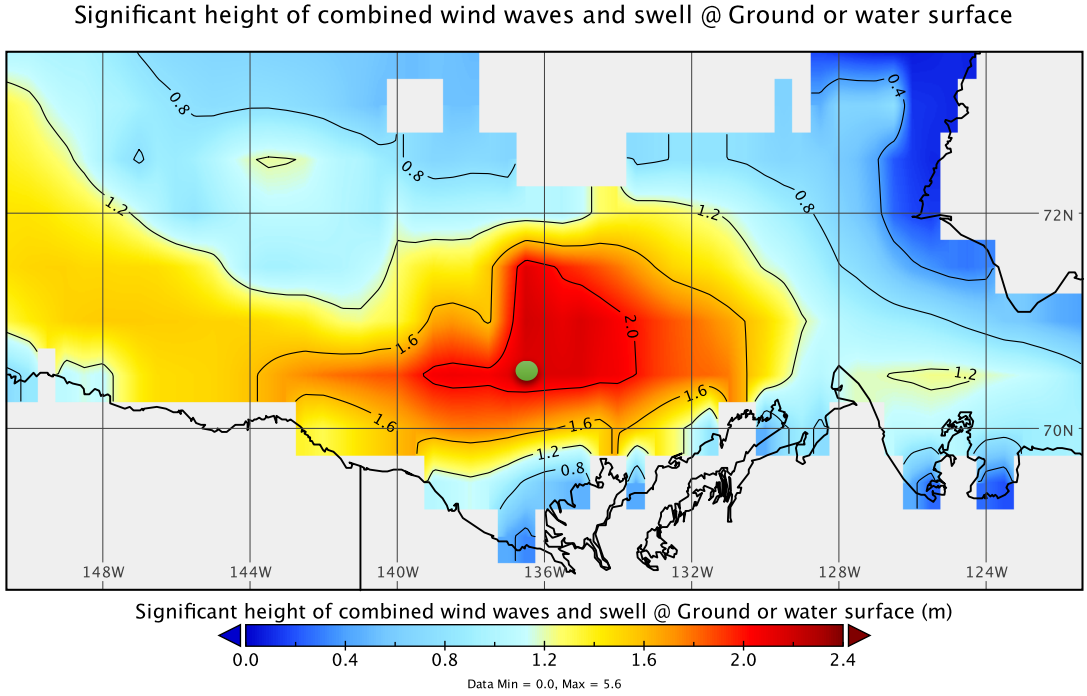

B.

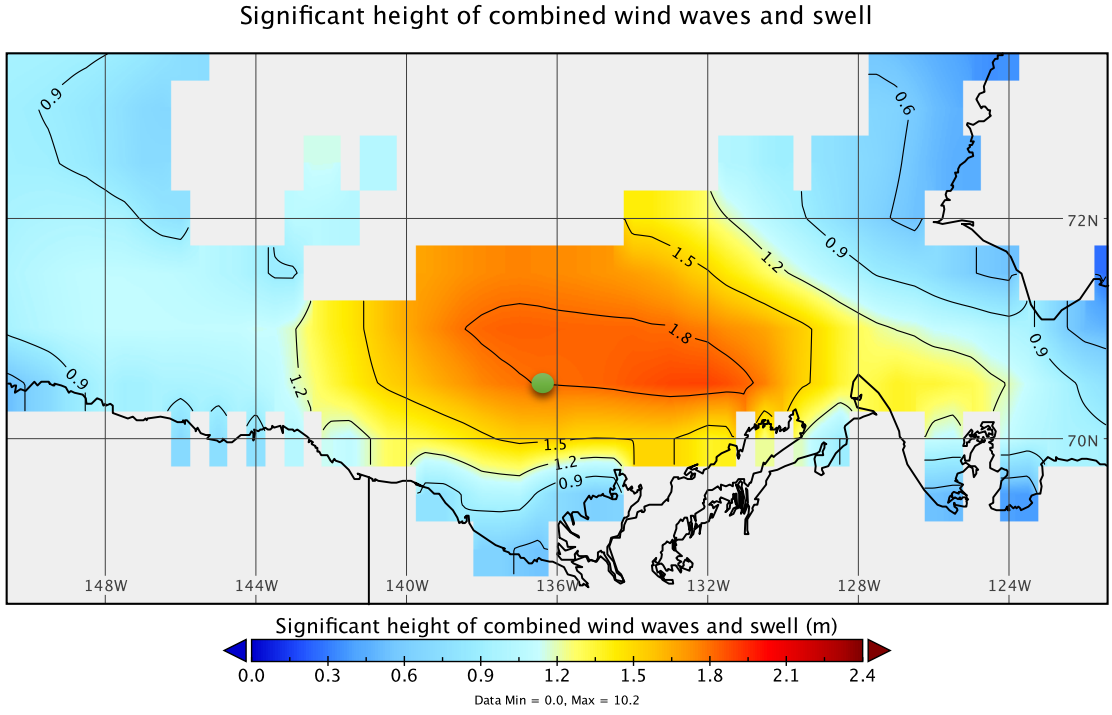

Figure 6.2: Significant wave heights (H_s) from A) ERA5 and B) Wavewatch III reanalyses on August 28 2009. The models are unable to resolve the MIZ and therefore grossly overestimate H_s. The green dot represents the mooring position that was actually in partial ice (~30% concentration) where an H_s of 0.2 m was observed, while the models report H_s of ~ 2m in completely open water.

Another consideration regarding the use of ice products for determining local wave growth in partial ice cover is that the ice product must be able to resolve individual floes, and thus most ice concentration products would not be very useful for this specific purpose. Nonetheless, once wave growth itself is established, its relationship with ice concentration is a key area that needs to be examined. Many ice concentration products, however, are still unable to provide the high-resolution ice information that is needed to model processes in the MIZ. One of the higher resolution satellite products is the AMSRE 12 km ice concentration data. It is shown in Figure 6.3, overtop optical imagery of the same-day ice field. The sections of the ice field close to the MIB where open water fetches (and wave growth) may be the greatest tend to be completely unresolved as Figure 6.3 shows, and the ice concentration values lower than 30% from AMSRE (the shaded regions that are very light blue to white) are often higher in actuality.

It is clear that for improved understanding of locally grown waves in partial ice, significant work must be done in terms of simulating the MIZ itself within wave models. In addition, in the context of the Arctic, there are relatively few datasets of waves in general (regardless of origin or characteristics), which limits the extent to which we can improve upon the current knowledge in this area of research. Nonetheless, although local wave growth in ice, specifically, presents itself as a relatively new research problem, we can simplify the process by applying already established open-water wave growth principles, with the caveat that the fetch is severely limited. Forecasting of waves in partial ice conditions is thus feasible, with the use of high-resolution ice information such as that obtained from synthetic aperture radar (SAR).

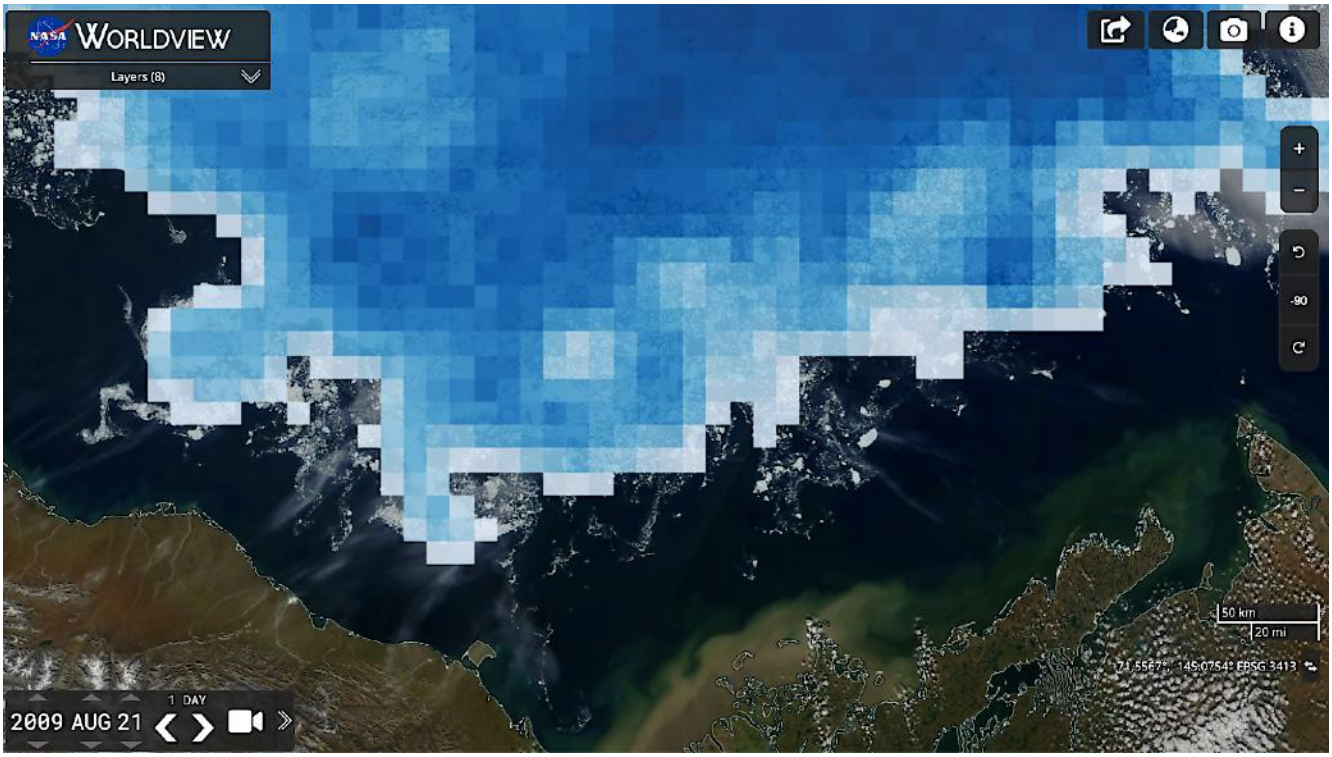

Figure 6.3: AMSRE 12 km ice concentration data is represented by the blue shading and plotted over true colour optical imagery. Lighter blues on the AMSRE image indicates lower ice concentration. The data is unable to accurately represent the ice field close to the boundary of the marginal ice zone, which is the area that is likely to produce the most notable in-ice wave growth events.

4.1 Future Work

My future work will be focused on using high resolution SAR imagery to characterize the MIZ in the Hudson Bay, Canada, looking specifically at trends in the in-ice fetches over the past few years as well as how they tend to vary throughout the breakup season. The next step would then be to hindcast and map local wave growth in the MIZ over the time, observing trends in wave growth in relation to changes in ice concentration and fetch patterns. Wind data from ERA5 will be utilized. This work will be a contribution to the BAYSYS (Hudson Bay System) study which is a 4-year study examining the contributions of climate change and hydroelectric regulation to the variability and change of freshwater-marine coupling in the Hudson Bay System. This study is

funded by Manitoba Hydro as well as NSERC and is spearheaded by the Center for Earth Observation Science (CEOS) at the University of Manitoba, where I will continue this research. Hudson Bay (HB) in northeastern Canada is described as the world's largest inland sea. It is almost completely surrounded by land but connects to the Arctic Ocean by means of the Foxe basin to the north, and to the Atlantic Ocean via Hudson Strait to the north-east. This is a relatively unexplored region of the sub-Arctic, with the BASYS study being one of the first bay-wide study to examine marine-freshwater coupling alongside the effects of climate change. The timing of sea ice growth and decay is quite different in HB in comparison to the Beaufort Sea. The HB becomes completely ice free each year, with a cycle of breakup starting in late May through early August, and freeze-up occurring from late October to early December (Andrews, Babb, and Barber 2017). Ice melt begins in the north and produces a distinct marginal ice zone (MIZ). Figure 6.4 shows a section of the MIZ in Hudson Bay during early stages of breakup on June 4, 2019. Already there are fetches up to 10 km, with visible wave activity. Like much of the Arctic, the sea ice in Hudson Bay has been breaking up earlier and freezing up later as a result of surface air temperatures increasing significantly since the mid 1990s (Hochheim and Barber 2014). With this trend, the MIZ is expected to increase, along with open water fetches and wave development. Increase in wave activity (even relatively low waves) in the MIZ will undoubtedly have significant effects, increasing the overall heat and kinetic energy within the ice-ocean system. Mapping the patterns in open water fetches and wave growth has never been done in HB. This will provide an important contribution to the overall study of the marine system in HB and the impacts of climate change on this system.

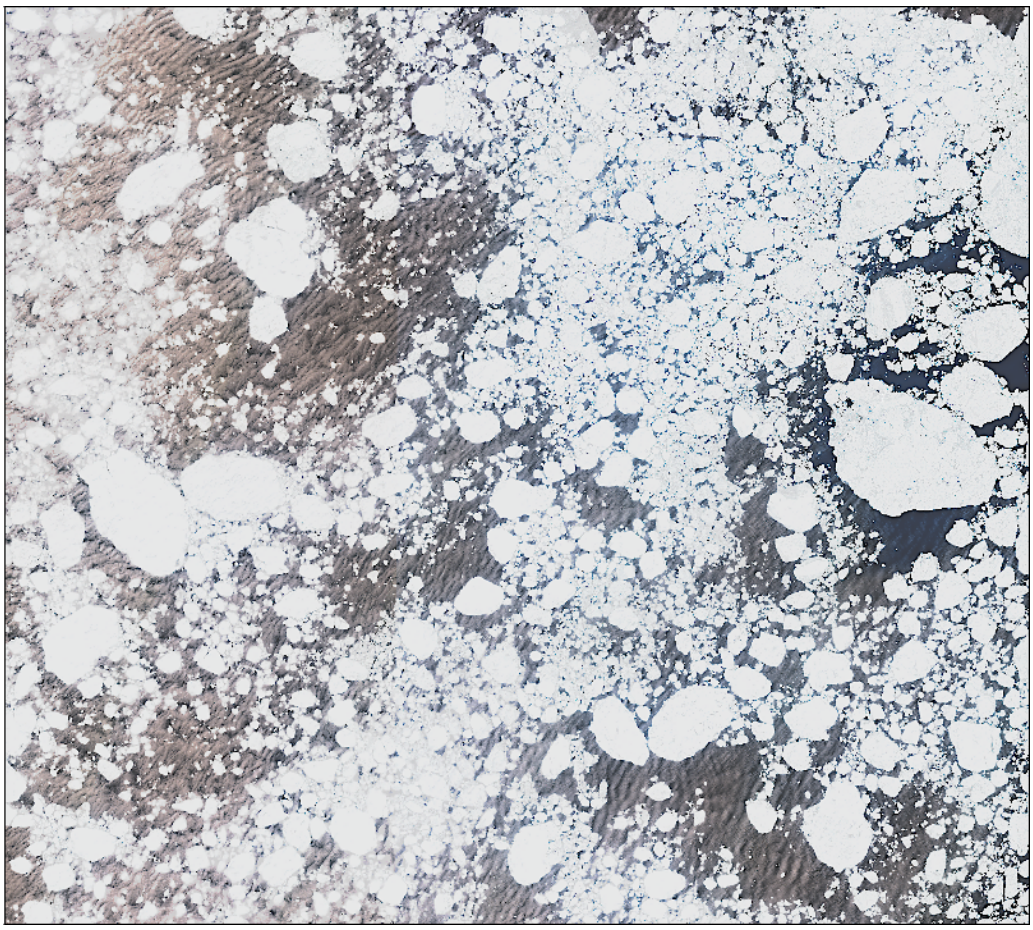

Figure 6.4: Sentinel-2 image of a section of the marginal ice zone of Hudson Bay on June 6 2019. Open water fetches are up to 10 km and waves can be clearly seen.

7. Conclusion

There has been very little research done on short waves generated within partial sea ice cover, as their longer counterparts have a much greater ability to invoke stress, fracture and breakage in sea ice and are therefore the focus of most waves-in-ice studies. Once leads have been formed in the sea ice, however, whether by these long waves, upwelling of warm water or by divergent wind conditions, the potential for waves to develop within these open water regions present another source of enhancing the heat fluxes between sea ice, ocean and atmosphere. The conclusion is that waves in partial sea ice, based on this study, are likely to remain below heights of 0.5 m and periods of 9 seconds. The observations in this study were collected in the year 2009, however, which did not see a significant sea ice decline in comparison to other (and more recent) years. As increasing temperature trends continue, the MIZ is expected to widen, and as a result, the quantity and sizes of open water segments in sea ice are also expected to increase. This will then have a direct impact on the wave evolution in sea ice. Waves, even when quite low affect the total balance of heat, momentum and gas in of the sea ice-ocean-atmospheric system and allows for these fluxes to occur more effectively. As Garbe et al. (2008) mentioned, ocean waves are the gearbox between the atmosphere and the ocean. Wave breaking, in particular, is the highest gear. Wave breaking not only increases the total kinetic energy (TKE) in the near-surface layer but also transfers gases, momentum and heat from the atmosphere to the ocean. In addition, the 'skin' layer at the ocean surface, typically around a millimeter in thickness hosts a temperature gradient which is vital in regulating vertical heat fluxes. At low wind speeds, the temperature gradient is at its maximum, however, with the development of waves both the gradient and thickness of this layer decreases (Geernaert and Plant 2013). The result is an increased heat flux across the ocean-atmosphere interface. He et al. (2018) found that surface waves could increase the transfer of momentum to the ocean surface by 15%. This is a feedback mechanism in itself, encouraging the generation and growth of waves. Thus, even though waves

in sea ice tend to be fairly low, they will play an increasingly important role in the energy balance of Arctic marine systems as the climate warms.

In this study, the local growth of waves was observed to be the dominant source of wave energy in the MIZ throughout the month of August 2009. Typically, wave energy in the MIZ is attributed to long waves propagating from the open ocean. In such cases, the average peak periods tend to increase as the sea ice selectively attenuates waves with shorter periods, while the wave energy is reduced. This study provided a different perspective of wave energy deep in a sea ice field. Throughout most of August, while all moorings were in sea ice, the wave heights were quite coherent with the peak periods, as opposed to having contrasting responses (that is, heights increasing and periods decreasing). This indicates that the waves were locally grown and were not as a result of open water waves propagating into the ice field. The contrast between H_s and T_p was predominantly seen towards the end of the month and close to the MIB. The positive correlation between the H_s and T_p also indicates that this contrasting behavior was not dominant. Thus, it is hypothesized that two main types of sea ice interactions took place in this wave environment. The first involves the attenuation of local waves where the sea ice acted as a low pass filter with the shorter waves being selectively dissipated. The second involves the attenuation of these short waves but more so at the longer wavelengths or periods. In the former case, the attenuation is expected to take place when the short waves interact with small floes, and hence the predominance closer to the MIZ at the end of the month (where there are large discrepancies between the wave heights and the peak periods). The latter case would occur when the short waves interact with large floes, which were the majority of the floes present in the MIZ in August. This type of interaction would produce more coherence with height and periods, as the large floes would decrease the heights and also decrease the periods (because the larger wavelengths are being selectively attenuated). Since a significant amount of the floes remained large throughout the month, there was likely to be a significant amount of backscattering from

the interaction between these large floes and the local short waves. This could lead to increases in heights close to a sea ice edge and choppy wave conditions.

The changes in the MIZ as a result of increasing Arctic warming is expected to have significant impacts on the energy balance of the marine system in the Arctic. Both long and short waves work conjointly together to increase the breaking of floes as well as the melting of the floes. An increase in local short-wave growth, as well as more energetic wave growth, enhances the distribution and impact of heat from the water to the sea ice, an effect that is likely to be more pronounced as Arctic warming continues.

References

- "An Update on the Ice Climatology of the Hudson Bay System: Arctic, Antarctic, and Alpine Research: Vol 46, No 1." n.d. Accessed September 9, 2019. https://www-tandfonline-com.uml.idm.oclc.org/doi/full/10.1657/1938-4246-46.1.66?scroll=top&needAccess=true.
- Andrews, Jonathan, David Babb, and David G. Barber. 2017. "Climate Change and Sea Ice: Shipping Accessibility on the Marine Transportation Corridor through Hudson Bay and Hudson Strait (1980–2014)." *Elem Sci Anth* 5 (0): 15. https://doi.org/10.1525/elementa.130.
- Ardhuin, Fabrice, Peter Sutherland, Martin Doble, and Peter Wadhams. 2016. "Ocean Waves across the Arctic: Attenuation Due to Dissipation Dominates over Scattering for Periods Longer than 19 s." *Geophysical Research Letters*.
- Asplin, Matthew G., Ryan Galley, David G. Barber, and Simon Prinsenberg. 2012. "Fracture of Summer Perennial Sea Ice by Ocean Swell as a Result of Arctic Storms." *Journal of Geophysical Research: Oceans* 117 (C6).
- Barber, David G., Haakon Hop, Christopher J. Mundy, Brent Else, Igor A. Dmitrenko, Jean-Eric Tremblay, Jens K. Ehn, Philipp Assmy, Malin Daase, and Lauren M. Candlish. 2015. "Selected Physical, Biological and Biogeochemical Implications of a Rapidly Changing Arctic Marginal Ice Zone." *Progress in Oceanography* 139: 122–150.
- Bennetts, L.G., A. Alberello, M.H. Meylan, C. Cavaliere, A.V. Babanin, and A. Toffoli. 2015. "An Idealised Experimental Model of Ocean Surface Wave Transmission by an Ice Floe." *Ocean Modelling* 96 (December): 85–92. https://doi.org/10.1016/j.ocemod.2015.03.001.
- Bennetts, Luke G., and Vernon A. Squire. 2011. "On the Calculation of an Attenuation Coefficient for Transects of Ice-Covered Ocean." *Proceedings of the Royal Society A: Mathematical, Physical and Engineering Sciences* 468 (2137): 136–162.
- Boutin, Guillaume, Fabrice Ardhuin, Dany Dumont, Caroline Sévigny, Fanny Girard-Ardhuin, and Mickael Accensi. 2018. "Floe Size Effect on Wave-Ice Interactions: Possible

Effects, Implementation in Wave Model, and Evaluation." *Journal of Geophysical Research: Oceans* 123 (7): 4779–4805. https://doi.org/10.1029/2017JC013622.

- Carter, D. J. T. 1982. "Prediction of Wave Height and Period for a Constant Wind Velocity Using the JONSWAP Results." *Ocean Engineering* 9 (1): 17–33.
- Chen, Chen-Tung Arthur, and Jacques C. J. Nihoul. 2009. *OCEANOGRAPHY– Volume I*. EOLSS Publications.
- Collins III, Clarence O., W. ERICK Rogers, and Aleksey Marchenko. 2016. "On Wave-Ice Interaction in the Arctic Marginal Ice Zone: Dispersion, Attenuation, and Ice Response." NAVAL RESEARCH LAB STENNIS DETACHMENT STENNIS SPACE CENTER MS OCEAN DYNAMICS ….
- Collins III, Clarence O., W. Erick Rogers, Aleksey Marchenko, and Alexander V. Babanin. 2015. "In Situ Measurements of an Energetic Wave Event in the Arctic Marginal Ice Zone." *Geophysical Research Letters* 42 (6): 1863–1870.
- Comiso, Josefino C. 2012. "Large Decadal Decline of the Arctic Multiyear Ice Cover." *Journal of Climate* 25 (4): 1176–1193.
- Doble, Martin J., Giacomo De Carolis, Michael H. Meylan, Jean-Raymond Bidlot, and Peter Wadhams. 2015. "Relating Wave Attenuation to Pancake Ice Thickness, Using Field Measurements and Model Results." *Geophysical Research Letters* 42 (11): 4473–4481.
- Dumont, D., A. Kohout, and L. Bertino. 2011. "A Wave-Based Model for the Marginal Ice Zone Including a Floe Breaking Parameterization." *Journal of Geophysical Research* 116 (C4): C04001. https://doi.org/10.1029/2010JC006682.
- Fissel, D B, N Kulan, A Kanwar, E Ross, K Borg, D Billenness, D Sadowy, and J Reitsma. 2012. "Ajurak- Pokak Marine Physical Environment Technical Data Report, Canadian Beaufort Sea, 2009-2011.," 271.

- Fox, Colin, and Vernon A. Squire. 1990. “Reflection and Transmission Characteristics at the Edge of Shore Fast Sea Ice.” *Journal of Geophysical Research: Oceans* 95 (C7): 11629–39. https://doi.org/10.1029/JC095iC07p11629.
- Francis, Oceana P., Gleb G. Panteleev, and David E. Atkinson. 2011. “Ocean Wave Conditions in the Chukchi Sea from Satellite and in Situ Observations.” *Geophysical Research Letters* 38 (24): L24610. https://doi.org/10.1029/2011GL049839.
- Garbe, Christoph S., Robert A. Handler, and Bernd Jähne. 2008. *Transport at the Air-Sea Interface: Measurements, Models and Parametrizations*. Springer Science & Business Media.
- Geernaert, G. L., and W. J. Plant. 2013. *Surface Waves and Fluxes: Volume I — Current Theory*. Springer Science & Business Media.
- Hasselmann, K. 1962. “On the Non-Linear Energy Transfer in a Gravity-Wave Spectrum Part 1. General Theory.” *Journal of Fluid Mechanics* 12 (4): 481–500. https://doi.org/10.1017/S0022112062000373.
- ———. 1963. “On the Non-Linear Energy Transfer in a Gravity Wave Spectrum Part 2. Conservation Theorems; Wave-Particle Analogy; Irrevesibility.” *Journal of Fluid Mechanics* 15 (2): 273–81. https://doi.org/10.1017/S0022112063000239.
- Hasselmann, Klaus, T. P. Barnett, E. Bouws, H. Carlson, D. E. Cartwright, K. Enke, J. A. Ewing, H. Gienapp, D. E. Hasselmann, and P. Kruseman. 1973a. “Measurements of Wind-Wave Growth and Swell Decay during the Joint North Sea Wave Project (JONSWAP).” *Ergänzungsheft 8-12*.
- Hasselmann, Klaus, TP Barnett, E Bouws, H Carlson, DE Cartwright, K Enke, JA Ewing, H Gienapp, DE Hasselmann, and P Kruseman. 1973b. “Measurements of Wind-Wave Growth and Swell Decay during the Joint North Sea Wave Project (JONSWAP).” Deutches Hydrographisches Institut.

- He, Hailun, Qiaoyan Wu, Dake Chen, Jia Sun, Chujin Liang, Weifang Jin, and Yao Xu. 2018. "Effects of Surface Waves and Sea Spray on Air–Sea Fluxes during the Passage of Typhoon Hagupit." *Acta Oceanologica Sinica* 37 (5): 1–7. https://doi.org/10.1007/s13131-018-1208-2.
- Healy, Terry R. 2005. "Coastal Wind Effects." In *Encyclopedia of Coastal Science*, edited by Maurice L. Schwartz, 312–13. Dordrecht: Springer Netherlands. https://doi.org/10.1007/1-4020-3880-1_91.
- Hochheim, Klaus P., and David G. Barber. 2014. "An Update on the Ice Climatology of the Hudson Bay System." *Arctic, Antarctic, and Alpine Research* 46 (1): 66–83. https://doi.org/10.1657/1938-4246-46.1.66.
- Holthuijsen, Leo H. 2010. *Waves in Oceanic and Coastal Waters*. Cambridge university press.
- Hunkins, Kenneth. 1962. "Waves on the Arctic Ocean." *Journal of Geophysical Research* 67 (6): 2477–89. https://doi.org/10.1029/JZ067i006p02477.
- Kohout, A. L., M. J. M. Williams, S. M. Dean, and M. H. Meylan. 2014a. "Storm-Induced Sea-Ice Breakup and the Implications for Ice Extent." *Nature* 509 (7502): 604–607.
- ———. 2014b. "Storm-Induced Sea-Ice Breakup and the Implications for Ice Extent." *Nature* 509 (7502): 604–7. https://doi.org/10.1038/nature13262.
- Kohout, Alison L., and Michael H. Meylan. 2008. "An Elastic Plate Model for Wave Attenuation and Ice Floe Breaking in the Marginal Ice Zone." *Journal of Geophysical Research: Oceans* 113 (C9).
- Kohout, Alison L., Michael H. Meylan, and David R. Plew. 2011. "Wave Attenuation in a Marginal Ice Zone Due to the Bottom Roughness of Ice Floes." *Annals of Glaciology* 52 (57): 118–22. https://doi.org/10.3189/172756411795931525.
- Koyama, Tomoko, Julienne Stroeve, John Cassano, and Alex Crawford. 2017a. "Sea Ice Loss and Arctic Cyclone Activity from 1979 to 2014." *Journal of Climate* 30 (12): 4735–4754.

- ———. 2017b. “Sea Ice Loss and Arctic Cyclone Activity from 1979 to 2014.” *Journal of Climate* 30 (12): 4735–54. https://doi.org/10.1175/JCLI-D-16-0542.1.
- ———. 2017c. “Sea Ice Loss and Arctic Cyclone Activity from 1979 to 2014.” *Journal of Climate* 30 (12): 4735–54. https://doi.org/10.1175/JCLI-D-16-0542.1.
- Lee, Craig M., Jim Thomson, Marginal Ice Zone, and Arctic Sea State Teams. 2017. “An Autonomous Approach to Observing the Seasonal Ice Zone in the Western Arctic.” *Oceanography* 30 (2): 56–68.
- Li, Jingkai, Alison L. Kohout, Martin J. Doble, Peter Wadhams, Changlong Guan, and Hayley H. Shen. 2017. “Rollover of Apparent Wave Attenuation in Ice Covered Seas.” *Journal of Geophysical Research: Oceans* 122 (11): 8557–66. https://doi.org/10.1002/2017JC012978.
- Lin, Lihwa, Zeki Demirbilek, Jinhai Zheng, and Hajime Mase. 2010. “Rapid Calculation of Nonlinear Wave-Wave Interactions in Wave-Action Balance Equation.” ENGINEER RESEARCH AND DEVELOPMENT CENTER VICKSBURG MS COASTAL AND HYDRAULICS LAB.
- Lynn, Paul A. 2013. *Electricity from Wave and Tide: An Introduction to Marine Energy*. John Wiley & Sons.
- Masson, D., and P. H. Leblond. 1989. “Spectral Evolution of Wind-Generated Surface Gravity Waves in a Dispersed Ice Field.” *Journal of Fluid Mechanics* 202 (May): 43–81. https://doi.org/10.1017/S0022112089001096.
- Masson, Diane. 1987. “Spectral Evolution of Wind Generated Surface Gravity Waves in a Dispersed Ice Field.” University of British Columbia. https://doi.org/10.14288/1.0053103.
- McCormick, Michael E. 2010. *Ocean Engineering Mechanics: With Applications*. Cambridge University Press.
- Meylan, M. H., and L. G. Bennetts. 2018. “Three-Dimensional Time-Domain Scattering of Waves in the Marginal Ice Zone.” *Philosophical Transactions. Series A, Mathematical, Physical, and Engineering Sciences* 376 (2129). https://doi.org/10.1098/rsta.2017.0334.

- Meylan, Michael H. 2002. “Wave Response of an Ice Floe of Arbitrary Geometry.” *Journal of Geophysical Research: Oceans* 107 (C1): 5-1-5–11. https://doi.org/10.1029/2000JC000713.
- Meylan, Michael H., and Diane Masson. 2006. “A Linear Boltzmann Equation to Model Wave Scattering in the Marginal Ice Zone.” *Ocean Modelling* 11 (3–4): 417–27. https://doi.org/10.1016/j.ocemod.2004.12.008.
- Meylan, Michael H., Vernon A. Squire, and Colin Fox. 1997. “Toward Realism in Modeling Ocean Wave Behavior in Marginal Ice Zones.” *Journal of Geophysical Research: Oceans* 102 (C10): 22981–91. https://doi.org/10.1029/97JC01453.
- Meylan, Michael, and Vernon A Squire. 1994. “The Response of Ice Floes to Ocean Waves.” *JOURNAL OF GEOPHYSICAL RESEARCH-ALL SERIES-* 99: 891–891.
- Miles, John W. 1957. “On the Generation of Surface Waves by Shear Flows.” *Journal of Fluid Mechanics* 3 (2): 185–204.
- Overeem, Irina, Robert S. Anderson, Cameron W. Wobus, Gary D. Clow, Frank E. Urban, and Nora Matell. 2011. “Sea Ice Loss Enhances Wave Action at the Arctic Coast.” *Geophysical Research Letters* 38 (17): L17503. https://doi.org/10.1029/2011GL048681.
- Perrie, W., and Y. Hu. 1996. “Air–Ice–Ocean Momentum Exchange. Part 1:Energy Transfer between Waves and Ice Floes.” *Journal of Physical Oceanography* 26 (9): 1705–20. https://doi.org/10.1175/1520-0485(1996)026<1705:AMEPTB>2.0.CO;2.
- Phillips, Owen M. 1957. “On the Generation of Waves by Turbulent Wind.” *Journal of Fluid Mechanics* 2 (5): 417–445.
- Pierson, Willard J., and Lionel Moskowitz. 1964. “A Proposed Spectral Form for Fully Developed Wind Seas Based on the Similarity Theory of SA Kitaigorodskii.” *Journal of Geophysical Research* 69 (24): 5181–5190.
- Prinsenberg, Simon, Ingrid Peterson, David Barber, and Matthew Asplin. 2010. “Long Period Swells Break up the Canadian Beaufort Sea Pack Ice in September 2009.” In . International Society of Offshore and Polar Engineers.

- Robin, G de Q. 1963. “Wave Propagation through Fields of Pack Ice.” *Philosophical Transactions of the Royal Society of London A: Mathematical, Physical and Engineering Sciences* 255 (1057): 313–39.
- Sergienko, O. V. 2017. “Behavior of Flexural Gravity Waves on Ice Shelves: Application to the Ross Ice Shelf.” *Journal of Geophysical Research: Oceans* 122 (8): 6147–64. https://doi.org/10.1002/2017JC012947.
- Singh, H. A., O. A. Garuba, and P. J. Rasch. 2018. “How Asymmetries Between Arctic and Antarctic Climate Sensitivity Are Modified by the Ocean.” *Geophysical Research Letters* 45 (23): 13,031-13,040. https://doi.org/10.1029/2018GL079023.
- Small, David, Eyad Atallah, and John Gyakum. 2011. “Wind Regimes along the Beaufort Sea Coast Favorable for Strong Wind Events at Tuktoyaktuk.” *Journal of Applied Meteorology and Climatology* 50 (6): 1291–1306. https://doi.org/10.1175/2010JAMC2606.1.
- Smith, Madison, and Jim Thomson. 2016. “Scaling Observations of Surface Waves in the Beaufort Sea.” *Elem Sci Anth* 4 (0): 000097. https://doi.org/10.12952/journal.elementa.000097.
- Squire, V. A. 2007. “Of Ocean Waves and Sea-Ice Revisited.” *Cold Regions Science and Technology* 49 (2): 110–33. https://doi.org/10.1016/j.coldregions.2007.04.007.
- Squire, V.A. 2007. “Of Ocean Waves and Sea-Ice Revisited.” *Cold Regions Science and Technology* 49 (2): 110–33. https://doi.org/10.1016/j.coldregions.2007.04.007.
- Squire, Vernon A. 2018. “A Fresh Look at How Ocean Waves and Sea Ice Interact.” *Philosophical Transactions. Series A, Mathematical, Physical, and Engineering Sciences* 376 (2129). https://doi.org/10.1098/rsta.2017.0342.
- Squire, Vernon A., Gareth L. Vaughan, and Luke G. Bennetts. 2009. “Ocean Surface Wave Evolvement in the Arctic Basin.” *Geophysical Research Letters* 36 (22): L22502. https://doi.org/10.1029/2009GL040676.

- Stammerjohn, Sharon, Robert Massom, David Rind, and Douglas Martinson. 2012. “Regions of Rapid Sea Ice Change: An Inter-Hemispheric Seasonal Comparison.” *Geophysical Research Letters* 39 (6). https://doi.org/10.1029/2012GL050874.
- Stegall, Steve T., and Jing Zhang. 2012. “Wind Field Climatology, Changes, and Extremes in the Chukchi–Beaufort Seas and Alaska North Slope during 1979–2009.” *Journal of Climate* 25 (23): 8075–89. https://doi.org/10.1175/JCLI-D-11-00532.1.
- Stopa, J. E., F. Ardhuin, Jim Thomson, Madison M. Smith, Alison Kohout, Martin Doble, and Peter Wadhams. 2018. “Wave Attenuation Through an Arctic Marginal Ice Zone on 12 October 2015: 1. Measurement of Wave Spectra and Ice Features From Sentinel 1A.” *Journal of Geophysical Research: Oceans* 123 (5): 3619–34. https://doi.org/10.1029/2018JC013791.
- Stroeve, Julienne C., Mark C. Serreze, Marika M. Holland, Jennifer E. Kay, James Malanik, and Andrew P. Barrett. 2012. “The Arctic’s Rapidly Shrinking Sea Ice Cover: A Research Synthesis.” *Climatic Change* 110 (3–4): 1005–1027.
- Strong, Courtenay, Dallas Foster, Elena Cherkaev, Ian Eisenman, and Kenneth M. Golden. 2017. “On the Definition of Marginal Ice Zone Width.” *Journal of Atmospheric and Oceanic Technology* 34 (7): 1565–84. https://doi.org/10.1175/JTECH-D-16-0171.1.
- Thomson, Jim, Stephen Ackley, Fanny Girard-Ardhuin, Fabrice Ardhuin, Alex Babanin, Guillaume Boutin, John Brozena, et al. 2018. “Overview of the Arctic Sea State and Boundary Layer Physics Program.” *Journal of Geophysical Research: Oceans* 123 (12): 8674–87. https://doi.org/10.1002/2018JC013766.
- Thomson, Jim, and W. Erick Rogers. 2014. “Swell and Sea in the Emerging Arctic Ocean.” *Geophysical Research Letters* 41 (9): 3136–40. https://doi.org/10.1002/2014GL059983.
- Wadhams, Peter. 2014. *Ice in the Ocean*. CRC Press.
- Wadhams, Peter, Vernon A. Squire, Dougal J. Goodman, Andrew M. Cowan, and Stuart C. Moore. 1988. “The Attenuation Rates of Ocean Waves in the Marginal Ice Zone.” *Journal of*

Geophysical Research: Oceans 93 (C6): 6799–6818. https://doi.org/10.1029/JC093iC06p06799.

- Waseda, Takuji, Adrean Webb, Kazutoshi Sato, Jun Inoue, Alison Kohout, Bill Penrose, and Scott Penrose. 2018. "Correlated Increase of High Ocean Waves and Winds in the Ice-Free Waters of the Arctic Ocean." *Scientific Reports* 8 (March). https://doi.org/10.1038/s41598-018-22500-9.
- Weeks, Willy. 2010. *On Sea Ice*. University of Alaska Press.
- Zhang, Yuanyuan, Xiao Cheng, Jiping Liu, and Fengming Hui. 2018. "The Potential of Sea Ice Leads as a Predictor for Summer Arctic Sea Ice Extent." *The Cryosphere* 12 (12): 3747–57. https://doi.org/10.5194/tc-12-3747-2018.
- Zhao, Xin, Hayley H. Shen, and Sukun Cheng. 2015. "Modeling Ocean Wave Propagation under Sea Ice Covers." *Acta Mechanica Sinica* 31 (1): 1–15. https://doi.org/10.1007/s10409-015-0017-5.
- Zippel, Seth, and Jim Thomson. 2016. "Air-Sea Interactions in the Marginal Ice Zone." *Elem Sci Anth* 4 (0): 000095. https://doi.org/10.12952/journal.elementa.000095.